Synthesis and Characterization of Epitaxial Thin Film β-SiC and TiC

Qinghua Zhao
B.S., Central-South University of Technology, Changsha, P. R. China, 1985
M.S., Central-South University of Technology, Changsha, P. R. China, 1988
M.S., Oregon Graduate Institute of Science and Technology, 1993

A dissertation submitted to the faculty of the
Oregon Graduate Institute of Science & Technology
in partial fulfillment of the requirements for the degree of
Doctor of Philosophy
in
Materials Science and Engineering

October, 1994

The dissertation "Synthesis and Characterization of Epitaxial Thin Film β-SiC and TiC" by Qinghua Zhao has been examined and approved by the following Examination Committee:

David A. Downham, Thesis Advisor
Assistant Professor

James D. Parsons,
Associate Professor

Lemmy Meekisho
Assistant Professor

Margret Moroz
Assistant Professor

To my mother, the source of my strength.

Acknowledgement

First, I would like to thank my research advisor, Dr. David Downham, for his guidance, support, and friendship during the period of my Ph.D study. I am grateful to Dr. James Parsons for his helpful discussions and suggestions, I benefited a lot from his pioneer work in the field of β-SiC semiconductor research. I would also like to thank Dr. Lemmy Meekisho and Dr. Margret Moroz for their friendship and efforts in reviewing the manuscript.

Thanks are also extended to Gregg Kruval for his help and co-operations. I am also thankful to all the students, staff, and faculty members in the Materials Science and Engineering Department for their friendship and support, they made my stay at OGI enjoyable.

I would like to express my special thanks to my husband John Simmons, his love, friendship, and moral support, offered me the strength to overcome all the difficulties. Finally, I want to thank my family and friends in China, their love and support made my dream come true.

Table of Contents

List of Tables

List of Figures

ABSTRACT

Synthesis and Characterization of Epitaxial Thin Film β-SiC and TiC

Qinghua Zhao, Ph.D

Supervising Advisor: David A. Downham

Epitaxial thin film β-SiC and TiC were synthesized in a inverted-vertical CVD reactor, and the defects formed in the thin films were characterized using transmission electron microscopy.

The TiC_x material was used as the substrate for β-SiC epitaxial growth. Due to the growth technique limitations, TiC_x crystals are nonstoichiometric and contain substructures and inter-subgrain defects. Three configurations of sub-boundaries are: (i) wide-extended, fault-like defects (WEFLD), (ii) edge dislocation arrays, and (iii) dislocation networks. The planar defects, present within the substructures, resemble an stacking fault-like characteristics. Annealing of TiC_x at 2300°C in contact with graphite, caused a significant reduction in the misorientation level and/or density of subgrains.

Studies of surface morphology and crystallinity of β-SiC epitaxial growth on TiC_x substrates using scanning electron microscopy (SEM) showed that the optimum growth conditions were T_s = 1157 -1180 °C and Q_{DSE} = 3.2 sccm. Microtwins and double positioning boundaries (DPBs) were formed in all the β-SiC epilayers grown on TiC_x substrates. The defect density was affected by the growth conditions and TiC_x substrate orientations. Non-optimum growth conditions and off-(111) orientations of TiC_x led to high density of microtwins and DPBs. The β-SiC grown on a (111) TiC_x contained less

concentration of microtwins and DPBs.

TiC epitaxial thin films were obtained on (110)β-SiC, (111)β-SiC, and (0001)6Hα-SiC surfaces, the TiC/SiC interface remained flat and stable after annealing at 1300-1400°C for two hours. The TiC films grown on 6Hα-SiC was superior to these on β-SiC, due to the better crystal quality of bulk-grown 6Hα-SiC, although threading dislocations were formed in all the TiC films. The quality of TiC epilayers were also dependent on their thickness. Large TiC/6Hα-SiC interface incoherence was observed when TiC thickness exceeded 1750Å, and non-uniform TiC layers were produced when the thickness was less than 160Å.

Chapter 1

INTRODUCTION

Beta silicon carbide (β-SiC) has been considered as a potential semiconductor material for high temperature, high frequency, and high power electronic devices.[1-5] This is because of its superior electrical and physical properties, such as wide band gap (E_g = 2.35 ev at 300 °K),[6-8] high breakdown electric field ($5x10^6$ V/cm),[8,9] high saturated electron drift velocity ($2.5x10^7$ cm/s),[10-12] low dielectric constant (K = 9.7),[13] and high thermal conductivity (ρ_T = 4.9 W/cm-°C).[14]

Silicon carbide has over 170 polytypes;[15] one common polytype is β-SiC which has a zincblend structure with cubic (C) symmetry, and all the other polytypes are denoted as α-SiC and occur in hexagonal (H) or rhombohedral (R) structures. The most abundant α-SiC polytype is the 6Hα-SiC. The bandgap of SiC increase in proportion to "hexagonality", i.e., from 2.35 ev in 3C- or β-SiC to 3.2 ev in 2Hα-SiC.[1] The β-SiC exhibits higher electron mobility than α-SiC because of the smaller phonon scattering in cubic crystals. Thus, β-SiC is currently considered more desirable than any of the alpha polytypes for use in high performance solid state devices.[1]

Unfortunately, the development of β-SiC as an electronic material has been inhibited due to the difficulties in obtaining high quality and large size single crystal β-SiC. Traditional bulk single crystal growth methods from solutions or from vapors are not suitable. From the equilibrium phase diagram of the Si-C system,[16] it can be seen that SiC is a peritectic reaction product. It is very unlikely that SiC can be obtained from a stoichiometric melt at atmospheric pressure. The other problem with β-SiC single

crystal growth is that β-SiC tends to transform to alpha-SiC polytypes above 2000°C,[17] therefore, growth of β-SiC needs to be conducted below 2000°C.

Synthesis of single crystal β-SiC is focussing on the epitaxial growth using the chemical vapor deposition (CVD) technique, on a foreign material substrate. Substrates materials primarily used are Si,[18-27] 6Hα-SiC[28-33] and TiC_x substrates.[34-36] The quality of β-SiC films depends critically on the substrate structure, orientation, and surface condition and, of course, the growth conditions used.

Beta-SiC epitaxial thin films grown on Si substrates generally contain a high concentration of defects including misfit dislocations, threading dislocations, twins, stacking faults, and antiphase boundaries (APBs).[20,23-24,26] The formation of these defects can be attributed to the lattice mismatch (about 20%), the thermal expansion coefficient difference between the epilayer β-SiC and substrate Si, and the growth process. These high energy defect APBs can be eliminated from the epilayers by using off-axis (100) Si substrates,[21,25] however, the high concentration of dislocations, twins, and stacking faults are unavoidable due to the large lattice mismatch and the thermal expansion coefficient mismatch between β-SiC and Si. The β-SiC epitaxial films grown on (0001) orientation 6Hα-SiC substrates have much lower density of defects in comparison to β-SiC/Si system, owing to the identical lattice constant and chemical compositions on the $(111)_{\beta\text{-}SiC}/(0001)_{6H\alpha\text{-}SiC}$ interface plane. However, double positioning boundaries (DPBs) generally occur, and it is not always possible to achieve epitaxial films containing cubic β-SiC devoid of α-SiC polytypes.[29,31,33] A DPB is an incoherent twin boundary with high internal energy; the potential applications of β-SiC demand the removal of DPBs from the thin films. However, previous studies,[30] aimed at eliminating DPBs by tilting the substrate were not successful. Therefore, β-SiC thin films synthesized on either Si or 6Hα-SiC substrates are far from perfect and are not suitable for electronic device applications.

Titanium carbide (TiC_x) has been chosen as an substrate material for β-SiC epitaxial growth.[34-36] This is because TiC_x has a cubic crystal structure, a small lattice mismatch with β-SiC (0.6%), and excellent chemical stability within the required

Chapter 2

BACKGROUND

The superior electronic properties of β-SiC make it a potential semiconductor material for high performance device applications. However, a high quality single crystal β-SiC is not available at the present time. Extensive studies on single crystal synthesis of β-SiC were inspired by a two-step CVD process developed by Nishino and his co-workers in 1980, from which β-SiC epitaxial thin films were obtained on Si substrates.[18]

The purpose of this chapter is to review the crystal structures and electronic properties of SiC especially β-SiC, the advantages of β-SiC as a semiconductor material, the current status on the study of single crystal β-SiC synthesis, and general defects formed in epitaxial thin films.

2.1 Physical and Electronic Properties of SiC

2.1.1 Polytypes of SiC

Silicon carbide can exist in over 170 polytypes, but only three crystal structures, hexagonal (H), rhombohedral (R) or trigonal, and cubic (C).[15] There is only one polytype of cubic SiC, denoted as 3C- or β-SiC; the additional 170 polytypes of SiC with hexagonal and rhombohedral structures are collectively referred to as α-SiC.

The several common polytypes of SiC are listed in Table 2.1, where A, B, and C denote the close-packed atomic plane. The differences between these polytypic SiC

can be described by the differences in the closed-packed atomic plane stacking sequences. These polytypes are alike in the two dimensions of the close-packed planes but differ in the stacking sequence in the dimension perpendicular to the close packed plane.

Table 2.1. Several Common SiC Polytypes

Type	Notation	Stacking Sequence
cubic or beta	3C	ABC..
alpha	2H	AB...
	4H	ABAC...
	6H	ABCACB...
	15R	ABCBACABACBCACB...

Various explanations have been proposed to account for the polymorphism in SiC. Frank's dislocation model,[37] Ramsdell and Kohn's polymer model,[38] Schneer's transformation model,[39] and Jagodzinski's disorder model[40] have been proposed. These models seem to be fairly satisfactory when they are applied to the longer-period polytypes such as 4H-, 6H-, and 15R-SiC. However, none of these models can account for the occurrence of short-period polytypes such as 2H- and 3C-SiC. An electrostatic model proposed by Yoo and Matsunami[41] recently successfully explained the formation of these two polytypes of SiC.

Different polytypes of SiC have similar physical and chemical properties, but different electronic properties.[42] Since β-SiC and 6Hα-SiC are the two most important types of SiC, their electronic properties and their merits for electronic device applications are reviewed below.

2.1.2 Superior Electronic Properties of β-SiC

The key properties of β-SiC and 6Hα-SiC for high temperature, high frequency,

and high power circuit applications are compared with commercial semiconductor materials Si, GaAs, and InP in Table 2.2.[6-14] Since the electronic properties of Si, GaAs, and InP can be found in numerous text books, the listed references only apply to β-SiC and 6Hα-SiC.

Table 2.2. Important Properties of Semiconductor Materials

Properties (at 300°K)	Si	GaAs	InP	β-SiC	6Hα-SiC	Ref.
Bandgap Energy (E_g, ev)	1.12	1.43	1.29	2.35	2.86	6-8
Breakdown Electric Field (E_b, V/cm)	$3x10^5$	$4x10^5$	$6x10^5$	$>5x10^6$	$>5x10^6$	8,9
Saturated Electron Drift Velocity (v_s, cm/s)	$1x10^7$	$2x10^7$	$2x10^7$	$2.5x10^7$	$2.0x10^7$	10-12
Dielectric Constant, (κ)	11.8	12.8	14.0	9.7	≥ 9.7	13
Thermal Conductivity, (σ_T, w/cm-°K)	1.5	0.5	0.7	4.9	4.9	14

Semiconductors with larger bandgaps (E_g) are less susceptible to thermal runaway, and are able to handle higher current densities, and usually have a higher breakdown electric field (E_b). Based upon the properties listed in Table 2.2, figures of merit are used to predict relative high frequency and high power performance limitations of semiconductor materials. Two well known figures of merit have been proposed by E.

O. Johnson[43] and R. W. Keys.[44]

In 1965, Johnson developed a simple theoretical relationship between the breakdown voltage (E_b), the electron saturated drift velocity (v_s), and the power and frequency limits of transistors. This analysis can give a simple benchmark value for comparing semiconductors with respect to the power and the frequency limits of the devices, and is important in comparing candidate materials for high power, high frequency devices. Johnson's figure of merit is obtained from the expression:

$$M_J = (P_m X_c)^{1/2} f_T = \frac{E_b v_s}{2\pi} \qquad (2.1)$$

where P_m = maximum power, X_c = relative impedance at f_T, and f_T = the cutoff frequency. The values of this expression for the several semiconductor materials are listed in column 1 of Table 2.3. The ratios of the figure of merit with respect to Si are shown in column 2 of Table 2.3.

Table 2.3. Figures of Merits

Material	Johnson's Figure of Merit		Key's Figure of Merit	
	$(E_b v_s)/2\pi$, x10^{11} (volts/sec)	Ratio to Si	$\sigma_T(v_s/\kappa)^{1/2}$, x$10^2$ (w/cm$^{1/2}$-sec$^{1/2}$-°C)	Ratio to Si
Si	10.6	1.0	13.8	1.0
GaAs	28.3	2.7	6.3	0.5
InP	42.4	4.0	8.4	0.6
6H α-SiC	353.6	33.5	70.4	5.1
β-SiC	442.0	41.7	78.7	5.7

Another important figure of merit was developed by Keyes[44] as a relationship between high frequency limitations, minimum device dimensions, and the semiconductor properties σ_T, v_s and κ. The numerical value for Keys' figures of merit is given by:

$$M_K = \sigma_T (v_s / \kappa)^{1/2} \qquad (2.2)$$

where σ_T is the thermal conductivity, v_s is the saturated electron drift velocity, and κ is the dielectric constant. The values of this expression are listed in column 3 of Table 2.3. Ratios of this figure of merit relative to Si for the various semiconductors are shown in column 4 of Table 2.3.

From Table 2.3, it is seen that both β-SiC and 6Hα-SiC are superior to Si, GaAs, and InP for electronic applications, no matter which figure of merit is used for the evaluations. Since the existing commercial semiconductor materials, i.e., Si and GaAs, have been pushed to their upper limits of performance capabilities[45] in today's electronic industry, SiC seems to be an ideal candidate for the further development of high temperature, high frequency, and high power devices. Because of the smaller phonon scattering in the cubic crystal, the electron mobility of β-SiC is greater than that of α-SiC, thus, β-SiC is currently considered more desirable than any alpha polytypes.[1]

2.2 Single Crystal Growth of β-SiC

Silicon carbide is the only compound that exists in a solid state in the Si-C binary system as shown in the phase diagram Fig.2.1.[16] Because of the peritectic nature of the reaction form SiC, it is very unlikely that SiC can be obtained from a stoichiometric melt at atmospheric pressure. In fact, SiC does not melt but sublimes at temperatures above 1800°C[5] at atmospheric pressure. Therefore, the conventional bulk single crystal growth methods from solutions, i.e., Czochralski and float-zone methods, cannot be used for SiC crystal growth.

A sublimation method for SiC single crystal growth was first developed by Lely.[46] Owing to its simplicity, efficiency, flexibility, and controllability, this process

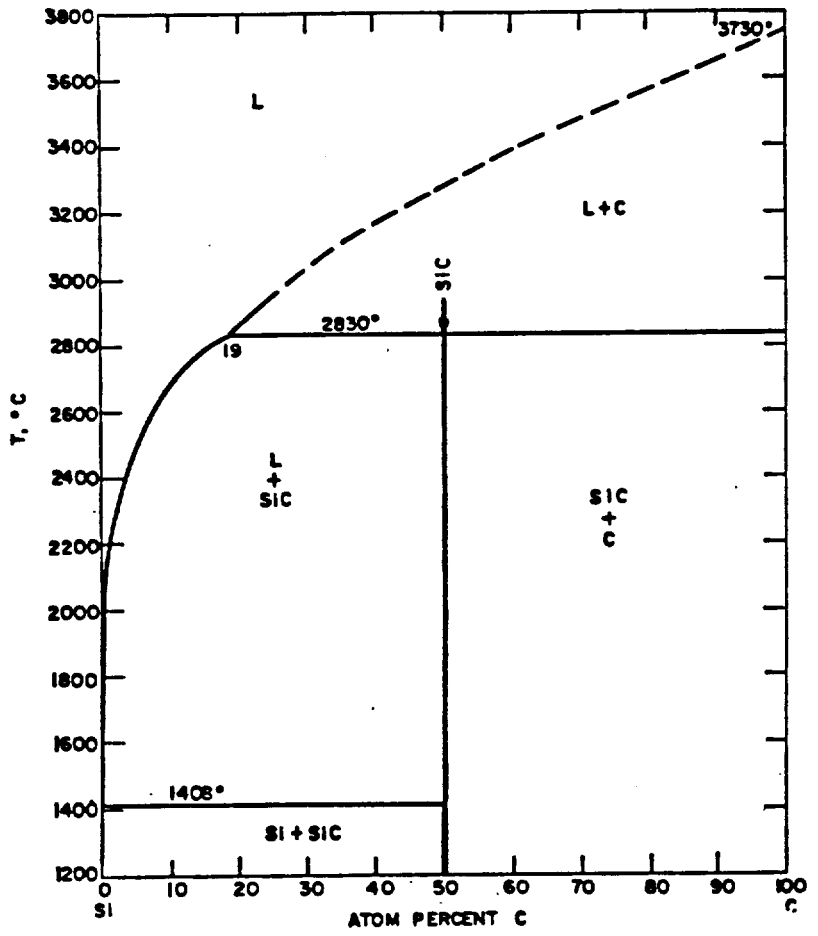

Fig.2.1 Phase diagram of Si-C system.

was studied in great effort and 6Hα-SiC has been successfully produced using the Lely sublimation method.[47-49] However, the Lely sublimation method fails to produce β-SiC single crystals. This is mainly because that β-SiC is a metastable modification of α-SiC, and it transforms to α-SiC at temperatures above 2000°C according to the Ostwald rule.[15] This temperature is below the sublimation temperature.

Epitaxial growth on a single crystal foreign material substrate is the only successful approach for obtaining single crystal β-SiC. Early studies of vapor phase epitaxial deposition of SiC on single crystal substrates had largely been confined to substrates of silicon,[50-53] sapphire[54] and hexagonal alpha SiC polytypes.[54-56]

In recent years, the major efforts have been concentrated on the synthesis of β-SiC on substrates of Si,[18-27] 6Hα-SiC,[28-33] and TiC_x using CVD.[34-36] The crystal parameters of Si, 6Hα-SiC, TiC_x and β-SiC, and the lattice mismatch relative to β-SiC are listed in Table 2.4.[57-58] The current research status on β-SiC single crystal synthesis using these three substrates will be reviewed below.

Table 2.4. Crystal Data of β-SiC, Si, 6Hα-SiC and TiC[57,58]

Material	Crystal Structure	Lattice Parameter	Space Group	Lattice Mismatch Relative to β-SiC
β-SiC	cubic (zincblend)	a = 0.436 nm	$F\bar{4}3m$	0%
Si	cubic (diamond)	a = 0.543 nm	$Fd\bar{3}m$	20%
6Hα-SiC	hexagonal	a = 0.309 nm c = 1.512 nm	$P6_3mc$	0% at interface $(111)_{\beta\text{-SiC}}/(0001)_{6H\alpha\text{-SiC}}$
TiC_x	cubic (rocksalt)	a = 0.433 nm (when x = 0.85)	$Fm\bar{3}m$	0.6%

2.2.1 β-SiC Grown on Si Substrate

Single crystal silicon is the most widely available commercial semiconductor, it has very high purity, and is virtually defect free. However, there is a large lattice mismatch (20% as shown in Table 2.4) between ß-SiC (a = 0.436 nm) and Si (a = 0.543 nm), which makes direct epitaxial growth of ß-SiC on Si almost impossible.

Chemical conversion of a Si substrate was the first successful method by which large area monocrystalline β-SiC films were produced, although the film thicknesses were very thin. In this process, SiC films were formed by the reaction (carburization) of a monocrystalline Si substrate with gaseous hydrocarbons, such as C_2H_2,[59-64] C_2H_4,[65] C_3H_8,[66] and CH_4.[67-69]

A two-step process which combines buffer-layer formation on Si and chemical vapor deposition (CVD) of single crystal β-SiC thin films was developed in 1980.[18] In this method, a sputtered ß-SiC layer was formed as a buffer layer on the Si substrate surface prior to the CVD epitaxial growth. This technique was further improved by growing the buffer-layer *in situ* prior to the CVD epitaxial growth of β-SiC. Large area monocrystalline β-SiC on Si was then first obtained by Nishino et al. in 1983. using this modified two-step method.[19] Since single crystal Si substrates are readily available and inexpensive, this two-step approach has been duplicated and modified worldwide.[22-23,26,28,70-73]

The CVD system used for ß-SiC growth on Si consists of a conventional horizontal water-cooled quartz tube reactor. Three major steps included in this method are (1) etching, (2) buffer layer growth, and (3) crystal growth. The purpose of etching is to clean the Si surface, and is performed by heating the Si to 1200°C in a mixture of HCl and H_2. The second step provides the buffer layer which is necessary to obtain single crystal ß-SiC on the Si substrate. In this step, propane C_3H_8 carried by H_2 gas flows through the reaction chamber and reacts with the Si surface forming a SiC buffer layer. After the formation of the buffer layer, a mixture of SiH_4 and C_3H_8 (in a certain ratio) is established and flows through the reaction chamber, forming β-SiC deposition film on top of the buffer layer. The buffer layer formed has been identified as a single

crystal ß-SiC layer,[70] which makes further single crystal epitaxial growth of ß-SiC film possible.

The crystallinity of epitaxially grown ß-SiC films is strongly affected by Si substrate orientation.[20,21] It was found that, single crystal ß-SiC can be obtained on (100) and (111) orientation Si substrates, but polycrystalline ß-SiC is obtained if (110) and (211) Si substrates are used. Since β-SiC epilayers grown on (111) Si substrates tend to result in cracking, curling and twinning,[20] Si substrates with (100) orientation have become the most popular choice.

The dependence of ß-SiC crystallinity on the substrate orientation can be explained by considering the arrangement of atoms around the ideal ß-SiC/Si interfaces for various orientations. The Si(100) and (111) have polar surface planes, that is the (100) or (111) plane consists of C atoms only (or Si atoms only). Therefore, substrate surface must contain C atoms only (or Si atoms only) to form a single crystal β-SiC epilayer. This condition is satisfied by the carburization process prior to the β-SiC growth. After carburization, the substrate surface can be considered to be covered by C atoms only. Hence, a single crystal β-SiC can be obtained by subsequent CVD growth on Si(100) and (111). On the other hand, in the case of nonpolar surfaces such as SiC(110) and (211), both C and Si atoms are needed to form an ideal β-SiC lattice. As stated above, there are only C atoms available on the substrate surface after carburization, therefore, a single crystal SiC cannot be obtained on these two orientations of Si substrates using the two-step CVD method.

Generally, a high concentration of defects including misfit dislocations, threading dislocations, twins, stacking faults, and antiphase boundaries (APBs) are generated in the β-SiC thin films on Si substrates.[18-26] An antiphase boundary (APB) is a special type of planar defects, which will be discussed later. The formation of defects are due to several factors, the lattice mismatch, the thermal expansion coefficient mismatch, and the growth process performed. By using off-axis (100) Si substrates, the high internal energy APBs can be eliminated from the epilayers.[21-25] However, the large lattice mismatch (20%) between β-SiC and Si determines that, there is little hope of reducing

the concentration of dislocations, twins, and stacking faults formed in ß-SiC on Si to values suitable for semiconductor device applications.[74]

Recently, a single molecule reactant source, hexamethydisilane $Si_2(CH_3)_6$ (denoted as HMDS) was developed by Nishino and his coworkers[22] for single crystal ß-SiC films synthesis. Using this single source HMDS, single crystal ß-SiC can be obtained epitaxially on a (111) Si substrate without the necessity of a buffer-layer. However, a buffer-layer is required to form single crystal ß-SiC on a (001) Si substrate. A growth temperature of 1100°C was used for this new reactant source, which is lower than the growth temperature (1400°C) used in the previous two-step process which utilized separate Si- and C-containing reactant sources.[21] Detailed studies on the crystal quality and electronic properties of ß-SiC formed by the HMDS source have not been reported.

2.2.2 β-SiC Grown on 6Hα-SiC Substrate

Development of 6Hα-SiC bulk crystal growth capabilities has spurred interest in its use as a substrate for ß-SiC epitaxial growth. There are two major advantages using 6Hα-SiC as substrates. First, the lattice parameters are identical at the interface $(111)_{\beta\text{-SiC}}/(0001)_{6H\alpha\text{-SiC}}$, see Table 2.4. Secondly, 6Hα-SiC has a similar linear thermal expansion coefficient as the β-SiC. Therefore, lattice mismatch and thermally induced stress between the epilayer and substrate will be minimized.

Single crystal β-SiC was produced on the basal plane of 6Hα-SiC substrate (either (0001) Si face or $(000\bar{1})$ C face).[29] Compared to β-SiC grown on Si substrates, the epitaxial thin films of β-SiC produced on 6Hα-SiC substrates contained much lower density of defects such as misfit dislocations or stacking faults. Unfortunately, double positioning boundaries (DPBs) were formed in the β-SiC on 6Hα-SiC.[31-33] The occurrence of DPBs arises because of the "multiple positioning " during deposition of cubic β-SiC. The formation mechanism of a DPB is described in section 2.3.3. Since a DPB is an incoherent twin boundary, it contains a high internal energy. Therefore, the presence of DPBs seriously degrades the electronic properties of ß-SiC and makes the development of lateral integrated circuits highly unlikely.

Elimination of DPBs was attempted by inclining the 6Hα-SiC substrate, as it was performed by using off-axis Si substrates to eliminate APBs in β-SiC.[21,25] However, experimental evidence showed that 6Hα-SiC substrates with a small angle off the basal plane (0001) resulted in the formation of homoepitaxial growth of 6Hα-SiC instead of ß-SiC.[30,75,76] To create an inclined 6Hα-SiC substrate surface, patterning was performed to form 1 $(mm)^2$ die size areas.[77,78] The CVD epitaxial thin films grown on the patterned 6Hα-SiC substrate contained mixed polytypes of β-SiC and 6Hα-SiC domains. The distribution of β-SiC was random and uncontrollable. Therefore, high quality β-SiC epitaxial thin films can not be produced on 6Hα-SiC substrates using the present CVD process.

2.2.3 β-SiC Grown on TiC_x Substrate

Titanium carbide was first chosen as a substrate material by Parsons et al.[79] This choice was based on the consideration of several properties such as crystal structure, lattice parameter, thermal expansion coefficient, and chemical stability.

Titanium carbide has a cubic crystal structure which enables the epitaxial growth of cubic β-SiC. The phase diagram of the Ti-C system is shown in Fig.2.2.[58] From the phase diagram, it can be seen that the TiC single phase has an extraordinarily wide composition range, and therefore, TiC_x (x is less than 1) is used to denote the titanium carbide. The lattice parameter of TiC_x varies with the C/Ti ratio x. The minimum lattice mismatch between TiC_x (a = 0.4331 nm, when x = 0.85) and ß-SiC (a = 0.4358 nm) is about 0.6% (see Table 2.4).

The thermal expansion coefficient of TiC_x is higher than that of β-SiC over the temperature range of interest (from room temperature to CVD deposition temperature below 2000°K).[35] The difference between the thermal coefficient of the two materials is about 0% at 200°K to about 50% at 2000°K. The higher thermal expansion coefficient of TiC_x will result in compressive loading on the epilayer, which reduces the chances of forming microcracks and pinholes in β-SiC.

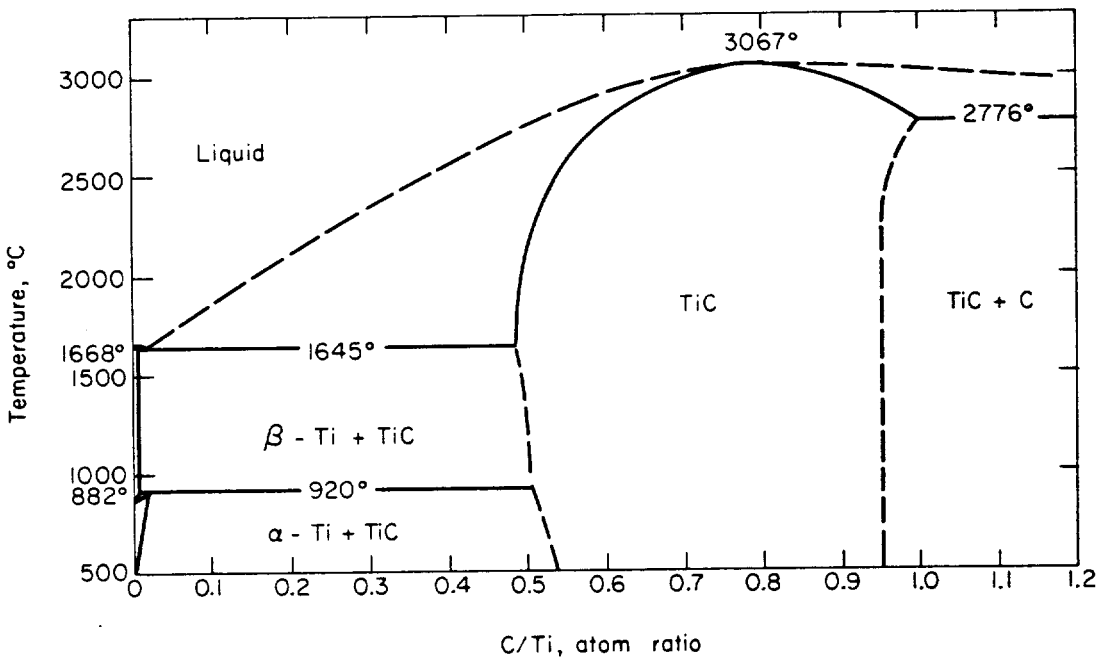

Fig.2.2 Phase diagram of Ti-C system.

The TiC_x does not decompose or undergo phase transformations in the temperature range of β-SiC epitaxial growth. Therefore, TiC_x will exhibit minimal surface reactivity with the chemical environment in the CVD reaction chamber.

An additional advantage of TiC_x as a substrate for ß-SiC epitaxial growth is that it forms an almost ideal Schottky interface with β-SiC. The barrier height is controlled by the work function difference between TiC_x (< 3.0 ev) and ß-SiC (~ 4.5 ev).[36] This is extremely beneficial for forming ohmic contacts between n-type β-SiC and TiC_x.

Previous studies showed that single crystal β-SiC can be successfully obtained on TiC_x substrates.[34-36,80-85] Compared to thin films grown on Si and 6Hα-SiC substrates, β-SiC grown on TiC_x has lower defect densities and a smoother surface. Most importantly, controllable and repeatable β-SiC epitaxial thin films have been produced on TiC_x substrates by using a single reactant source 1,2-disilylethane (DSE or $Si_2C_2H_{10}$), which provides equal numbers of Si and C atoms.[86,87]

However, to date, high quality β-SiC epilayers with suitably low defect densities have not been obtained. One of the reasons for this is that the TiC_x available at the present time is nonstoichiometric and contains substructures. The development of TiC single crystal growth technique is still under way. Improvement of the TiC_x crystal quality is necessary for it to be considered as a suitable substrate material for epitaxial growth of semiconductor material β-SiC.

2.3 Defects in Epitaxial Thin Films

As discussed in the previous section, defects were formed in the β-SiC epilayers grown on Si, 6Hα-SiC, or TiC_x substrates. The formation of defects in epitaxial films have been studied for a long time, it has been found that higher densities of defects are usually contained in epitaxial deposits than in crystals grown by other methods. This is due to the constraints imposed by the substrate. Some configurations of defects seem to be specific to epitaxial films. The formation of defects is certainly associated with the

nucleation or initial growth mode of the thin film, it is relevant to briefly review some of the prominent features of epitaxial growth mechanisms before considering the formation of crystalline defects.

2.3.1 Nucleation Mode

The nucleation mode of an epitaxial film is strongly governed by the bonding between the deposit and the substrate. It is convenient to employ surface and interfacial free energies to describe the initial stage of deposition.[88] If the deposit is in the form of a hemispherical cap, then, at equilibrium,

$$\sigma_{sv} = \sigma_{xs} + \sigma_{xv}\cos\theta \tag{2.3}$$

where σ_{sv}, σ_{xv}, and σ_{xv} are the free energies of the substrate-vapor, deposit-substrate, and deposit-vapor interfaces, respectively, and θ is the contact angle.

Three types of nucleation modes can be formed and are descried in Figure 2.3. First, if the contact angle $\theta = 0$, which means the deposit "wets" the substrate, equ.(2.3) has the relation: $\sigma_{sv} = \sigma_{xs} + \sigma_{xv}$. In this case, it is to be expected that growth will occur in a *layer-by-layer mode*, as shown in Fig.2.3(a). When $\sigma_{xs} + \sigma_{xv} > \sigma_{sv}$, θ is finite; the deposit forms by the nucleation of discrete particles that grow three dimensionally (see Fig.2.3(b)); and eventually these particles agglomerate into a continuous film. This is called *island mode growth*. As θ increases, the bonding between substrate and deposit becomes progressively weaker than the cohesive bonding between the deposit particles. The third category corresponds to $\sigma_{xs} + \sigma_{xv} < \sigma_{sv}$, and here the deposit substrate bonding is stronger than that within the deposit. Initially, the deposit grows as strongly bound layers, on top of which discrete nuclei may form at a later stage, as depicted in Fig.2.3(c).

The most closely studied mode of thin-film formation systems occurs in the second case, the *island mode* of the moderate-to-weak bonding situation ($\theta > 0$). Here the deposited atoms (or molecules) initially are thermally equilibrated with the substrate

on which they diffuse and interact to form polyatomic clusters (nuclei). The nuclei continue to grow, because of their nonuniform spatial distribution on the substrate, and eventually agglomerate when they merge together. The mode of epitaxial growth plays an important role in determining defect structures of the subsequent epitaxial deposits.

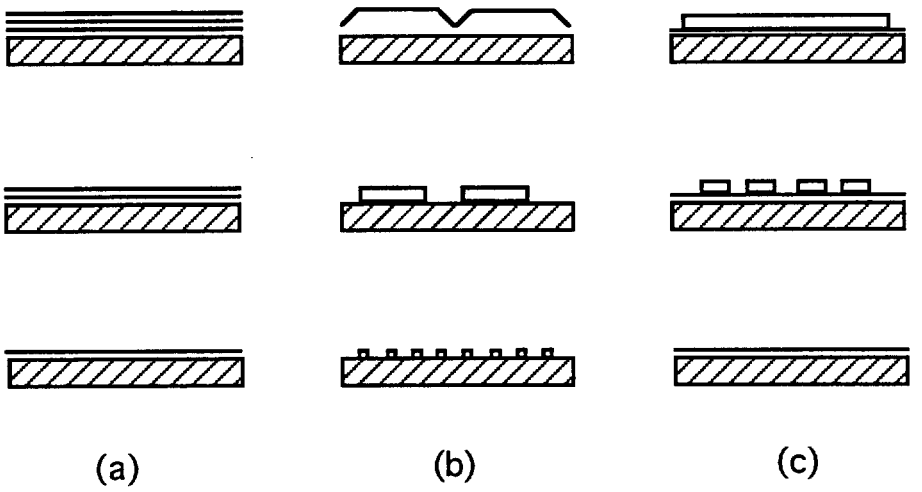

Fig.2.3 Three nucleation modes of epitaxial growth.

2.3.2 Relation Between Nucleation Mode and Epitaxial Growth

The relation between nucleation process and the occurrence of epitaxial growth is not yet completely clear. In the *island growth* case, there has been a strong move in recent years, to the belief that epitaxy is a postnucleation phenomenon.[89,90] Clusters can reorient themselves through rotation and migration processes and move over on the substrate. This type of movement has been reported by many authors.[90-92] Motois et al.[91] observed that in the case of Au-KCl (100) growing at low temperature (20°C), the (100) gold orientation resulted from the coalescence of (111) oriented islands which migrated into each other and rotated to (100) orientation during the subsequent annealing at $T \geq 200°C$. There is little doubt that cluster rotation and migration processes are important in establishing epitaxial orientation. However, some controversy remains as to whether the migration-coalescence processes are necessary, or even occur, to establish epitaxy in a high temperature deposition. All the experiments performed by the aforementioned authors were conducted in low deposition temperatures and followed by annealing,[90-92] which leads to some doubt.

For *layer-by-layer* growth, indications are that epitaxy results in almost all circumstances providing the substrate surface is clean.[89,93] Generally, it is believed that the substrate has a very strong influence on the form of the thin film produced.[89] The growing film has little option but to choose the best orientation for epitaxial growth. The initial layers are more or less forced to be related epitaxially to the substrate. Epitaxy can be "destroyed" by influencing the growth process in a later stage with impurities or defects. Joyce and co-workers[94-97] found that a smooth layer-by-layer fashion with no islands present at all in the Si on Si growth was achieved after removal of carbon impurities from the system, although island growth was observed initially. A ultra clean environment is definitely necessary for layer-by-layer growth.

2.3.3 Defect Formation Mechanisms

It is apparent that the constraints imposed by a substrate, and the often highly nonequilibrium conditions under which epitaxial growth is obtained, can both markedly

influence the defect structures formed. The dominant source of imperfections in epitaxial films is misfit between deposit and substrate (and any contaminant that may exist on the substrate). If the misfit is small, the defects arise mainly as a result of coherency loss between substrate and overgrowth.

The common defects formed in a epitaxial film are dislocations, stacking faults, twins, and antiphase boundaries (APBs) which may occur in alloys or compounds. The possibilities for dislocation introduction during epitaxial growth can be attributed to various sources:[98-103]

(1) the extension of substrate defects;
(2) plastic deformation of the thin film, both during growth and subsequent cooling;
(3) the formation of dislocation loops by the aggregation of point defects;
(4) the accommodation of translational and rotational displacements between agglomerating islands that are close to epitaxial orientation.

Among these possibilities, the fourth, dislocation generation due to the accommodation of translational and rotational displacements between agglomerating islands, which is also called "island-misfit' model, has gathered strong experimental support especially from work involving *in-situ* observations of epitaxial growth. This model was confirmed by Jacos et al.[104] in the study of Au films grown on MoS_2. The most striking evidence was obtained by their direct observations of epitaxial growth inside a TEM. It was found that the initial nuclei were defect-free, but when coalescence occurred, dislocations were often found in the composite island.

A stacking fault is a planar defect. The formation of stacking faults in epitaxial deposits have been considered to be associated with the imperfections in the growth system and the fluctuations of growth conditions. The "island-misfit" model is also the most acceptable stacking fault generation mechanism. For example, most of the nuclei grow in the correct relation with respect to the substrate, the stacking sequence above the "a" substrate layer is bcabc... for a fcc deposit. If one nucleus is incorrectly placed it

subsequently grows in the stacking sequence cabcab... . When the incorrect nucleus and the correct nuclei grow together, an outward-growing "triangular" fault is formed. Various suggestions such as oxygen contamination[105] and metallic impurities[106] have been proposed as initiation sites for the cause of the incorrect nuclei, which subsequently cause the formation of stacking faults. The occurrence of stacking faults is also related to the growth conditions performed. The stacking fault density has been observed to vary exponentially with growth temperature, and proportionally with the deposition rate.[88]

Twinning defects can also be formed in epitaxial deposits. In many cases, twins were considered to be generated as a consequence of misfit between coalescing islands, as discussed in dislocation and stacking fault generation mechanisms. A special form of twinning seems to be unique to epitaxial thin film, it is called a "double-positioning boundary (DPB)". This occurs as a result of "multiple positioning", whereby the deposit is oriented in several crystallographically equivalent ways on the substrate. Fig.2.4. illustrates a DPB formed in a fcc epitaxial thin film. One island (phase I) grows in the sequence of bcabca... on top of substrate, another island (phase II) grows in the sequence of cbacba... . The boundary between these two islands is a DPB. As a DPB is an incoherent twin boundary, at which the atomic structure is disordered, it provides a source of high internal energy; the free energy of an incoherent twin boundary is about 2/3 that of a high angle grain boundary.[88]

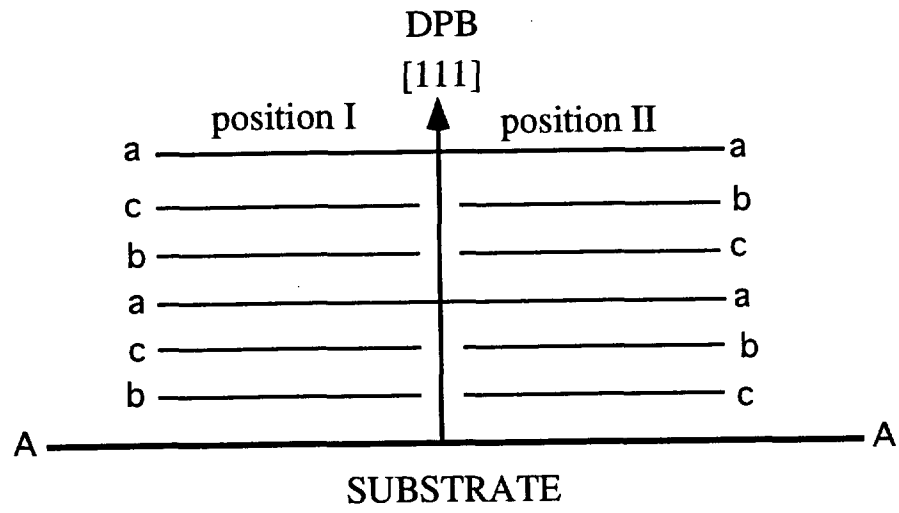

Fig.2.4 Illustration of a double positioning boundary (DPB) due to equivalent stacking sequence ABC... and ACB... in a cubic structure deposit.

If the epitaxial film is a compound, a special type of planar defect can be formed, that is an anti-phase boundary (APB). The formation of APBs arises due to the identity change of atoms at a given lattice point; but there is no atomic stacking change as in a stacking fault. For example, two distinct {111} surfaces can exist that contain either all A or all B atoms in a sphalerite structure compound AB. Holt[107] examined, theoretically, the defect structures in this lattice and showed that two different types of APBs are possible; these are illustrated in Fig.2.5. In Fig.2.5(a), an APB is drawn at which there are equal numbers of wrong A-A and B-B bonds (type I APB), whereas in Fig.2.5(b) and (c) respectively, only wrong A-A and B-B bonds exist (type II APB). The later type of APB is important in that it represents an excess of one class of atom in the crystal; it may be viewed as a thin planar precipitate.

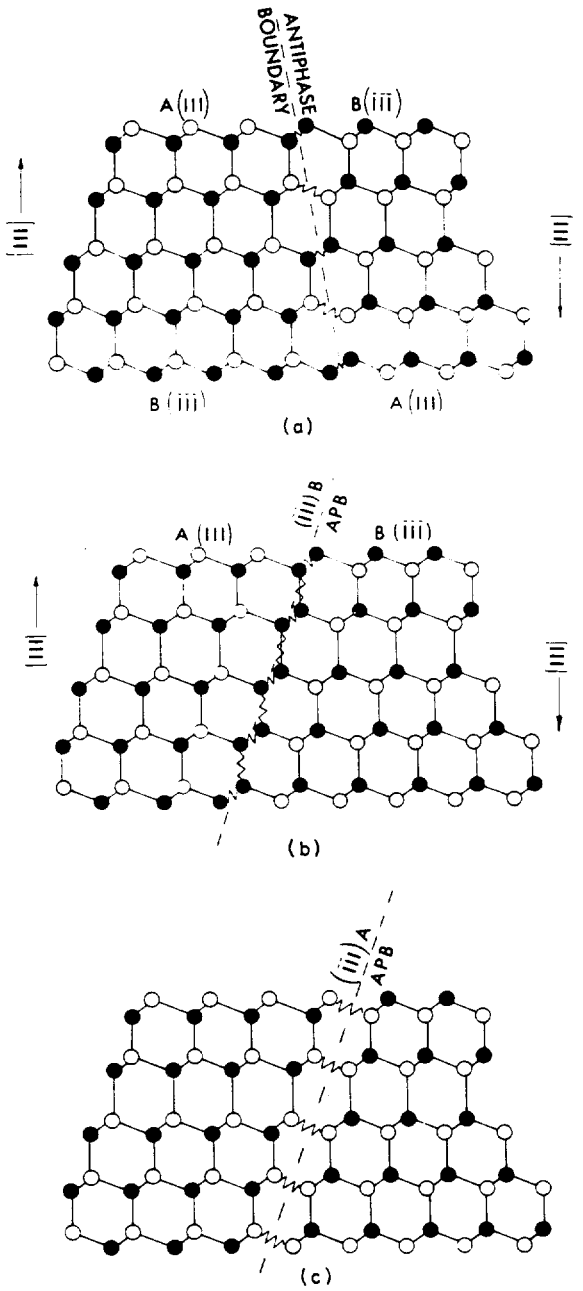

Fig.2.5 Illustration of an antiphase boundary (APB) formed in a compound AB: (a) type I APB with equal number wrong A-A and B-B bonds, (b) type II APB with only wrong A-A, and (c) B-B bonds.

2.4 Heteroepitaxial Structures

2.4.1 Mismatch Induced Strains

Heteroepitaxy refers to epitaxial growth of dissimilar materials on each other. There are two types of heteroepitaxial structures, lattice matched and mismatched. A lattice mismatched heterostructure can be represented by the schematic cross section shown in Fig.2.6. Both the substrate and the film have a cubic structure, with lattice constant a_s and a_f, respectively. The epitaxial layer is either unstrained (Fig.2.6(a)) or strained (Fig.2.6(b)).[108] The former case is usually called relaxed, where the film and the substrate maintain their lattice constants and cubic structures. Therefore, there cannot be an interfacial alignment on an atomic basis; the mismatch is taken up by defects, called "misfit dislocations". The misfit (f) between substrate and film is defined as:

$$f=\frac{|a_s-a_f|}{a_s} \tag{2.4}$$

Misfit dislocations may be represented as edge dislocations uniformly spaced along the interface. The average spacing s of misfit dislocations depends on the mismatch f and is of the order of a_s/f. For f = 1% and a_s = 0.4 nm, s = 40 nm, that is there is one misfit dislocation every 40 nm on the interface plane.

For a strained system, which is also called pseudomorphic growth, the lattice constant of the film in the plane of the interface is equal to that of the substrate. A cubic cell is then distorted into a tetragonal cell. The in-plane strain is defined as:

$$\epsilon_{\parallel} = \frac{(a_{f\parallel} - a_f)}{a_f} \tag{2.5}$$

where $a_{f\parallel}$ is the parallel-to-the-interface or in-plane lattice constant of the deposited film material, and a_f is the lattice constant of the film material in the bulk or unstrained state. The in-plane strain is often called the coherency strain. The strain in the direction perpendicular to the interface is defined as:

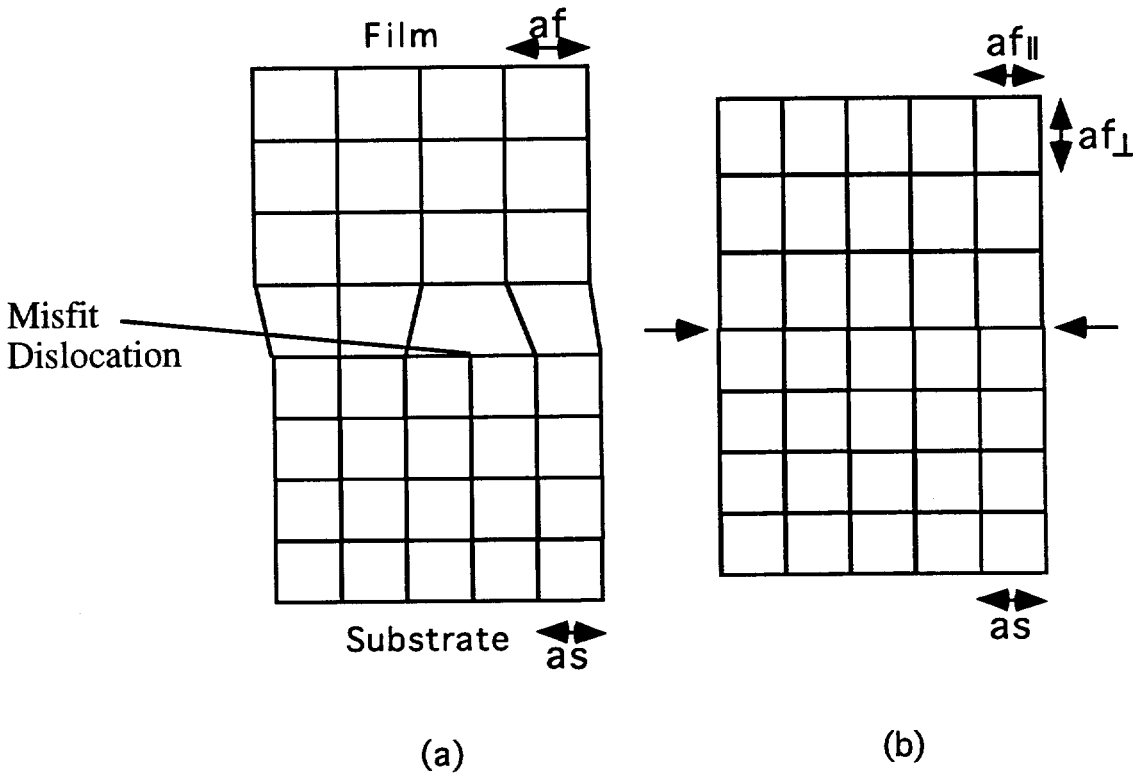

Fig.2.6 Heteroepitaxial growth under (a) relaxed and (b) strained conditions.

$$\epsilon_{\perp} = \frac{(a_{f\perp} - a_f)}{a_f} \tag{2.6}$$

where $a_{f\perp}$ is the lattice constant perpendicular to the interface.

2.4.2. Critical Thickness of Pseudomorphic Growth

For a small lattice mismatched heteroepitaxial structure, pseudomorphic growth is possible when the film thickness is less than a critical value. That is, the deposit grows under strained condition and therefore, the lattice constant of the film in the plane of the interface precisely matches that of the substrate.

The critical thickness h_c for pseudomorphic growth is derived by considering the thickness dependence of the strain energy and the misfit dislocation energy, and by minimizing the total energy.[108-120] This model was developed by Matthews,[109-113] based on the original model by van der Merwe.[114-116] A number of reviews of the critical thickness models have recently been published.[117-120] The mechanism assumed in the models is that glissile dislocations, threading from the film/substrate hetero-interface to the free surface, may move due to the forces caused by the lattice-mismatch-induced strain in the film. Such a dislocation could glide only on an inclined slip plane, and so would leave a misfit dislocation with an inclined Burgers vector. The glide force depends on the film thickness. As the threading dislocation glides, a restoring force will be introduced due to the energy of the new misfit dislocation core created. The critical thickness can be approximated from the balance of these two forces.

In an elastic approximation, the strain energy of a thin film with a thickness h is given by Cahn[121] as

$$E_{\epsilon} = B\epsilon^2 h \tag{2.7}$$

where ϵ is the in-plane strain of the film ($\epsilon = \epsilon_{\parallel}$). The constant B is a complicated function of the elastic constants of the film material.[108]

The energy density of misfit dislocations is given by

$$E_{\perp} = \frac{\mu_f b}{2\pi(1-\nu)} (f - \epsilon_l) \left[\ln\left(\frac{h}{b}\right) + 1\right] \tag{2.8}$$

where μ_f is the shear modules, ν is the Poisson's ratio, and b is the Burger's vector.

The combined energy of strain energy and dislocation energy is then given by

$$E_{tot} = \epsilon_l^2 Bh + \frac{\mu_f b}{2\pi(1-\nu)} (f - \epsilon_l) \left[\ln\left(\frac{h}{b}\right) + 1\right] \tag{2.9}$$

The strain that minimizes the total energy is obtained by setting $dE_{tot}/d\epsilon_l = 0$, to yield the critical strain, ϵ^*. Then

$$\epsilon^* = \frac{\mu_f b}{4\pi(1-\nu)hB} \left[\ln\left(\frac{h}{b}\right) + 1\right] \tag{2.10}$$

where, constant B is given for an elastically isotropic film as

$$B = 2\mu_f \frac{(1 + \nu)}{(1 - \nu)} \tag{2.11}$$

Since the largest possible value of ϵ^* is the misfit f, if the value of ϵ^* is equal to f, the film will be strained to precisely match the substrate. Of course, ϵ^* can never be greater than f. The film thickness h_c, at which it becomes energetically possible for the first misfit dislocation to be made, is obtained by setting $\epsilon^* = f$. Then this critical thickness is given by

$$h_c = \frac{b}{8\pi (1 + \nu) f} \left[\ln\left(\frac{h_c}{b}\right) + 1\right] \tag{2.12}$$

As discussed, the derivation of the critical thickness relies on the energy balance between strain energy and dislocation energy. Since the contribution to the dislocation energy from the heavily disordered dislocation core is somewhat uncertain, it follows that the formula for the critical thickness, eq.(2.12), should be considered only as an estimate.

2.5 Research Plans

The potential applications of β-SiC as a high performance semiconductor material have been recognized for a long time. However, the superior electrical properties of β-SiC has not been demonstrated experimentally due to the lack of high quality single crystal β-SiC.

The peritectic phase transformation nature of SiC makes it very unlikely to growth SiC from solution. The metastable property of β-SiC relative to α-SiC determined that growth of β-SiC needs to be conducted at temperatures below 2000°C. Epitaxial growth of β-SiC using CVD processes has been shown as a successful approach. The three substrate materials used for β-SiC growth are Si, 6Hα-SiC, and TiC_x. Beta-SiC grown on Si substrates contained large amount of defects, such as, dislocations, stacking faults, twins, and high internal energy defect APBs. There is a little hope of reducing the concentration of these defects to values suitable for semiconductor applications, due to the large lattice mismatch (20%) between β-SiC and Si. Single crystal β-SiC produced on the basal plane of 6Hα-SiC substrates contained much lower density of defects compared to β-SiC films grown on Si substrates. Unfortunately, DPBs were formed in the β-SiC thin films. The presence of DPBs seriously degrades the electronic properties of β-SiC and makes the development of lateral integrated circuits highly unlikely.

Titanium carbide was chosen as the substrate material because of its small lattice mismatch with β-SiC (0.6%), cubic crystal structure, and excellent chemical stability. However, TiC single crystal growth technique is still not fully developed, the available titanium carbide crystals are far from perfect. First, the TiC is not stoichiometric with carbon deficiency, and thus referred as TiC_x ($x < 1$), secondly, these TiC_x crystals contain many substructures. These substructures will be replicated into β-SiC thin films during epitaxial growth. Therefore, it is necessary to remove these substructures from TiC_x crystals to make them suitable substrates for β-SiC growth.

The intentions of this research were from three aspects: (1) to characterize the defect structures especially the subgrain boundaries in as-grown TiC_x, and then to

improve the TiC_x crystal quality through an annealing process; (2) to synthesize β-SiC on the improved TiC_x substrates. The growth conditions will be optimized based on the β-SiC surface morphology and crystallinity. Defect structures formed in β-SiC will be examined using TEM in cross-section, by considering the effect of growth conditions and the TiC_x substrate orientations; (3) to synthesize TiC epitaxial films on β-SiC and 6Hα-SiC substrates. This approach is designed to obtain a stoichiometric TiC with suitably low density of defects, and therefore, the TiC thin film can be used as a substrate for the further growth of β-SiC. Another desired benefit of this approach is that TiC can form ideal ohmic contacts with n-type β-SiC or 6Hα-SiC and rectifying contacts with p-type β-SiC or 6Hα-SiC.

There is no doubt that the results of this study will provide significant information on the understanding of defect formation mechanisms associated with β-SiC grown on TiC_x, on the semimetal/semiconductor (TiC/SiC) interface structures, and on a further exploring of β-SiC synthesis on stoichiometric TiC thin films. Therefore, this study will be a significant contribution to obtain a high performance β-SiC semiconductor material.

Chapter 3

DEFECT CHARACTERIZATION IN SINGLE CRYSTAL TiC_x

3.1 Introduction

Several properties of single crystal titanium carbide (TiC_x) make its use as a substrate for nucleation and growth of ß-SiC epilayers potentially advantageous.[36,79] These advantages are based on its crystal structure, lattice parameter, thermal expansion coefficient, and chemical stability. Titanium carbide has a rock salt crystal structure which can exist, as a single phase, within an extraordinarily wide composition range, as shown in phase diagram Fig.2.2.[58] The minimum lattice parameter mismatch between TiC_x and ß-SiC (a = 4.358Å) is about 0.6% when x=0.86 (a_{TiC}=4.331Å), see Table 2.4. The thermal expansion coefficient of TiC_x is greater than that of ß-SiC; thus, ß-SiC epilayers grown on TiC_x are under compressive strain, which reduces the chances of formation of microcracks and pinholes in ß-SiC.[36] The melting temperature of TiC_x is about 3100°C,[58] and it does not decompose or undergo phase transformations in any temperature range of interest for epitaxial growth of ß-SiC.

At the present time, single crystal TiC is not available commercially, and the crystal growth technique is still under development. Titanium carbide has a very high melting point (about 3100°C),[58] at this high temperature there is no suitable crucible material which does not react or contaminate the melt. The High-Pressure Floating-Zone (HPFZ) method is one of the few options used for titanium carbide single crystal growth.[122-125] The problem with this method is that it tends to produce non-stoichiometric composition TiC_x (x = C/Ti, x is less than 1).

The TiC_x crystals grown from HPFZ are not single crystal strictly speaking. Each wafer contains several grains with size range from ~ 5 mm^2 to ~ 1 cm^2. Device fabrication can be achieved within a grain as long as the grain size is larger than the device structure. However, the TiC_x crystals are not perfect even within each grain, pits can be observed after polishing in naked eyes. These pits are the reflection of defects present in TiC_x.

The predominant defects in single crystal TiC_x are sub-boundaries. The sub-boundaries are thought to be due to thermal stress caused by non-uniform temperature gradients at the solid-liquid interface and across the solidified crystal during high pressure float zone (HPFZ) growth.[126] These sub-boundaries in TiC_x can be reproduced in ß-SiC epilayers, which will provide electrical shorting paths for current leakage. Therefore, they are a major obstacle to TiC_x as a substrate for epitaxial growth of device quality ß-SiC. Development of TiC_x single crystals which can serve as substrates for epitaxial growth of device quality ß-SiC, requires the removal of these sub-boundaries from TiC_x.

Planar defects, associated with the sub-boundaries in TiC_x, are thought to be due primarily to impurities, such as boron.[126-133] The apparent stacking fault defects observed by Williams,[128,129] were subsequently identified as platelet TiB_2 precipitates.[126,131-133] Equilibrium stacking faults are not anticipated in TiC_x, because of its high stacking fault energy.[130] The high stacking fault energy of TiC_x is explained by the d-band electron structure model.[131] In this model, the magnitude of the stacking fault energy is related to the d-band filling; where, metals with a filled d-band have a lower stacking fault energy than those with partially filled bands. Titanium carbide has a d-band structure identical with that of the first long-period transition metals.

This chapter describes the details of the: (1) characterizations of defect structures formed in the as-grown TiC_x crystals using TEM, and (2) removal of the sub-boundaries from TiC_x single crystals through high temperature annealing.

3.2. Experiment

The TiC_x ingot was grown by high pressure float zone (HPFZ) method. Slices for TEM sample preparation (0.9 mm thick) were cut - parallel to the ingot growth axis - from 10 mm diameter x 1.0 mm thick TiC_x wafers, using a Buehler ISOMET low speed saw. Each slice was mounted on a supportive cylinder and prepared from two sides.

The first side was lapped with 15 μm diamond paste and polished with 6 μm and 1 μm diamond paste. The polished surface was laminated to a molybdenum (Mo) washer for mechanical support. The sample was then turned over and the second side was lapped. The thickness of the slice was reduced to 50 μm using 15 μm diamond paste, and to a thickness of 30 μm using 6 μm diamond paste. The second surface was then polished and dimpled with 1 μm diamond paste, until the thickness at the center of the TEM sample was 15-20 μm. A Mo washer was laminated to this side. Finally, the sample was ion-milled from both sides, simultaneously, until perforation was observed.

A Hitachi-800 TEM (operated at 200 kV) was used to examine defects in as-grown TiC_x. Two-beam conditions and trace analysis methods were used to characterize the defects.[134,135] Two-beam conditions were obtained by tilting the TEM sample, such that the image was formed by the transmitted beam plus one diffracted beam. The (hkl) plane which produced the diffracted beam is referred to as the reflecting plane, and the plane normal (g) is called the operating reflection. Trace analysis methods were used by combining the crystallographic and orientation information provided by selected area diffraction patterns with the geometry of the electron micrograph. From this analysis, some important crystallographic details of the defects, such as the habit planes, the direction of the dislocation lines, can be deduced.

The invisibility criteria of dislocations and stacking fault fringes were used to analyze the defects.[135] It should be pointed out that the invisibility criteria of $\mathbf{g} \cdot \mathbf{b} = 0$ was used for a unit dislocation, both a screw and an edge dislocation. There is no problem for a screw dislocation using this criteria, however, it is known that an edge dislocation has a complete invisibility when both $\mathbf{g} \cdot \mathbf{b} = 0$ and $\mathbf{g} \cdot \mathbf{b} \times \mathbf{u} = 0$; where,

b is the Burgers vector and u is the dislocation line direction. In practice, $g \cdot b = 0$ can be used as the invisibility criteria; because the residual contrast was very faint under this condition even if $g \cdot b \times u$ is not zero.

The stacking fault extrinsic/intrinsic nature was determined based on the direction of the operating reflection g vector used relative to the out-fringe formed by the fault.[135] If the origin of the g vector is placed at the center of the fault in a DF image, g points away from the light out fringe if the fault is extrinsic and towards it if it is intrinsic for all {200}, {222}, and {440} (type A) reflections. If the operating reflection is of type B {400}, {111}, {220}, the reverse is true.

The as-grown TiC_x wafers were annealed at 2300°C for 24 hours in Ar. Heating of the TiC_x wafers, sandwiched between 2 graphite discs, was accomplished by passing a DC current through a graphite block, as shown in Fig.3.1. The temperature was read from the edge of the wafer with a Leed and Northrup disappearing filament optical pyrometer. The temperature, observed through a process chamber window, was not corrected for emissivity. The effect of annealing on the crystallinity and sub-boundaries in TiC_x was examined by comparing the X-ray rocking curves obtained before and after annealing. The X-ray spot size was 2 mm x 1 mm for all measurements.

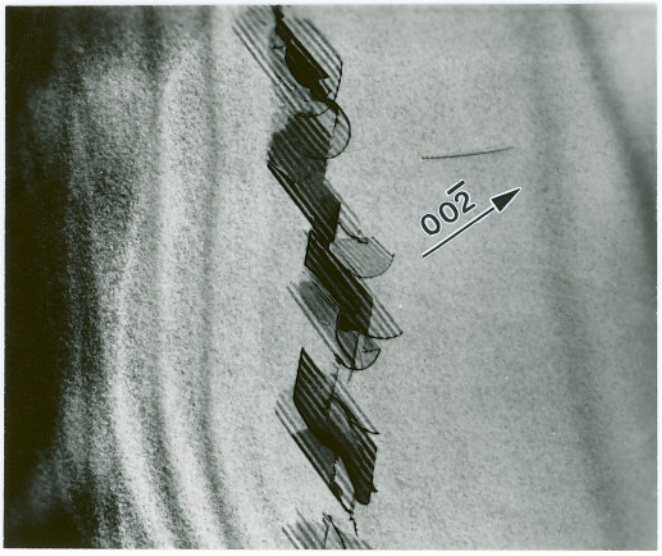

(a) 1 μm

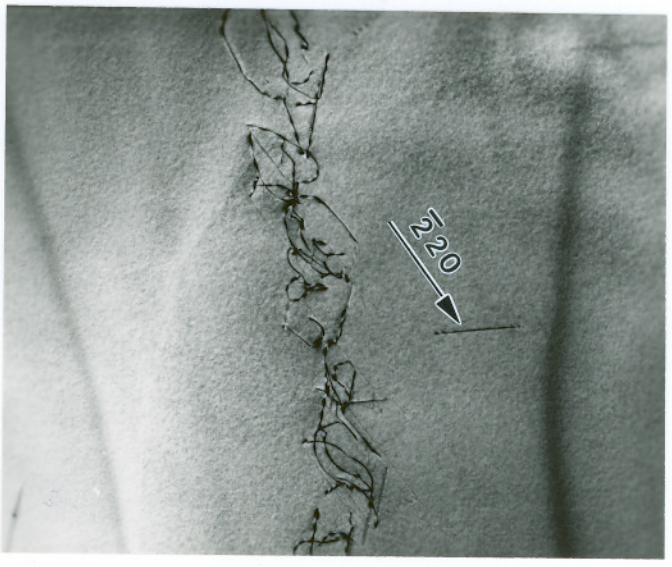

(b) 1 μm

Fig.3.2 A sub-boundary consisted of wide-extended, fault-like planar defects in the as-grown TiC_x: (a) g = [00$\bar{2}$], (b) g = [$\bar{2}$20].

A sub-boundary can also be formed by two sets of these fault-like planar defects, as shown in Fig.3.3. The planar defect set A was composed of very fine fringes, which were almost invisible at the low magnification. Fringe patterns of set B were clearly seen in Fig.3.3(a) when using g = [002]. The TEM images of Fig.3.3(a) and (b) clearly show the cross slip of partial dislocations which bound the fault-like planar defects.

(b) dislocation arrays

Two merging sub-boundaries are shown in Fig.3.4(a). Each of them is formed by an edge dislocation array. The two sets of dislocations are labeled as A and B with Burgers vectors b_A and b_B, respectively. The invisibilities of the two dislocation arrays and the $g \cdot b$ values under various operative reflections are listed in Table 3.1. From the values listed in Table 3.1, the Burgers vector of the two dislocation arrays are $b_A = \frac{1}{2}[0\bar{1}1]$ and $b_B = \frac{1}{2}[011]$ using the $g \cdot b = 0$ dislocation invisible criteria. The parallel dislocation array is the result of pure symmetrical tilted sub-boundaries,[136] each dislocation of the dislocation arrays is an edge type dislocation, the boundary can be illustrated as Fig.3.4(b). The dislocation directions (u), the sub-boundary plane, and the dislocation slip plane were determined by the combination of the geometry and trace analysis, and listed in Table 3.2.

(c) dislocation networks

Fig.3.5(a), (b) and (c) are the BF images of a dislocation network under g = $[00\bar{2}]$, g = $[\bar{1}1\bar{1}]$, and B = [110], respectively. A change in the dislocation visibility with respect to the g vectors can be observed in the images Fig.3.5(a)-(c). In Fig.3.5(c), which was taken with the electron beam along [110], triangular planar defects with fault-fringes were observed at the dislocation nodes of the sub-boundary network.

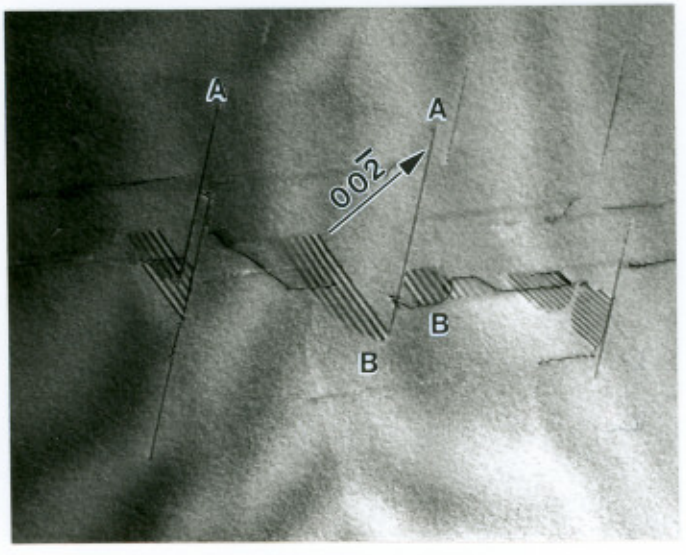

(a) 1 μm

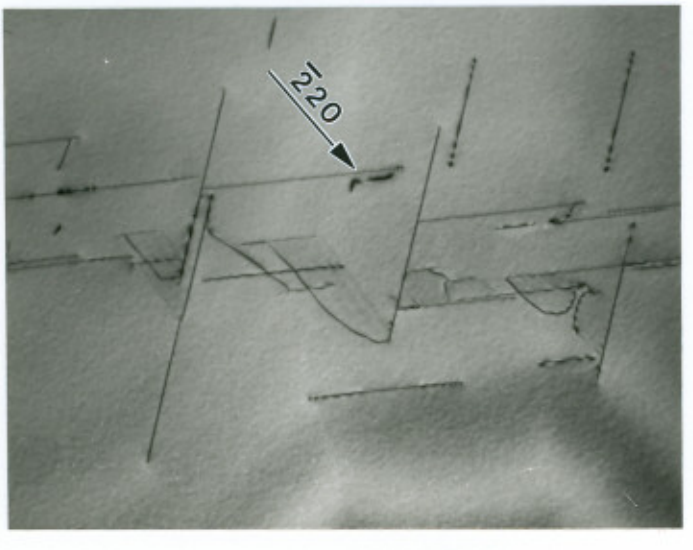

(b) 1 μm

Fig.3.3 A sub-boundary consisting of two sets of fault-like planar defects.

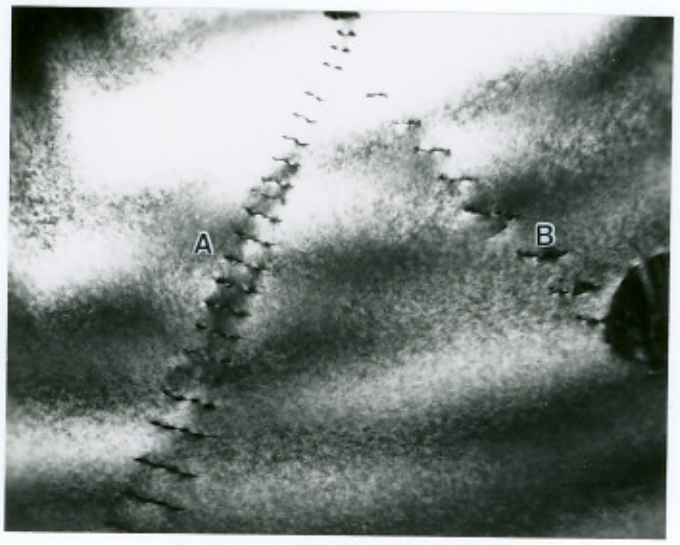

(a) 0.2 μm

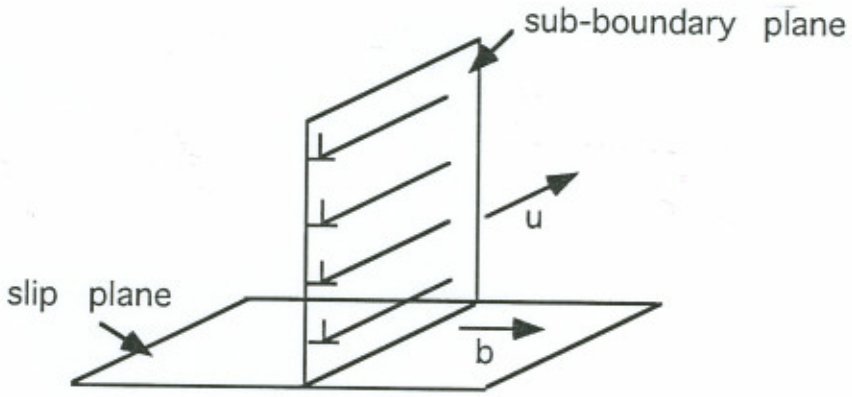

(b)

Fig.3.4 (a) Two symmetrical pure tilted sub-boundaries consisting of parallel edge dislocation arrays A and B, respectively, (b) illustration of the geometric relation between the Burgers vector, the dislocation direction, the sub-boundary plane, and the dislocation slip plane.

Table 3.1 Visibility of Dislocation Arrays A and B

g	g · b values and dislocation visibility							
	½[101]	½[011]	½[110]	½[1$\bar{1}$0]	½[0$\bar{1}$1]	½[$\bar{1}$01]	A	B
1$\bar{1}\bar{1}$	0	-1	0	1	0	-1	no	yes
$\bar{1}$1$\bar{1}$	-1	0	0	-1	-1	0	yes	no
00$\bar{2}$	-1	-1	0	0	-1	-1	yes	yes
$\bar{2}$20	-1	1	0	-2	-1	1	yes	yes
$\bar{1}$1$\bar{3}$	1	2	0	-1	1	2	yes	yes
2$\bar{4}$2	2	-1	3	1	3	0	yes	yes
$\bar{2}$02	0	1	-1	-1	1	2	yes	yes

Table 3.2 Important Parameters of the Symmetrical Tilted Sub-boundaries A and B in Fig.3.4

Dislocation	Burgers vector	boundary plane	direction	slip plane
A	½[0$\bar{1}$1]	(0$\bar{1}$1)	[$\bar{2}$11]	(111)
B	½[011]	(011)	[2$\bar{1}$1]	(11$\bar{1}$)

A third set of unit dislocations, not visible in Fig.3.5(a) and (b) under two-beam conditions, was observed in Fig.3.5(c). The three sets of unit dislocations (A, B, and F) and the three sets of Shockley partial dislocations (C, D, and E) which bound the triangular planar defects, are illustrated in Fig.3.5(d).

By imposing the dislocation invisibility criteria of $g \cdot b = 0$, the Burgers vectors of the three sets of unit dislocations, A, B and F, are ½[101], ½[011], and ½[110], respectively. The habit plane of the triangular defects was determined to be γ-(11$\bar{1}$) from trace analysis. Therefore, the Burgers vector of dislocation F does not lie on this γ-(11$\bar{1}$) habit plane. This set of dislocation F did not dissociate, from Fig.3.5(c).

The three possible Burgers vectors of Shockley partial dislocations on a γ-(11$\bar{1}$) plane can be determined from Thompson's tetrahedron net,[137] which shows all the unit dislocations and partials dislocations existing in a fcc crystal. The dislocation A and B (with b_A = ½[101] and b_B = ½[011]) can have dissociation reactions: Aγ + γD = A and Bγ + γD = B. Using the dislocation nodal sum rule, the dislocations illustrated in Fig.3.5(d) have relations: C + D = A and E + D = B. Therefore, the Burgers vectors of the three partial dislocations C, D and E are b_C = 1/6[2$\bar{1}$1], b_D = 1/6[112] and b_E = 1/6[$\bar{1}$21], respectively. The values of the Burgers vectors (b_{C-E}) obtained above were consistent with the invisibility criterion of $g \cdot b_p = 0$ or $g \cdot b_p = 1/3$, for a Shockley partial dislocation.[148] The Burgers vectors of the six dislocations and the habit plane of the triangular planar defects are listed in Table 3.3.

Table 3.3 Burgers Vectors of the Dislocation Network and the Habit Plane of the Triangular Planar Defects in Fig.3.5

A	B	C	D	E	F	habit plane
1/2[101]	1/2[011]	1/6[2$\bar{1}$1]	1/6[112]	1/6[$\bar{1}$21]	1/2[110]	γ-(11$\bar{1}$)

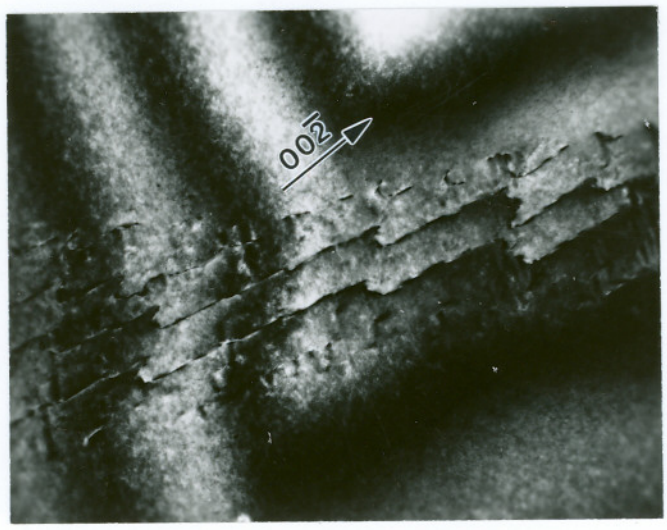

(a) 0.2 μm

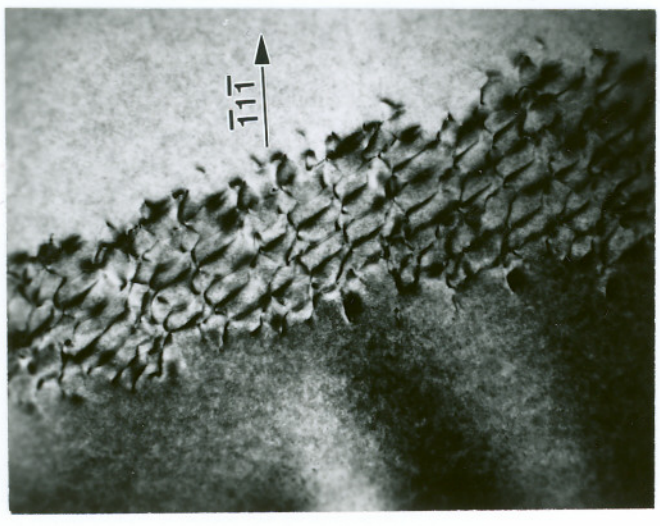

(b) 0.2 μm

Fig.3.5 BF images of a sub-boundary dislocation network under different observation conditions: (a) g = $[00\bar{2}]$, (b) g = $[\bar{1}1\bar{1}]$, (c) electron beam parallels to [110], (d) illustration of image (c).

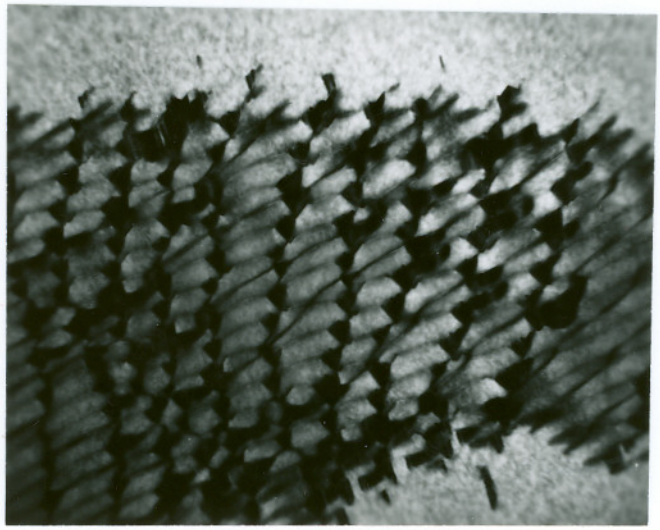

(c) 0.2 μm

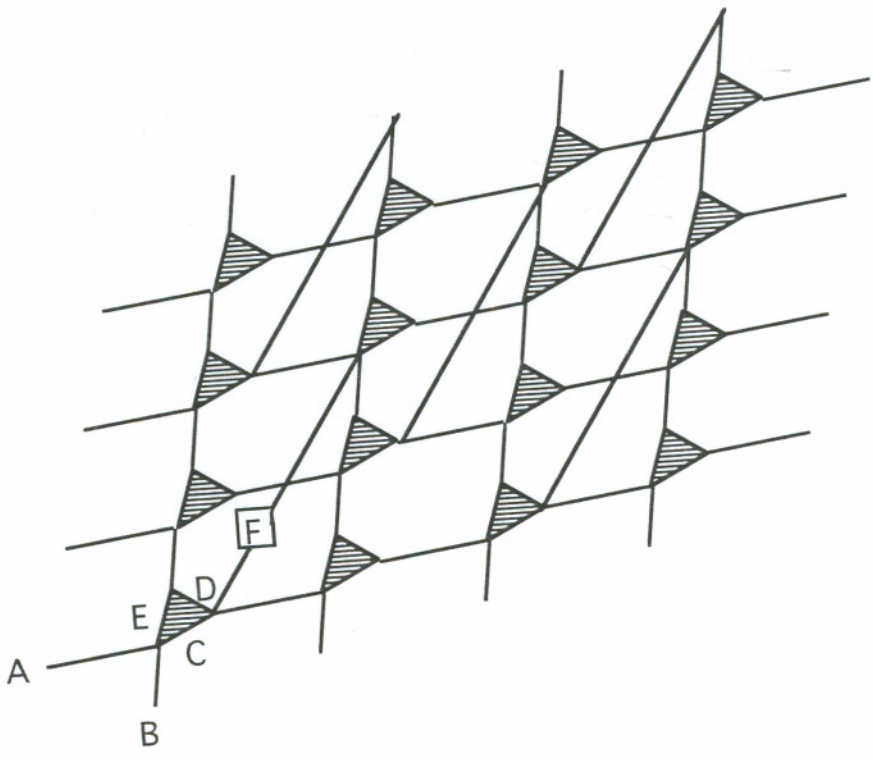

(d)

Fig.3.5 Continued.

These dislocation network structures are very common in the as-grown TiC_x crystals. Fig.3.6(a)-(d) show another this type of sub-boundaries consisted of two sets of unit dislocations, obtained using $g=[1\bar{1}\bar{1}]$, $[00\bar{2}]$, $[\bar{1}1\bar{3}]$, and $[\bar{1}\bar{1}1]$, respectively. The dislocation dissociations or knitings can be seen clearly in Fig.3.6(c) when $g=[\bar{1}1\bar{3}]$, where the three partial dislocations were formed at the dislocation nodal sites.

This type of fault-like defect is similar to that reported by Venable[131-133] and Chien[126], who identified that the formation of stacking fault like defects in TiC_x were due primarily to impurities, such as boron. Equilibrium stacking faults are not anticipated in TiC_x, because of its high stacking fault energy.[131] The fault-like defects in titanium carbide was first observed by William,[128-129] and identified to be related to boron impurities by Venables.[131-133] In a recent report, this type of defects was observed in the high pressure float-zone grown TiC_x crystals,[126] and were identified as platelet TiB_2 precipitates using high resolution electron microscopy techniques.

3.3.1.2 Inter-subgrain Planar Defects

Planar defects formed within the subgrains were observed in TiC_x, as shown in Fig.3.7(a) and (b). This is the first reported observation of inter-subgrain planar defects, to our knowledge. Fig.3.7(a) is the bright field (BF) and Fig.3.7(b) is the associated dark field (DF) images with g = [002]. These planar defects resemble stacking faults. The fault nature of these defects A-H shown in Fig.3.7 are determined and listed in Table 3.4, where I and E mean intrinsic- and extrinsic- stacking -fault, respectively.

Table 3.4 Nature of the Fault-Like Planar Defects in Fig.3.7

fault	A	B	C	D	E	F	G	H
Nature	E	I	E	E	E	I	E	I

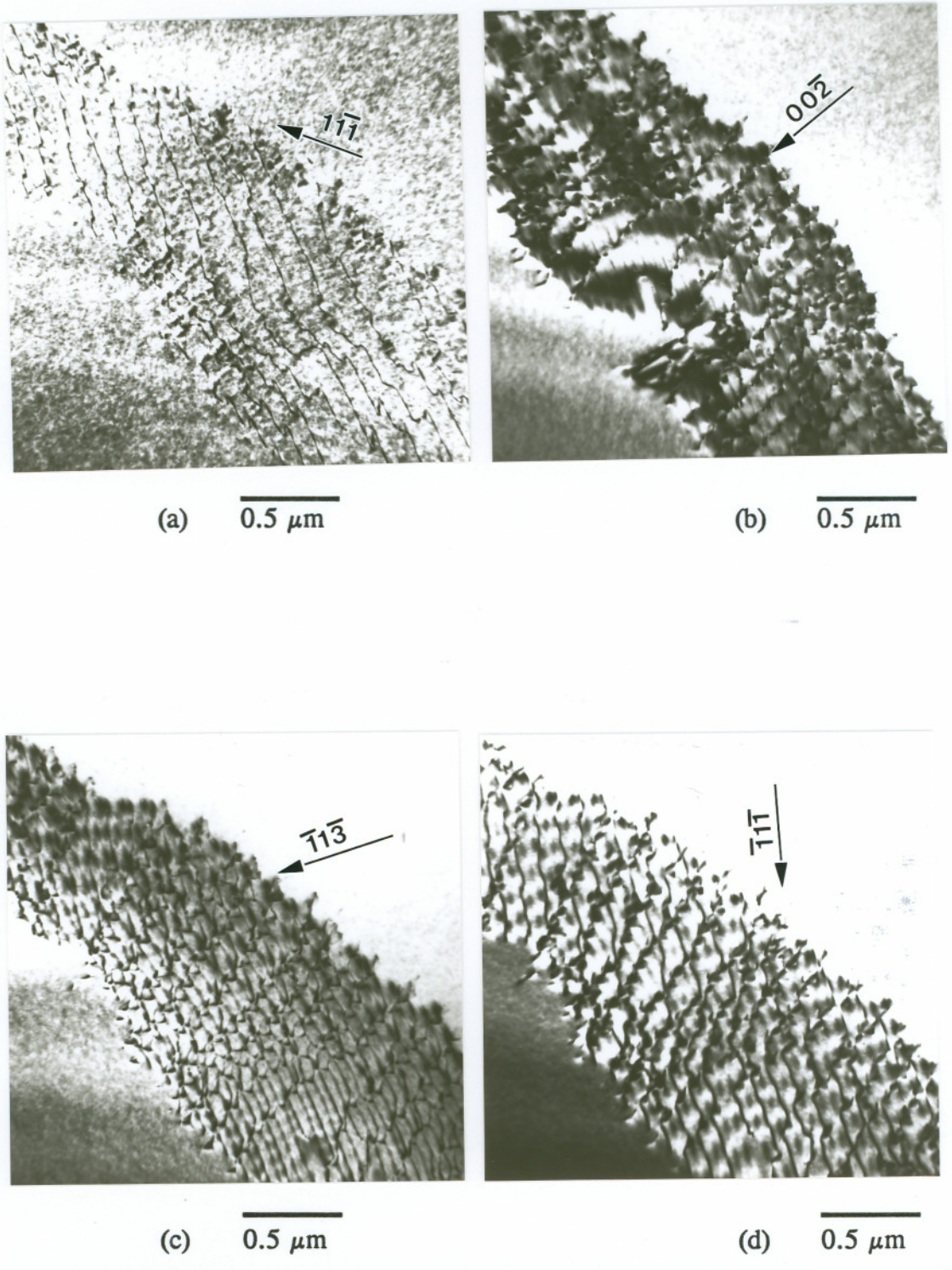

Fig.3.6 A sub-boundary consisting of dislocation networks obtained using (a) g=$[1\bar{1}\bar{1}]$, (b) $[00\bar{2}]$, (c) $[\bar{1}1\bar{3}]$, and (d) $[\bar{1}\bar{1}1]$.

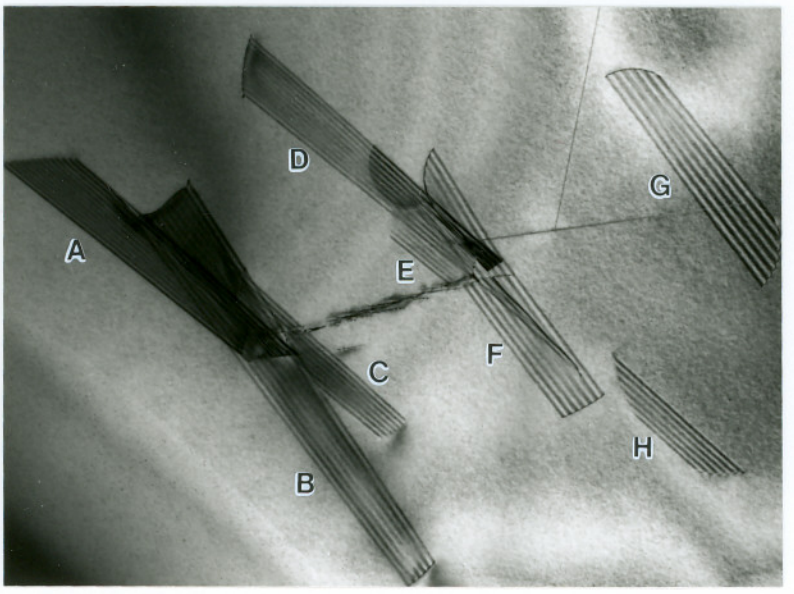

(a) 1 μm

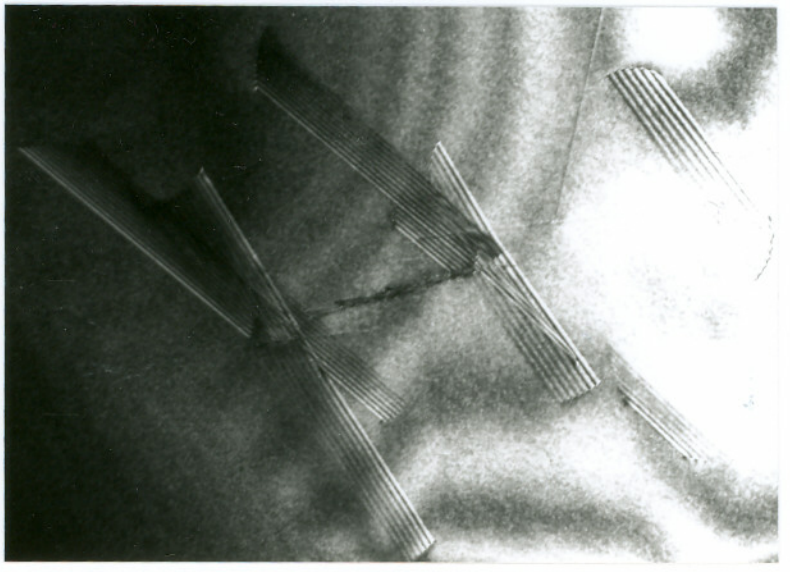

(b) 1 μm

Fig.3.7 Inter-subgrain planar defects with g = [002] and B = [110]: (a) BF and (b) DF images.

3.3.2 Defect Formation Mechanism

The formation of sub-boundaries in TiC_x is the result of dislocation rearrangement to lower the total strain energy. A variety of mechanisms exist to account for the introduction of dislocations into crystals grown from the melt:[138] (1) thermal stresses, (2) mechanical stresses, (3) vacancy and interstitial supersaturation, and (4) constitutional stresses. No matter what the mechanism of stress introduction into the crystal, if dislocation sources are readily available, the stress converts some of the total stress to plastic strain depending on the yield stress of the material. The number of dislocations per square centimeter introduced by the plastic strain is $n_d \sim 2[(\sigma-\sigma_y)/(E \cdot b)]$.[138] Where σ is the total stress, σ_y is the plastic stress, E is Young's modulus, and b is the Burgers vector of the dislocations. Since the yield stress near the melting point is approximately zero for metals or metallic compounds, many dislocations will be introduced into the solidified crystals.

For the crystals grown by the float zone method, thermal stress is certainly one of the major stress sources. If the crystal has a temperature distribution, as illustrated in Fig.3.8, the outside of the crystal wants to contract but cannot do so fully, because of the high temperature interior, thus, the outside will be in tension while the inside will be in compression. If the temperature difference between the inside and outside is ΔT, the thermal stress is $\alpha \cdot \Delta T \cdot E$, where α is the thermal expansion coefficient.

Dislocations generated in a crystal by various mechanisms will interact with each other behind the interface to form boundaries and arrays (Sub-boundaries) in order to lower the total dislocation energy.[139-141] The temperature of the solidified zone was still very high since it was next to the melt in the float zone growth. This high temperature provides thermal energy required for dislocation movement.

The formation of inter-subgrain stacking fault-like defects in TiC_x was associated with the segregation of boron impurity at dislocation sites. As stated in the formation of sub-boundaries, dislocations introduced in the crystal rearrange themselves into walls or sub-boundaries in order to lower the total dislocation energy. For those dislocations, which were not able to move to the sub-boundaries during the "recovery" stage, were left

within the subgrains, they were also the preferred sites for the diffusion of impurities such as boron. The high concentration of impurities at these dislocation lowered the stacking fault energy and promoted the dislocation dissociation into partials.

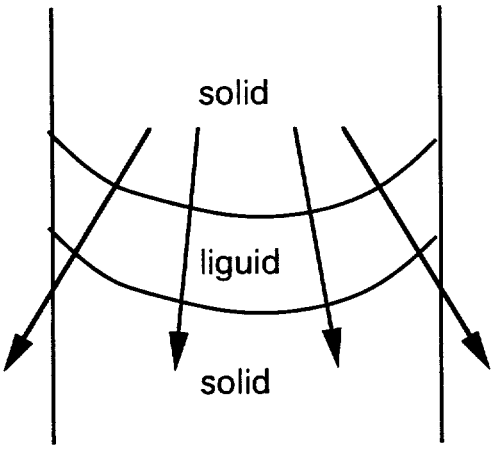

Fig.3.8 Illustration of temperature distribution during the float zone crystal growth.

3.3.3 Effect of Annealing on TiC_x Crystallinity

The as-grown TiC_x wafers were annealed at 2300°C for 24 hours in Ar, the annealing set-up is illustrated in Fig.3.1. The effect of annealing on the subgrain boundaries in TiC_x was examined by comparing the X-ray rocking curves obtained before and after annealing.

High temperature annealing of TiC_x, in contact with graphite, significantly reduced the misorientation level and/or the density of subgrains. This was substantiated by the double crystal X-ray rocking curves obtained from a $TiC_{0.8}$ wafer. Fig.3.9(a) and (b) show the X-ray rocking curves before- and after-annealing, respectively.

The as-grown $TiC_{0.8}$ wafer contained more than 5 subgrains per mm^2, with an average misorientation between the neighboring subgrains of approximately 0.05°, from Fig.3.9(a). The x-ray rocking curve, Fig.3.9(b), obtained from the TiC_x wafer after annealing indicates that the misorientation between subgrains has been reduced to less than 0.01°, and/or that the subgrain density has been reduced. This implys that some of the sub-boundaries formed in the as-grwon TiC_x crystals were removed through dislocation movement mechanisms.

Three conditions must be satisfied for the movement of a dislocation boundary. First, the geometrical aspects governing the movement of individual dislocations. If slip is involved the boundary can move only when the dislocations in the boundary are free to move on the slip planes defined by the dislocation lines and their Burgers vectors. Secondly, the thermodynamic condition is permittable that movement can result in a reduction in energy of the boundary. Thirdly, the driving force is sufficient to produce dislocation movement, for example, due to the excess vacancy concentration. Movement of boundaries, in the absence of an external stress, requires diffusion. High temperature annealing of TiC_x in contact with graphite provides the necessary driving force: the high thermal activation, higher vacancy concentration, and carbon atoms diffused from graphite to make-up the carbon deficiency in the as-grown non-stoichiometric TiC_x.

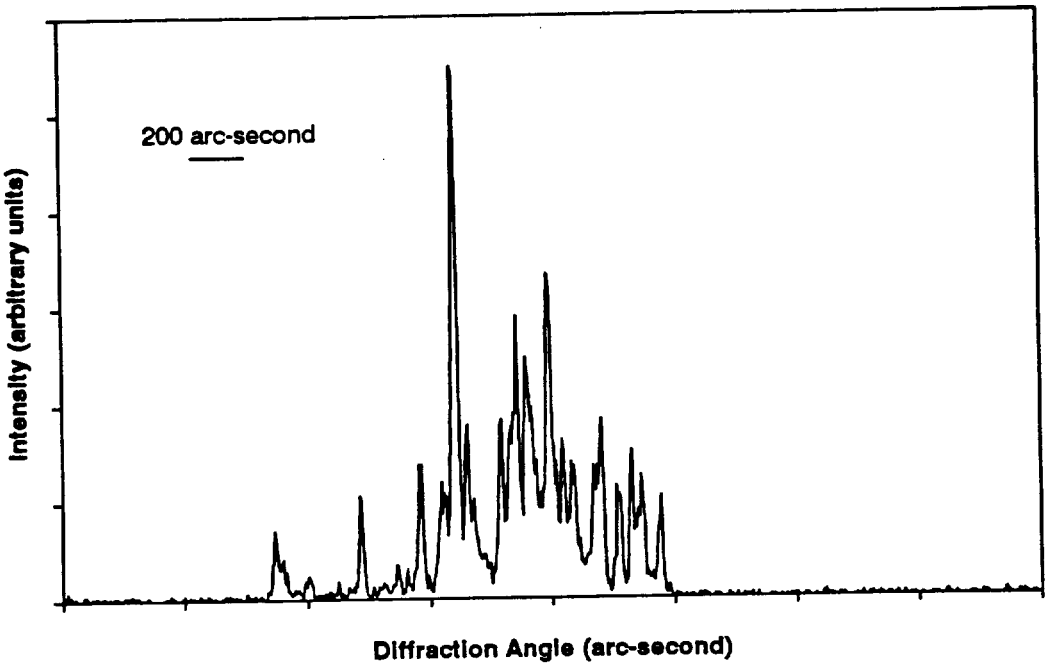

(a)

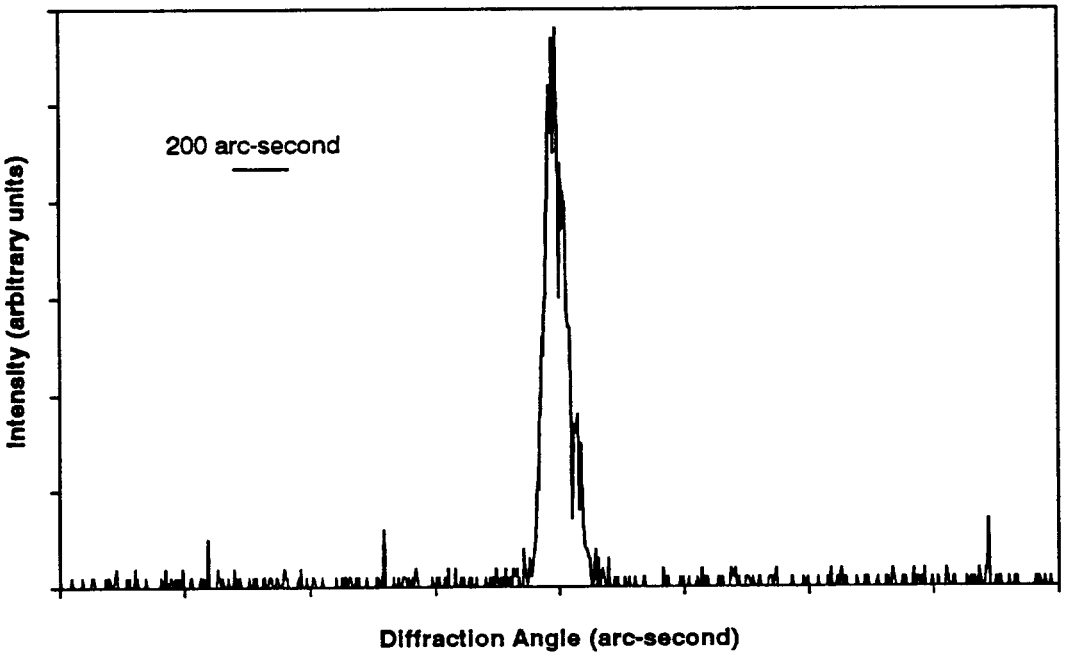

(b)

Fig.3.9. X-ray rocking curves from a $TiC_{0.8}$ crystal taken (a) before annealing, and (b) after annealing.

3.4 Conclusions

Three types of sub-boundaries and planar defects within subgrains were observed in the as-grown TiC_x crystals. The sub-boundaries were classified by their structures as: (i) wide-extended, fault-like defects (WEFLD), (ii) edge dislocation arrays, and (iii) dislocation networks. The planar defects, observed on sub-boundaries and within sub-grains, resemble an stacking fault-like characteristics. This is the first reported observation of planar defects formed within TiC_x subgrains, to our knowledge. Annealing of TiC_x at 2300°C in contact with graphite, caused a significant reduction in the misorientation level and/or density of subgrains. The improvement of TiC_x crystallinity through annealing makes it possible to use these TiC_x crystals as substrate for β-SiC epitaxial growth.

Chapter 4

EPITAXIAL GROWTH OF β-SiC ON TiC_x SUBSTRATES

4.1 Introduction

In this study, ß-SiC thin films were grown epitaxially on TiC_x substrates using 1,2-disilylethane (DSE or $Si_2C_2H_{10}$) as the single reactant source. The growth was conducted by chemical vapor deposition (CVD), in a water-cooled and inverted-vertical (IV) reactor. The interface structures (β-SiC/TiC) and defects formed in epilayer β-SiC were examined extensively using cross-sectional transmission electron microscopy (XTEM) technique.

4.2 Experiment

4.2.1 MOCVD Growth System

A schematic diagram of the CVD) system, used for the synthesis of β-SiC thin films, is shown in Fig.4.1. This technique was first developed at Hughes Research Lab.[86,87] The CVD reactor is a water-cooled, inverted-vertical (IV) reactor, as shown in Fig.4.2. This reactor configuration provides a true stagnation point flow pattern, theoretically ideal for achieving the best possible uniformity over the largest possible area, at atmospheric pressure. In addition, it eliminates backstreaming eddy currents by allowing the natural buoyancy of hot gases to expel them out of the reactor at high velocities.[83,84]

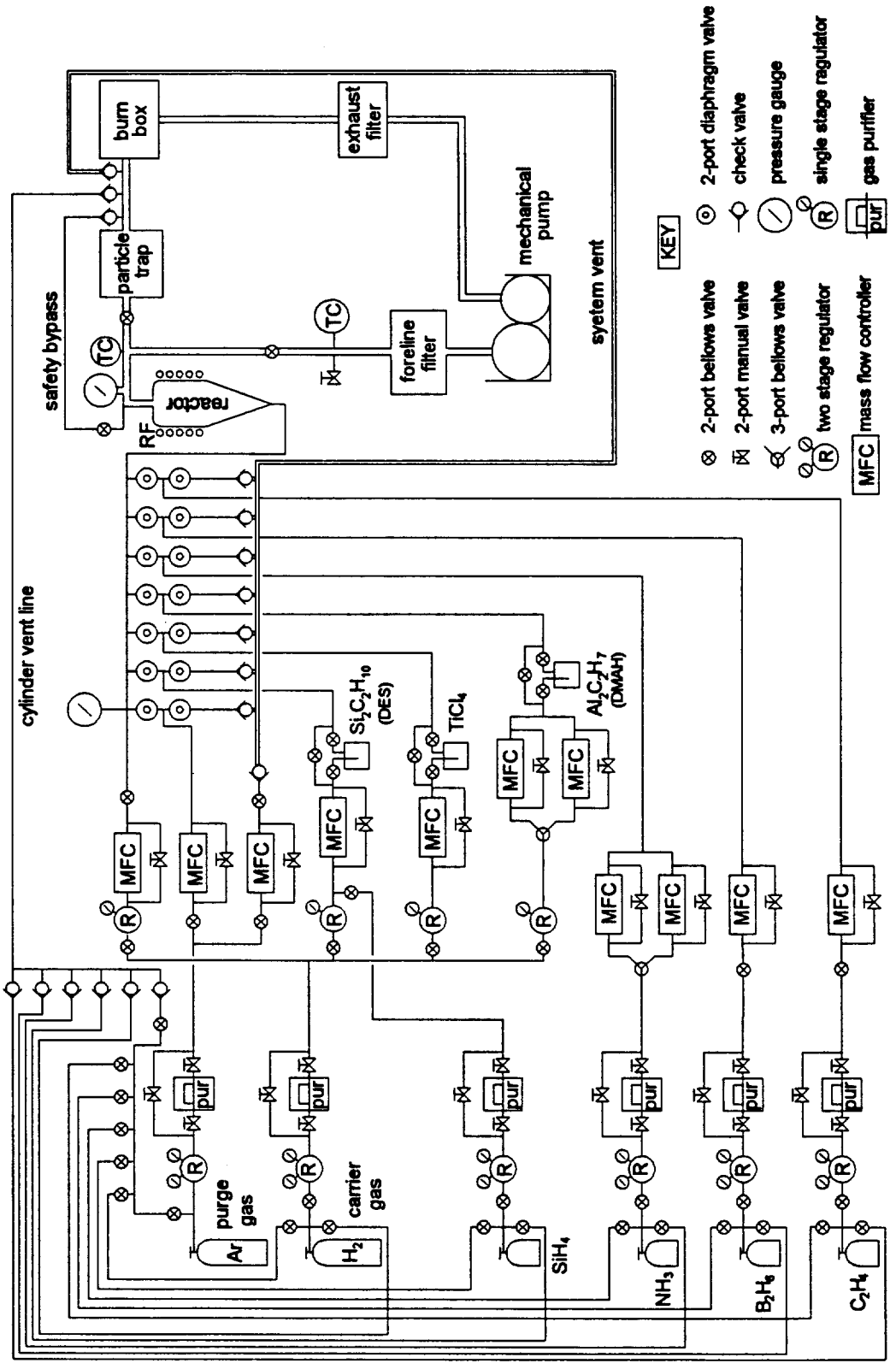

Fig.4.1 MOCVD epitaxial growth system.

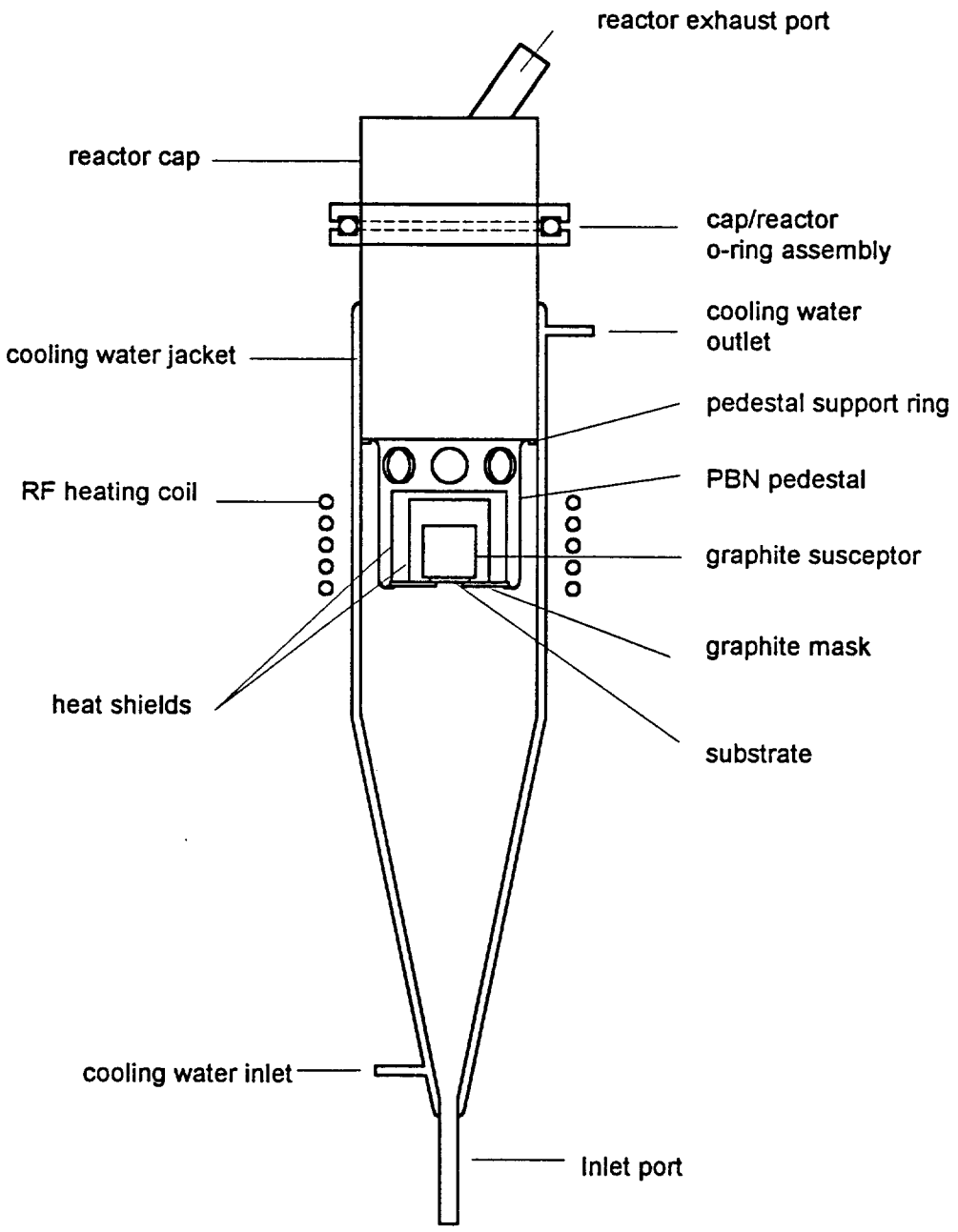

Fig.4.2 The inverted-vertical CVD reactor configuration.

In the MOCVD reactor, the growth-face-downward substrate is placed on a graphite mask which rests on the inside bottom of a pedestal. The pedestal is made of pyrolytic boron nitride (PBN), and is coaxially supported within the reactor by a support collar which rests on a pedestal support ring fused to the reactor wall. Two PBN heat shields are mounted over the graphite susceptor, between the susceptor and the pedestal vertical wall, to reduce heat loss.

The growth source enters from the bottom, below the downward-facing substrate. After decomposition of the source molecules, the gaseous reactant products are pushed radially outward until they reach the edge of the pedestal. Beyond this point, the pressure gradient in the reactor and buoyancy carry the reactant products upwards, through the annular volume between the outer pedestal wall and the inner wall of the reactor chamber. The reactant by-products exit through holes at the top of the pedestal, after which they exit through the exhaust port in the reactor cap.

4.2.2 Epitaxial Growth Procedure

The β-SiC epitaxial growth was conducted in the MOCVD systems described above. Before the growth, the system was pumped to below 1 millitorr and leak-checked, then backfilled with Ar.

Fig.4.3 illustrates the major procedures involved in an epitaxial growth of β-SiC on a TiC_x substrate. The TiC_x substrate was heated up, in the flow of C_2H_4, to the growth temperature by RF inductive heating through a graphite susceptor. The substrate temperature (or the growth temperature) was measured through the reactor chamber water cooling jacket with a Leeds and Northrup disappearing filament optical pyrometer. Growth of β-SiC was initiated by introducing the DSE (1,2-disilylethane: $Si_2C_2H_{10}$) reactant source into the reactor carried by H_2. The disilylethane source was in a liquid phase and stored in a stainless steel bubbler maintained at 15°C. The amount of the liquid transferred can be calculated by knowing the H_2 flowing rate and the vapor pressure of the liquid source at 15°C. Since there are equal molecule numbers of Si and C in the source, the Si/C ratio can be controlled precisely in the gas phase; and

therefore, complete nucleation or stoichiometric form of β-SiC can be obtained. The growth was terminated by bypassing the DSE source, and then the system was cooled down to room temperature.

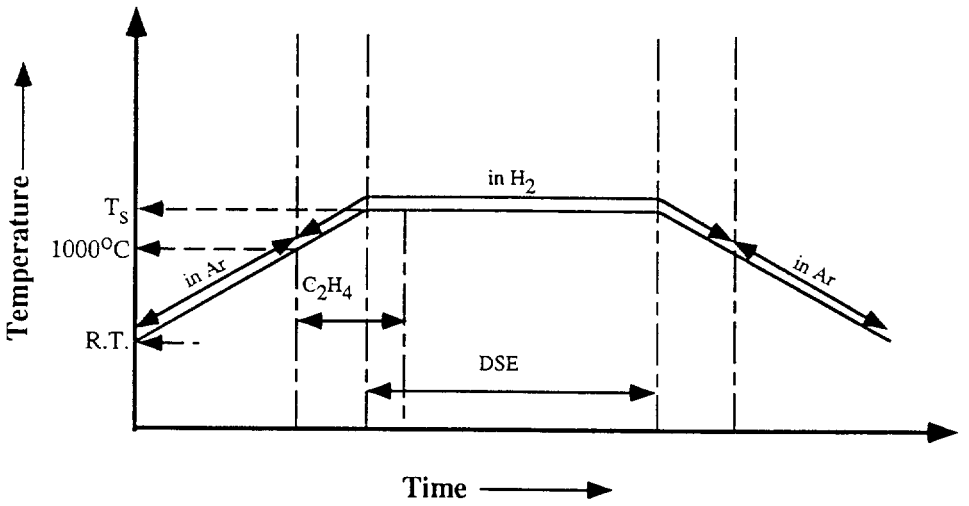

Fig.4.3 Major steps involved in β-SiC epitaxial growth on a TiC_x substrate.

4.2.3 Cross-Sectional TEM Sample Preparation

The β-SiC/TiC interfaces were examined in cross-section using transmission electron microscopy. Cross-sectional TEM (XTEM) provides the most detailed information on the interface structures, the defect initiation sites, and the relation between the β-SiC epitaxial layer and TiC_x substrate. The successful procedure developed during the research is illustrated in Fig.4.4.

Cross-sectional specimens were prepared by cutting the sample into two pieces using a low speed diamond saw and attaching them together using epoxy with ß-SiC layer face-to-face. Sandwich bars were sliced through the glue joint and mounted on a Gatan grinder using crystalbond, and ground with 15 μm and 6 μm diamond paste, respectively, and followed by 1 μm diamond paste polishing. Before turning over to another side, the sample was reinforced by laminating a 3 mm diameter molybdenum (Mo) washer to it, and ground the second side in the same way to a thickness of less than 30 μm. The second side was then dimpled using 1 μm diamond paste until the center of the disc was less than 20 μm thick. A Mo washer was also laminated to this side before final thining. Ar ion-milling was performed from two sides of the sample, with 5 kV working voltage and 1.1-1.5 A current. An 18° milling angle was used until perforation occured at which time the angle was reduced to 15° for further thining until the interface was electron transparent. A Hitachi-800 transmission electron microscope (TEM) operated at 200 kV was used for the TEM studies.

Two-beam conditions were used in the defect examinations by tilting the TEM sample, under which the images were formed by the transmitted beam plus one diffracted beam. The operative reflection $g_{(hkl)}$ used for each two-beam condition was then the vector from the transmitted spot (000) to the diffracted spot (hkl). The electron beam direction (B) was determined from the zone direction of the associated selected area diffraction pattern (SADP).

(1) Sandwiching

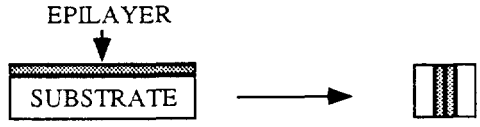

(2) Grinding

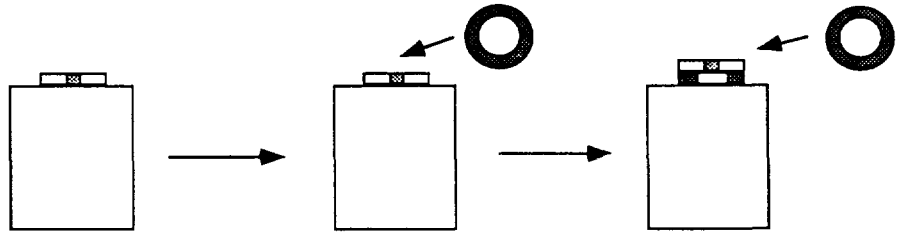

(3) Ion-milling

Fig.4.4 Illustration of cross-sectional TEM sample preparation procedures.

4.3 Results

4.3.1 Growth Condition Optimization

An optimized growth condition should be the controllable and repeatable growth parameters which lead to unpolytyped, single crystal or epitaxial β-SiC thin films with a smooth and shining surface.

Extensive studies on the growth conditions have been done previously.[34-36,80-87] The examinations of β-SiC crystallinity and surface morphology indicate that suitable growth conditions are the key factors to produce high quality single crystal β-SiC. Among these conditions, growth temperature is one of the most critical parameters in β-SiC nucleation and growth process. It directly controls the decomposition behavior of the reactant source DSE ($Si_2C_2H_{10}$). Within a certain temperature range, the reactant source decomposes to yield to equal number of Si and C atoms which then form stoichiometric β-SiC. On the other hand, if the growth temperature is too low, excess Si are produced after the decomposition of the DSE source. If the growth temperature is too high, excess C atoms are produced. Both cases would result in nonstoichiometric SiC layers that would deteriorate the surface morphology and crystal quality of the β-SiC films. A growth temperature in the range of 1157 - 1180°C with the DSE reactant source flow rate at about 3.2 sccm, were found to be the optimum growth conditions.

The surface morphologies of β-SiC thin films were examined in the SEM. The difference in the as-grown surface morphologies of the β-SiC epitaxial films grown under the optimum condition and non-optimum conditions are shown in Fig.4.5(a) and (b). The β-SiC film obtained under the optimum condition revealed uniform crystal facets (Fig.4.5(a)), no inclusions or domain structures were observed. However, the β-SiC film grown by non-optimum condition contained a lot of particles on the surface, as shown in Fig.4.5(b).

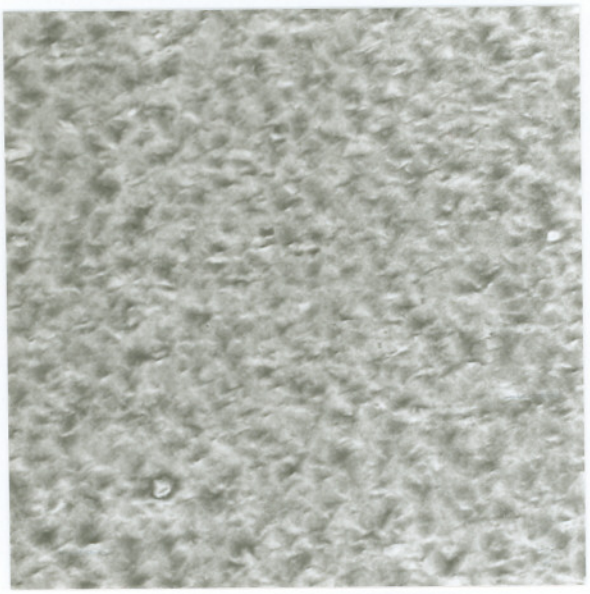

(a) 5 μm

(b) 5 μm

Fig.4.5 SEM micrographs showing the as-grown β-SiC surfaces obtained under (a) optimum and (b) non-optimum conditions.

However, the β-SiC thin films grown even under the optimum condition consisted of multiple large grains, see Fig.4.6(a). The large grain structure is the reproduction of grains in the TiC_x substrate. Since the TiC_x crystals used as the substrates were grown by the high pressure float zone method, they were not perfect single crystals as discussed in chapter 3. In fact, the TiC_x is not single crystal but contains many large grains. However, single crystal structure can be considered within each large grain. The crystallinity of a β-SiC thin film was determined using the selected area electron channelling pattern (SAECP). The SAECP is very similar in appearance to the reflection Kikuchi pattern formed in transmission electron microscopy (TEM). The detailed discussion of electron channeling contrast has been given in reference.[142] Fig.4.6(b) shows the SAECP obtained from a 2 μm thick β-SiC film grown on a (111) TiC_x substrate under the optimum growth condition. The sharp and clear SAECP with three-fold symmetry indicates that the β-SiC layer has repeated the (111) orientation of the substrate single crystal, and thus the growth was epitaxial.

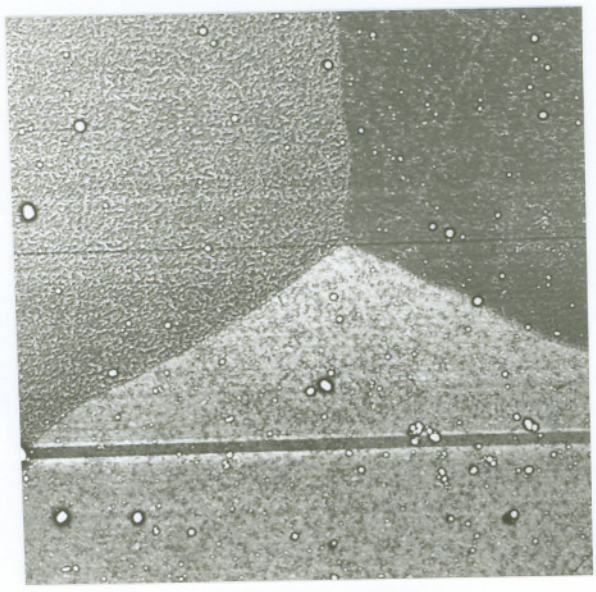

(a) 50 μm

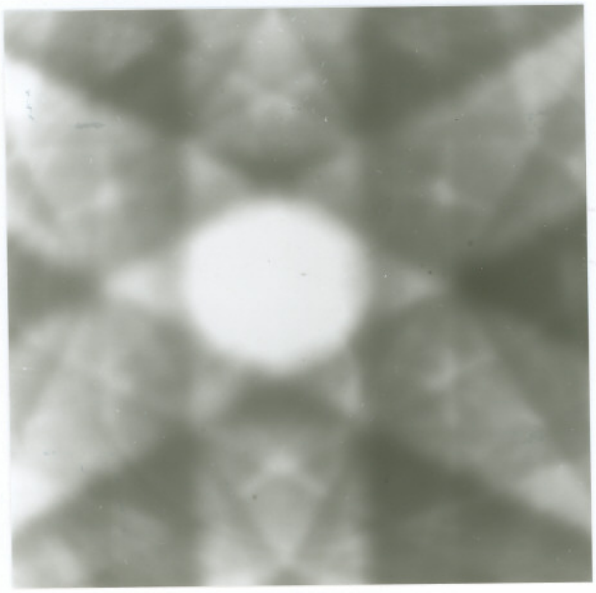

(b)

Fig.4.6 SEM micrographs of the as-grown β-SiC film on a TiC_x substrate showing (a) large grain structures and (b) selected area electron channelling pattern.

4.3.2. Interface Structures of β-SiC/(111)-TiC

4.3.2.1 Grown by Optimum Condition

The β-SiC epitaxial layers grown on (111)-oriented TiC_x substrates, even under the optimum growth conditions, contain a substantial number of defects. Microtwins were formed as the primary defects in β-SiC, and both coherent twin boundaries and incoherent twin boundaries were observed. Off-(111) orientation TiC_x substrates resulted in a higher concentration of defects in comparison to β-SiC epilayers grown on a (111) TiC_x.

(a) β-SiC grown on (111) TiC_x Substrate

Microtwins, as the primary defects, were formed in the β-SiC epilayers and were lying on {111} twinning planes as shown in Fig.4.7(a). These twins initiated from the interface (formed by the epitaxial layer β-SiC and the TiC_x substrate), and some of them propagated through the thickness of the β-SiC epitaxial thin film. Fig.4.7(b) is the associated selected area electron diffraction pattern (SADP) obtained from the interface area. The strongly diffracted spots in the SADP were from the reflective planes of β-SiC matrix with a $[\bar{1}10]$ zone. The extra spots were due to the presence of twins which diffracted the electron beam differently from the matrix.

The detailed description of twining structures can be found in a numerous textbooks. A twin is simply one part of a crystal that is oriented with respect to another according to a symmetry rule. From the TEM micrograph point of view, extra spots will arise in the SADP because a twin is oriented differently from the surrounding matrix relative to the incoming electron beam. In a face-centered cubic (fcc) crystal and those with diamond or zincblend structures (such as β-SiC), extra diffraction spots due to the presence of twins (including double diffraction spots) occur at $n \cdot \frac{1}{3} < 111 >$ positions of matrix spots in the diffraction pattern.[135,143]

In Fig.4.7(b), it seems that all the spots are shifted away except two spots [111] and $[\bar{1}\bar{1}\bar{1}]$. The twinning plane was then the (111) or $(\bar{1}\bar{1}\bar{1})$ plane, and the twinning axis

was [111] or [$\bar{1}\bar{1}\bar{1}$]. The extra spots caused by the presence of twins can be indexed by rotating the matrix diffraction spots 180° along the twining axis [111], as illustrated in Fig.4.7(c).[139] By comparing the image Fig.4.7(a) and the SADP Fig.4.7(b), the interface plane was perpendicular to [111] direction, and therefore, the interface plane was (111) plane. Since the twinning plane was also (111), twins lying parallel to the interface were expected. This direction of twins was seen at a higher magnification micrograph, Fig.4.8. It was also noticed that microtwins lying on the parallel-to-interface plane extended to about 28 nm from the interface and terminated as the film grows.

Besides the primary defect microtwins, a special type of twin boundary - double positioning boundaries (DPBs) were also observed in the β-SiC films. Fig.4.8 shows two DPBs (arrows) formed in the β-SiC epilayers. These DPB had a average spacing of 150 nm and extended about 175 nm in the epilayers. It's also noticed that microtwins were divided into small regions by the DPBs. The detailed analysis on DPBs will be discussed in a later section 4.3.2.2.

(b) β-SiC grown on off-(111) orientation TiC_x substrate

The TiC_x substrate with a small angle off the (111) orientation not only resulted in the formation of a higher concentration of defects, but also a rougher interface formed by the epilayer and the substrate. The comparison of β-SiC thin films grown on (111)-TiC_x and off-(111)-TiC_x were conducted by examining the samples using the same operating reflection from same zone axis.

Fig.4.9(a) and (b) show the XTEM micrographs of the epitaxial structures β-SiC/TiC with (111) and off-(111) orientations, respectively. Both the photographs were taken using g = [002] obtained by tilting the sample a small angle away from [$\bar{1}$10] zone axis. The difference in the defect concentration is clearly revealed from the microtwin spacings or densities shown in Fig.4.9(a) and (b). In Fig.4.9(a), only sparsely distributed microtwins along one direction were visible in the β-SiC epitaxial layer grown on a (111)-TiC substrate, the average microtwin spacing was about 338 nm. However,

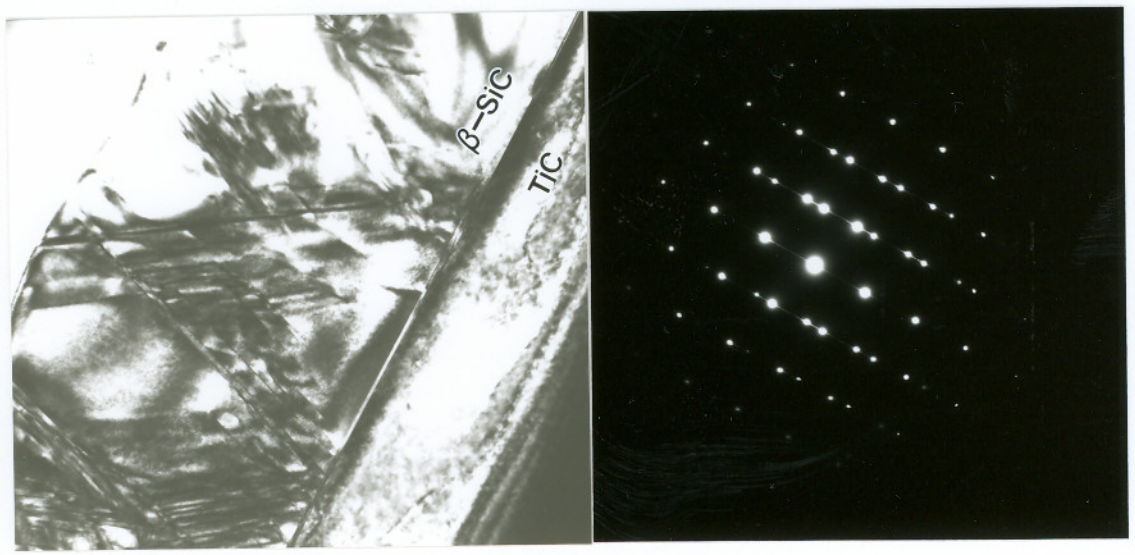

(a) $\overline{0.125\ \mu m}$ (b)

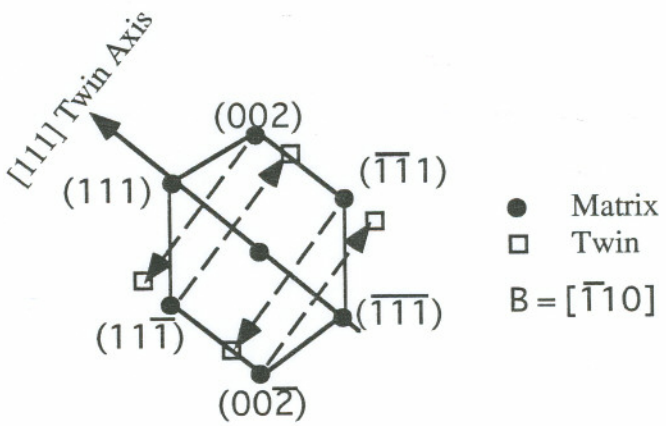

(c)

Fig.4.7 TEM micrographs showing (a) microtwins formed in β-SiC epilayer grown on a (111) TiC_x substrate, (b) the associated SADP, and (c) indexed pattern of (b).

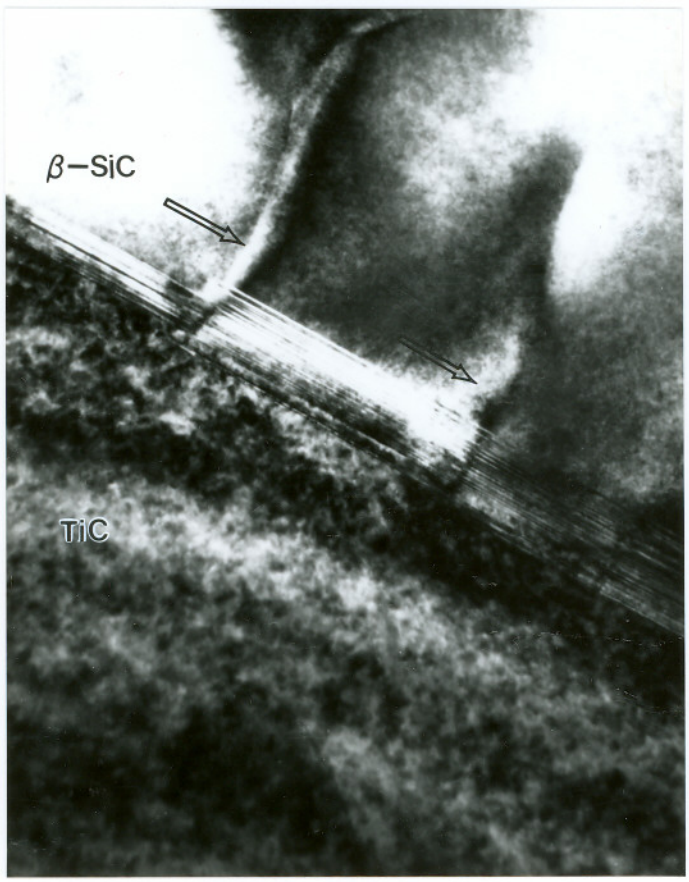

0.05 μm

Fig.4.8 DPBs extending from the β-S/TiC interface and dividing microtwins into small regions.

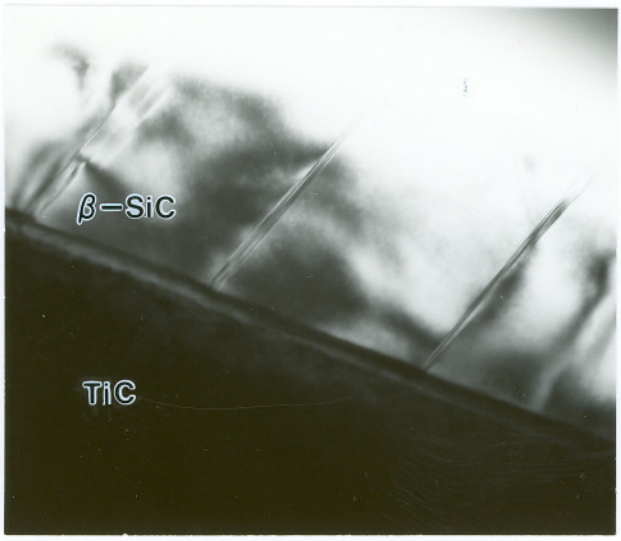

(a) 125 nm

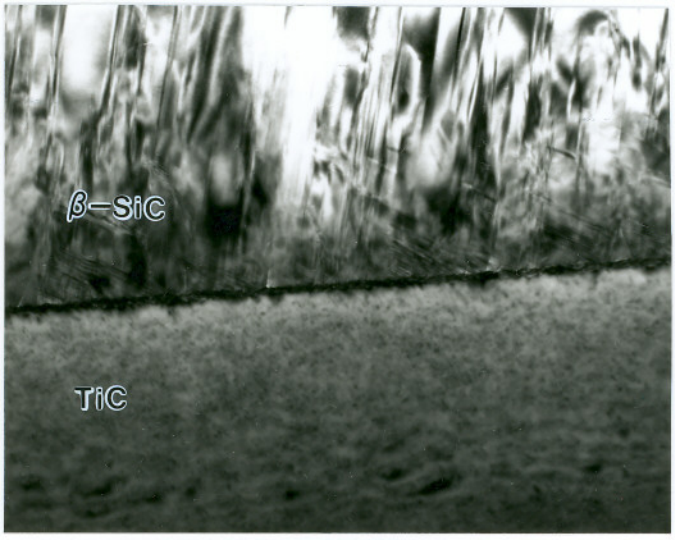

(b) 100 nm

Fig.4.9 XTEM micrographs showing defects formed in β-SiC epilayers grown on TiC_x substrates with orientations: (a) (111) and (b) off-(111). Both photos were taken with g = [002] and B = $[\bar{1}10]$.

a high density of twins lying on two different {111} planes were observed for the β-SiC thin film grown on a off-(111) orientation TiC substrate, as shown in Fig.4.9(b). Microtwins lying in one direction were closely packed and the twins lying along another direction had a spacing about 30 nm.

The β-SiC/TiC interface roughness was associated with the TiC substrate orientation. A rough interface was revealed for β-SiC grown on a TiC substrate with 16.5° off-(111) orientation, as shown in Fig.4.10. This is believed to be the result of surface steps due to mis-orientation, and will be explained in the discussion section.

A unique feature was also noticed for the microtwins formed near the interface of the β-SiC grown on TiC_x substrates. Samples shown in Fig.4.11(a) and (b) were grown on TiC_x substrates with (111) and 11° off-(111) orientations, respectively. The angles formed between the microtwins and the interface are approximated to be 0° in Fig.4.11(a) and 11° in Fig.4.11(b). This feature is attributed to the {111} twinning planes in a face-centered cubic (fcc) crystal. Twinning always occurs on a {111} plane in fcc structures. If the TiC substrate has a (111) orientation, twins formed on the (111) plane will be parallel to the β-SiC/TiC interface plane, as shown in Fig.4.11(a). If the substrate orientation has a small angle (θ) off the (111), twins still occur on the (111) plane for the fcc crystal structural β-SiC. Subsequently, twins form an angle (θ) with respect to the (111) interface (Fig.4.11(b)). Therefore, the angle between these microtwins and the interface resembled the substrate mis-orientation with respect to (111).

Fig.4.11(b) also shows that the density of DPBs formed in the epitaxial thin film β-SiC grown on a off-(111) orientation (11°-off) TiC_x substrate was higher than that in β-SiC grown on (111) TiC_x substrates, in Fig.4.8. The average spacing of the DPBs in off-(111) orientation was about 120 nm, while the spacing was about 150 nm in (111) orientation β-SiC.

Microtwins were formed as the primary defects in β-SiC epilayers in all the samples examined. Off-(111) orientation of TiC_x resulted in a higher concentration of microtwins and DPBs in the β-SiC epilayer due to rougher TiC_x substrate surface.

0.05 μm

Fig.4.10 A rough interface formed in the off-(111) β-SiC/TiC. B = [$\bar{1}$10].

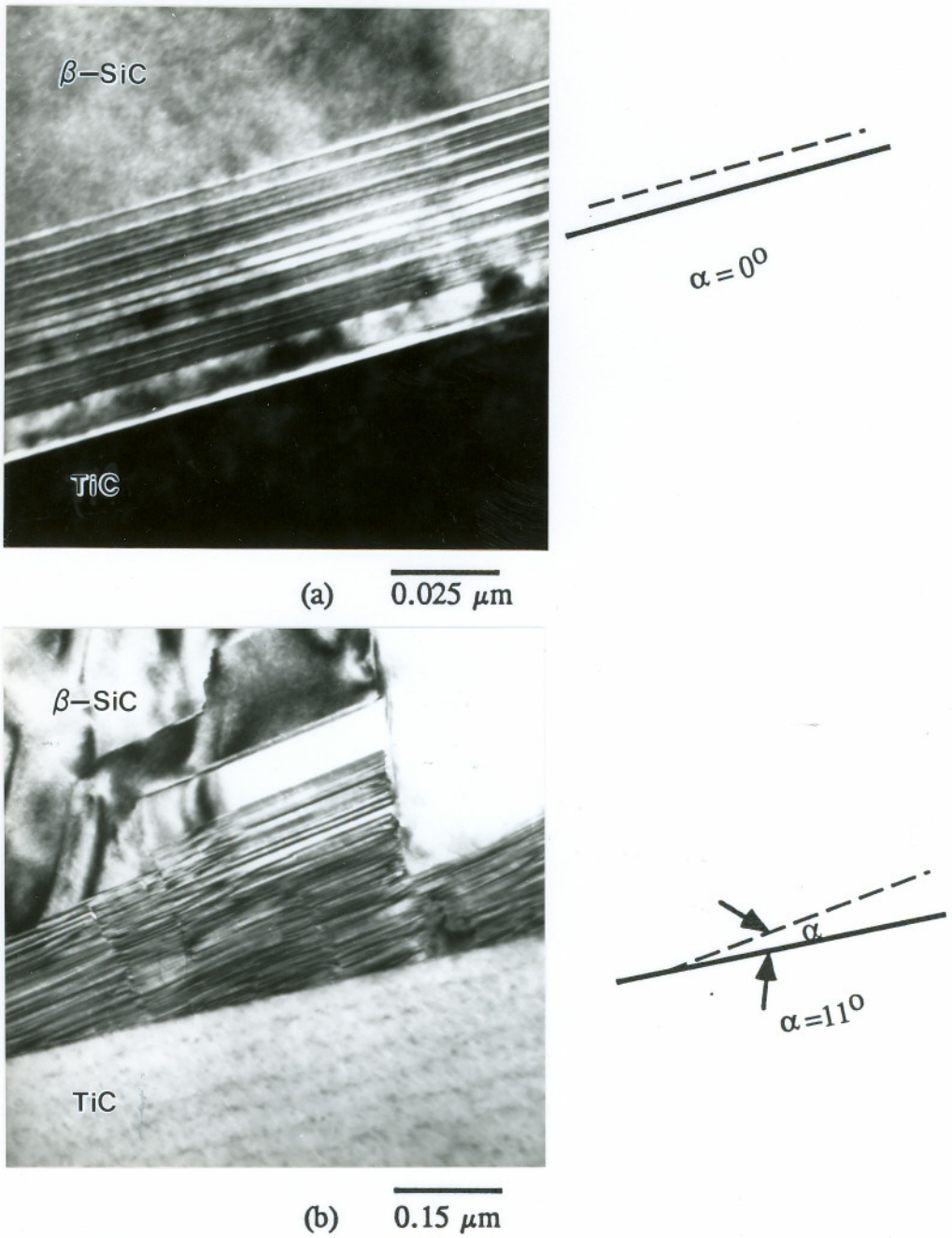

Fig.4.11 TEM micrographs showing that the angle (α) between microtwins and the interface plane resembled the TiC_x substrate misorientation level (θ): (a) $\alpha = 0°$ and $\theta = 0°$, (b) $\alpha = 11°$ and $\theta = 11°$.

4.3.2.2 Effect of Growth Condition

Compared to the β-SiC epitaxial thin films grown under optimum conditions, non-optimum conditions tend to result in a higher concentration of microtwins and a higher density of DPBs in the β-SiC epilayers. Fig.4.12(a) and (b) show the XTEM micrographs of β-SiC/TiC structures grown at reactant source (DSE) flow rates (Q_{DSE}) 10 sccm and 3.2 sccm, respectively. It can be seen that a higher density of twins were formed near the β-SiC/TiC interface due to the high flow rate (Fig.4.12(a)), in comparison to Fig.4.12(b) grown at 3.2 sccm.

Another deleterious effect of the non-optimum growth conditions is the introduction of a higher density of DPBs. Fig.4.13(a) shows one of the heteroepitaxial structures grown at a high growth temperature T_s = 1211°C, which was taken with electron beam direction approximately along [$\bar{1}$10] direction, see the SADP Fig.4.13(b). As shown in Fig.4.13(a), several regions were formed due to the presence of DPBs. It was also noticed that some of the DPBs disappeared as the thin film thickened (labelled as A), and some of them extended deep into the β-SiC (labelled as B).

These boundaries were determined to be DPBs according to their morphology and the diffraction patterns associated with the two neighboring regions. Fig.4.14(a) shows one example of the these DPBs. The two regions A and B shown in Fig.4.14(a) should have a twinning relation if the boundary is a DPB. This was confirmed from the electron diffraction patterns. Fig.4.13(b) is the SADP from region A and Fig.4.14(c) is the SADP from region B. Both of the diffraction patterns from either A or B has a <110> zone axis, the extra spots occurred in the diffraction patterns were due to the presence of microtwins within each region of A and B. By comparing Fig.4.14(b) and (c), it's noticed that there is a rotation between these two patterns. This is a simple case of twinning relation, which is the twinning plane lies parallel to the electron beam. The strong diffraction spots in Fig.4.14(b) and in Fig.4.14(c) were drawn in Fig.4.14(d) as solid dots and circle squares, respectively. The zone axis of the solid dot pattern from matrix A was arbitrarily defined as [$\bar{1}$10]. From Fig.4.14(d), the diffraction spots from B can be obtained by rotating spots from A about $[111]_A$ axis. Therefore, region A and

(a) 0.25 μm

(b) 0.3 μm

Fig.4.12 XTEM micrographs of β-SiC/TiC grown at reactant source flow rate Q_{DSE}: (a) 10 sccm, and (b) 3.2 sccm. Taken with g = $[11\bar{1}]$ and B = $[\bar{1}10]$.

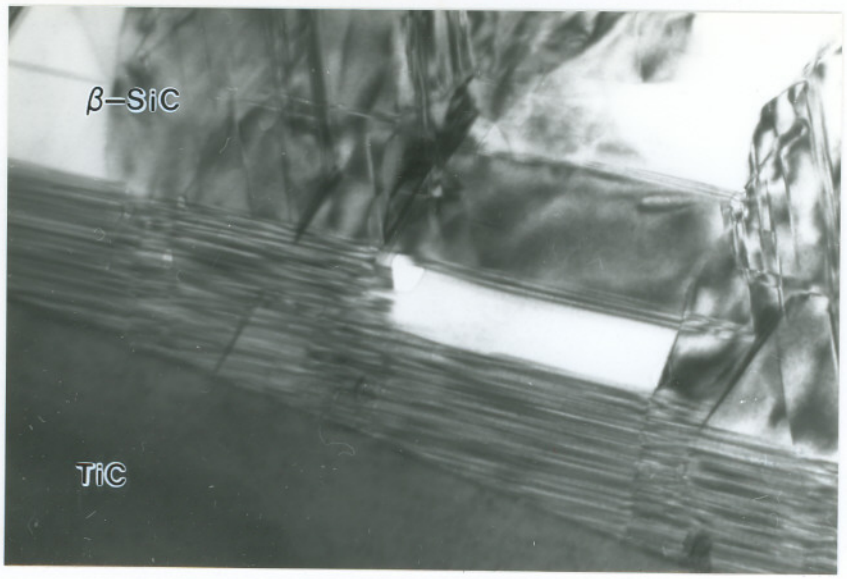

(a) 0.1 μm

(b)

Fig.4.13 TEM images showing: (a) DPBs formed in β-SiC grown at a high growth temperature T_s = 1211°C and (b) associated SADP with B = [$\bar{1}$10].

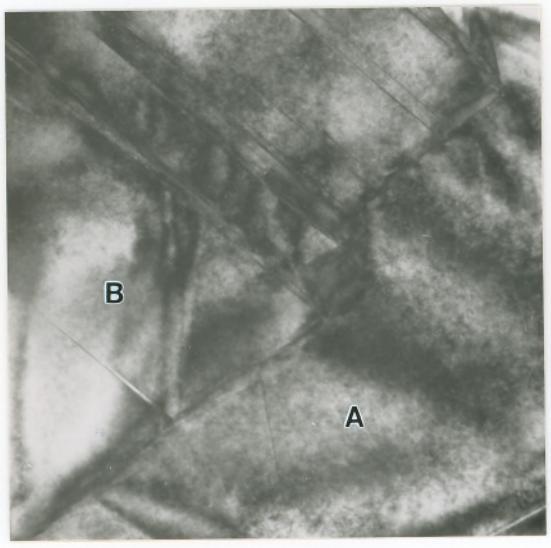

(a) 0.1 μm

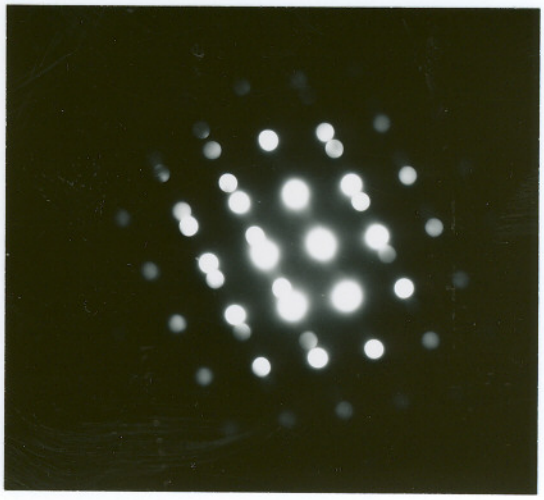

(b)

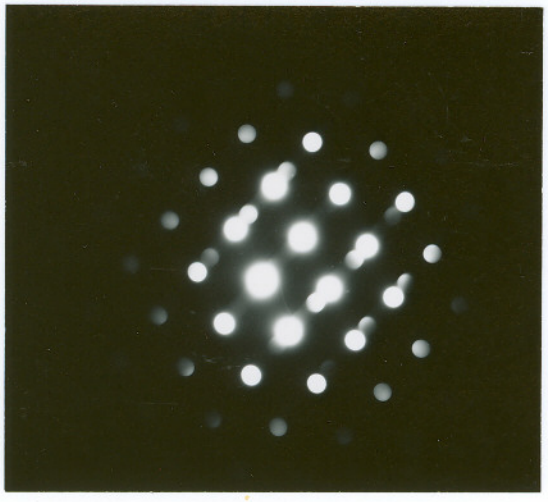

(c)

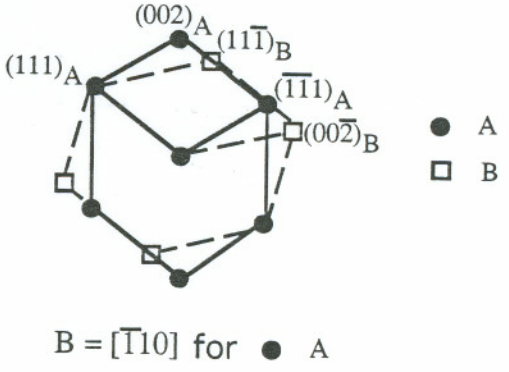

(d)

Fig.4.14 (a) A DPB formed in β-SiC grown at T_s = 1211°C, (b) SADP from region A, and (c) SADP from region B, and (d) diffraction spots from matrix in regions A and B showing that pattern (c) can be obtained by rotating (b) along $[111]_A$ twining axis.

region B have a twinning relation. Fig.4.15 shows another DPB formed in a β-SiC epilayer grown at a high flow rate (Q_{DSE} = 10 sccm). It's seen that microtwins can grow through the double positioning boundary or terminate at the boundary.

The DPB was not always a perfect line but contained a lot of small steps. This feature is attributed to the formation of alternating (111) coherent twin boundaries and $(11\bar{2})$ incoherent twin boundaries, as illustrated in Fig.4.16. When two twinning regions were stacked on top of each other, the boundary formed between them was a coherent twin boundary (C); however, when they positioned side-by-side, an incoherent twin boundary was then formed (I). The difference in the coherent twin boundaries and the incoherent twin boundaries can be clearly seen in Fig.4.17, a TEM image depicting the DPBs formed in β-SiC grown on a off-(111) TiC_x substrate.

4.3.3 Defects Formed in β-SiC Grown on (110)-TiC

The β-SiC epitaxial thin films grown on (110)-oriented TiC_x substrates contain a much higher concentration of microtwins and DPBs compared to β-SiC/TiC_x-(111) heteroepitaxial structures.

Fig.4.18 and Fig.4.19 are the TEM micrographs showing defects formed in β-SiC epilayers grown on (110) and (111) TiC_x substrates, respectively. From the micrographs, two important differences were noticed between the two orientations of β-SiC. First, microtwins formed in (110) β-SiC and (111) β-SiC epilayers revealed different orientations relative to the interface. In the (110) β-SiC epilayer, most microtwins were stacked on top of each other and were almost parallel to the interface. While the majority of microtwins in (111) β-SiC were initiated from the β-SiC/TiC interface and propagated perpendicular to the interface plane. Another difference between the two orientations of β-SiC epilayers is the density of defects. Higher densities of microtwins and DPBs were formed in the (110) β-SiC films, and also these DPBs extended all the way to the top surface of the β-SiC, while the DPBs formed in (111) β-SiC terminated within the film as it was thickening.

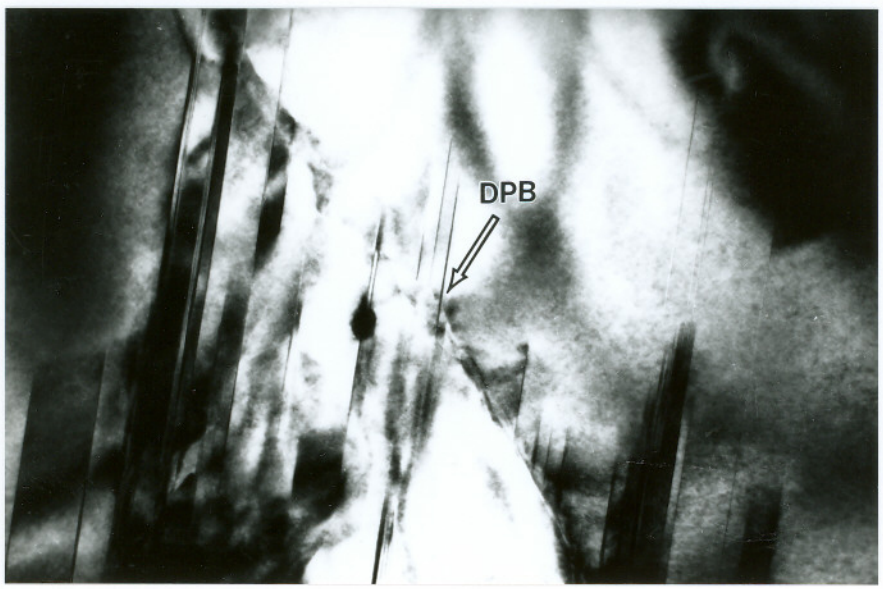

0.05 μm

Fig.4.15 A DPB formed in β-SiC grown by a high flow rate 10 sccm, showing that microtwins were either terminated or grown through the DPB.

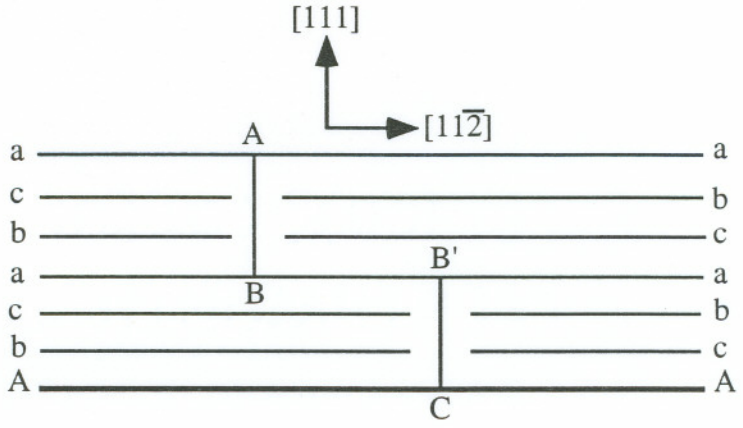

Fig.4.16 Illustration of a stepped DPB with (111) coherent twining plane and (11$\bar{2}$) incoherent twining plane.

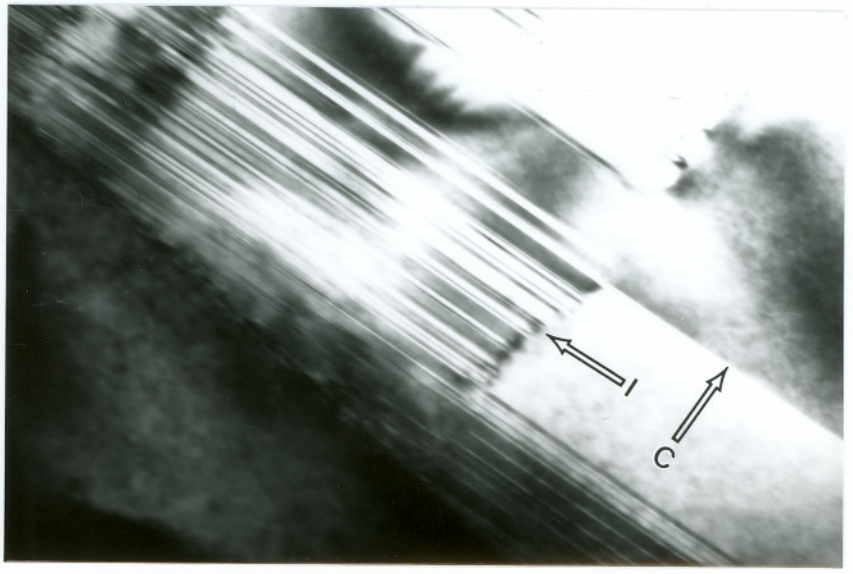

0.1 μm

Fig.4.17 Observations of alternating coherent and incoherent twining planes formed in a β-SiC epilayer grown on a off-(111) TiC_x substrate.

(a) 0.1 μm

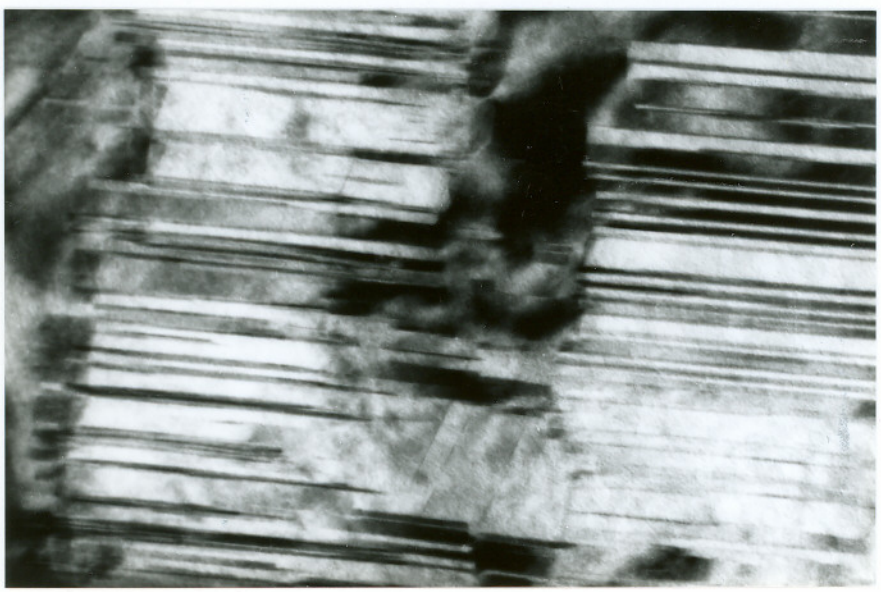

(b) 0.05 μm

Fig.4.18 Microtwins formed in β-SiC epilayer on a (110) TiC_x substrate with (a) $B = [\bar{1}10]$ and (b) $g = [111]$.

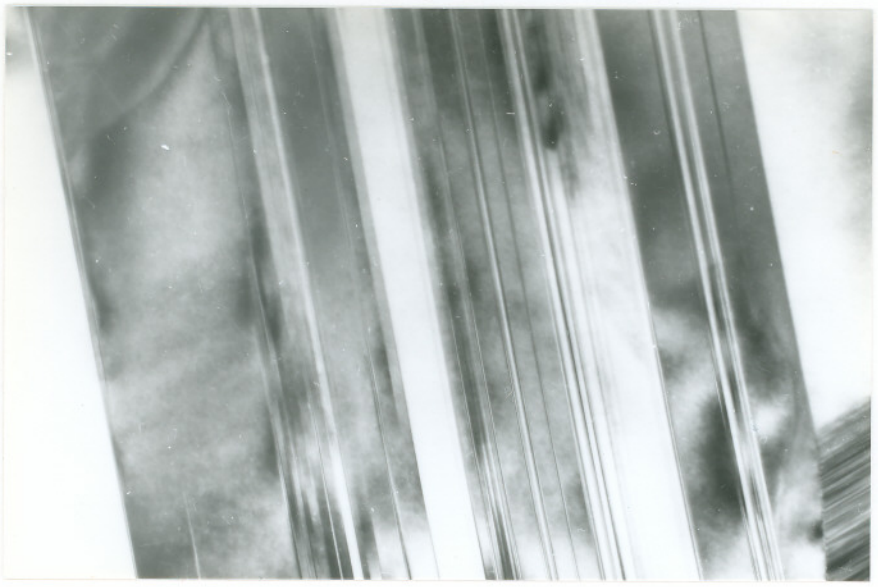

(a) 0.1 μm

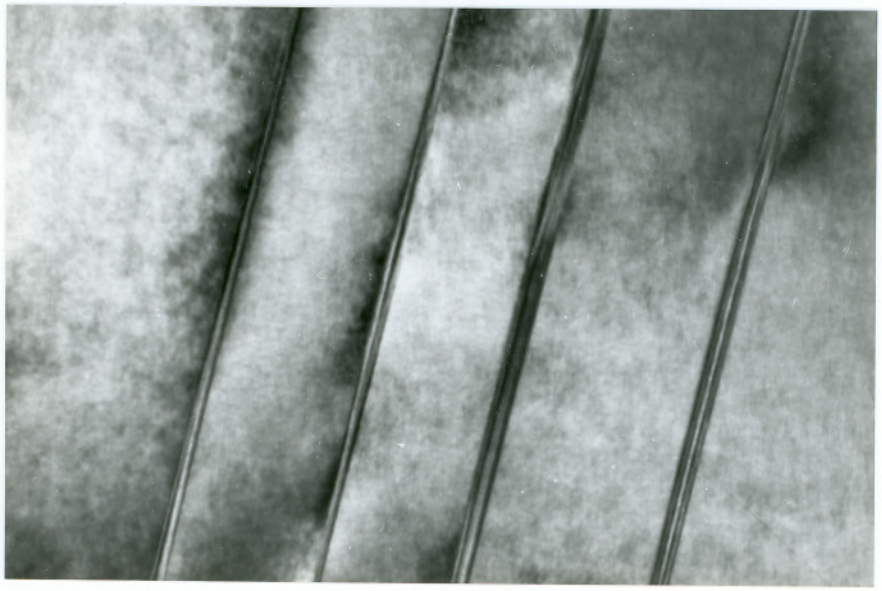

(b) 0.05 μm

Fig.4.19 Microtwins formed in β-SiC epilayer grown on a (111) TiC_x substrate with (a) $B = [\bar{1}10]$ and (b) $g = [111]$.

4.4. Discussion

4.4.1 Origins of Defects

Defects were formed in the β-SiC epitaxial films grown on a TiC_x substrate from the TEM examinations. Apparently, the constraints imposed by the TiC_x substrate, and the possibly impurities and unstable growth conditions, are the origins of defects. In the heteroepitaxial growth under the assumption of a clean system, three major sources are attributed to the defect introductions in the epilayers: (i) the lattice parameter mismatch, (ii) the thermal expansion coefficient difference, and (iii) the substrate surface defects.

4.4.1.1 Lattice Mismatch

Lattice mismatch in a heteroepitaxial growth system is one of the major defect formation sources. The lattice mismatch between β-SiC and TiC is very small (0.6%), however, its effect on the formation of defects in the epilayer is still not negligible. The direct effect of lattice mismatch is its introduction of misfit dislocations. The lattice misfit is also an important factor in controlling the critical thickness of an epitaxial thin film, which means the maximum thickness can be achieved to obtain misfit dislocation free epilayers.

For a heteroepitaxial system, the thin film can be grown under either strained or relaxed conditions, as discussed in chapter 2. If the thin film is under strained conditions, which means pseudomorphic growth, the atom positions match exactly on the interface plane between deposits and substrate, no mismatch dislocations are formed in the epitaxial thin film. However, pseudomorphic epitaxial growth can only be obtained for a very thin thickness of film, even theoretically. Further growth of the epilayer beyond the critical thickness will be energetically favorable to the formation of misfit dislocations. The critical thickness of a pseudomorphic layer is strongly related to the lattice mismatch, and is given by:[108,113,144]

$$h_c = \frac{b}{8\pi(1+\nu)f}\left[\ln\left(\frac{h_c}{b}\right)+1\right] \qquad (4.1)$$

where b is the Burger's vector of the misfit dislocations, ν is the Poisson's ratio for the epilayer material, and f is the lattice mismatch. The Burger's vector b is equal to $1/2[110]a_{SiC}$ in the β-SiC cubic crystal which is about 3.06×10^{-8} cm. The Poisson's ratio ν was calculated from the known stiffness constants of β-SiC as 0.28, see Table 4.1. The lattice mismatch f in the β-SiC/TiC heterostructure is 0.6%, from Table 2.4.

Table 4.1 Elastic Constants of β-SiC

Stiffness[145] ($\times10^{12}$ dynes/cm^2)	c11 = 3.523 c12 = 1.404 c44 = 2.329
Poisson's Ratio	$\nu = (c_{11} + c_{12})/c_{12} = 0.28$
Young's Modulus	$Y = [(c_{11} + c_{12})(c_{11} + 2c_{12})]/(c_{11} + c_{12})$ $= 2.71\times10^{12}$ (dynes/cm^2) $= 1.69\times10^{24}$ (ev/cm^3)
Shear's Modulus	$\mu = c_{44} = 2.329\times10^{12}$ (dynes/cm^2) $= 1.45\times10^{24}$ (ev/cm^3)

The equation (4.1) can then be written as

$$\frac{h_c}{b} = 5.208\left[\ln\frac{h_c}{b}+1\right] \qquad (4.2)$$

This equality is closely satisfied by $h_c/b = 21.08$. From the Burger's vector b = 3.06×10^{-8} cm, the critical thickness h_c is about 64.5 Å. This value is only about 25 ($h_c/d_{111} = 64.5/2.526 = 25$) monolayers of (111) β-SiC planes.

Since the derivation of the critical thickness equation (4.1) relies on the energy balance between strain energy and dislocation energy, the formula equ.(4.1) of h_c can only be considered as an estimate. Only a very thin pseudomorphic β-SiC can be produced on a TiC_x substrate, from the estimated value of critical thickness. It should also be mentioned that, a defect-free β-SiC epilayer can not always be obtained even if the thickness is less than the critical value. This is because a pseudomorphic epilayer is under strained or meta-stable condition, highly strained energies are stored within the crystal. If the epitaxial growth temperature is high enough for the strain energy to relieve, defects will then be formed as the result of stress relief. Therefore, a low growth temperature is one of the required conditions for pseudomorphic lattice growth. For the β-SiC/TiC_x system, the growth temperature is over 1000°C, this seems to be too high to keep the thin film under strained or unrelaxed condition.

4.4.1.2 Thermal Expansion Coefficient Difference

The difference in the linear thermal expansion coefficients between β-SiC and TiC acted as the most important factor in the introduction of defects in β-SiC thin films. The linear thermal expansion coefficients (α) of β-SiC and TiC are 3.9×10^{-6} /°C and 5.5×10^{-6} /°C, respectively.[145,146] From the growth temperature (about 1157°C) to room temperature (27°C), a big temperature drop occurred (ΔT was about 1130°C). The thermal stress introduced by the linear thermal expansion coefficient difference is:

$$\epsilon = \Delta\alpha \cdot \Delta T = 0.18\% \tag{4.3}$$

Since this strain is less than the value at yield stress, which is about 0.2%, the elastic approximation is assumed. Therefore, the stress can be calculated using the elastic coefficients of β-SiC:

$$\sigma = Y\epsilon = 3.04x10^{23} \quad (ev/cm^3) \tag{4.4}$$

where Y is the Young's modulus of β-SiC, which was calculated from stiffness constants as 2.71×10^{12} dynes/cm^2 or 1.69×10^{24} ev/cm^3, see Table 4.1.

It will be more understandable to describe this stress relative to each atom. The volume of each unit cell in β-SiC crystal is $(a_{SiC})^3 = 8.12\text{x}10^{-23}$ cm^3, and each unit cell contains 8 atoms, therefore, the atomic density is $9.8\text{x}10^{22}$ atoms/cm^3. The thermal stress applied on each atom will be:

$$\epsilon_{ta} = \frac{\sigma}{\rho} = \frac{3.04x10^{23}}{9.8x10^{22}} = 3.1 \quad (ev/atom) \tag{4.5}$$

This stress can be released by forming dislocations and twins in a β-SiC thin film. It is interesting to compare this stress to the energy generated by forming a dislocation in the β-SiC epitaxial films. It is known that the strain energy for the edge dislocation differs from that of the screw dislocation by a factor of $1/(1-\nu)$.[141] Since ν for most metals is near 1/3 (0.28 for β-SiC), the strain energy for the edge dislocation is thus larger than that for the screw dislocation. Therefore, it seems to be more reasonable to compare the strain energy of an edge dislocation with the strain energy introduced by thermal stress.

The strain energy per unit length around the core of an edge dislocation is approximately:[137]

$$\epsilon_e \approx \frac{\mu b^2}{4\pi(1-\mu)} = 1.5x10^8 \quad (ev/cm) \tag{4.6}$$

where the Poisson's ratio for β-SiC is about 0.28, the Burgers vector b is $3.06\text{x}10^{-8}$ cm, and the shear modulus μ is $1.45\text{x}10^{24}$ ev/cm^3, see Table 4.1.

To the first approximation, only the atoms around the dislocation core are considered, as illustrated in Fig.4.20. Considering a misfit dislocation lying on the interface plane with a length of L = 1 mm, the core volume around this dislocation is $2b \cdot 2b \cdot L = 3.75\text{x}10^{-16}$ cm^3. Each unit cell ($v = (a_{SiC})^3 = 8.12\text{x}10^{-23}$ cm^3) contains 8 atoms for a zincblend crystal structure, therefore, there are $N = 8\ (3.75\text{x}10^{-16}/8.12\text{x}10^{-23}) = 3.69\text{x}10^8$ atoms in this tunnel volume around the edge dislocation core. Therefore, the strain energy averaged on each atom will be:

$$\epsilon_{ea} = \frac{\epsilon_e}{N} = \frac{1.5x10^8}{3.69x10^7} = 4.06 \quad (ev/atom) \tag{4.7}$$

It is seen that the strain energy per atom around an edge dislocation is in the same level of magnitude as the strain energy generated by the thermal stress, by comparing equation (4.5) and (4.7). Therefore, the strain energy generated due to the thermal expansion coefficient difference can be a significant factor in the introduction of defects in β-SiC epitaxial films.

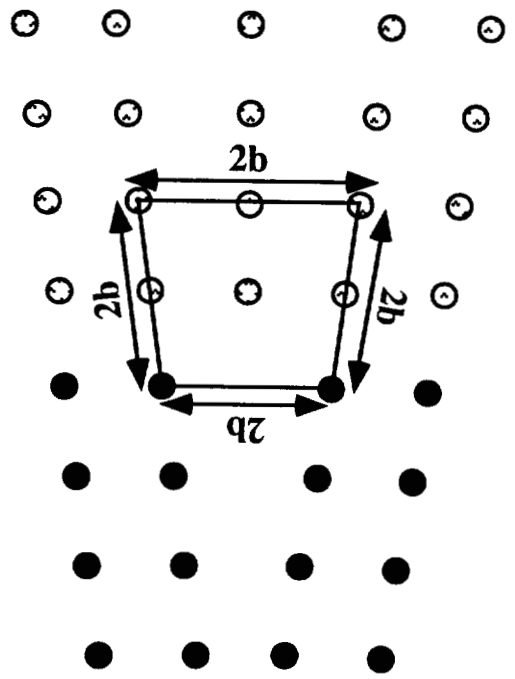

Fig.4.20 Illustration of an edge dislocation.

4.4.1.3 Substrate Surface Defects

The substrate surface is the starting place for epitaxial growth. An ideal surface should be completely smooth and absolutely clean, which means the surface lattice plane is occupied by correct atoms at the correct lattice sites, i.e., those determined by the ideal bulk crystal. However, in reality, the crystal surface exhibits irregular deviations from its perfect smoothness.

The surface has a microscopic structure associated with atomic displacements and a macroscopic structure associated with surface steps and other surface defects. In other words, the surface can contain terraces, steps, kinks, and others, as shown in Fig.4.21.[108,147] Steps or kinks, far from perfect, can form high-energy binding sites for deposited materials. The high binding energies at these surface defects can then be released by forming defects in the epitaxial films.

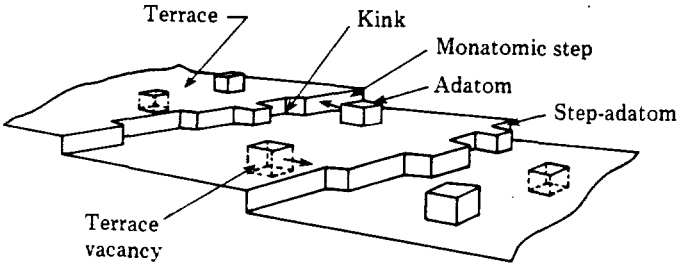

Fig.4.21 Schematic diagram of surface defects.[108,147]

The substrate surface steps were generated from two ways: (a) a bulk dislocation intercepts the surface, and (b) crystal miscut or off-orientation growth. The termination of a dislocation can give rise to a surface step. As shown in Fig.4.22, a surface step can be formed due to the movement of a edge dislocation to the free surface. This is also true for a screw dislocation. The TiC_x crystal used as the substrate for β-SiC epitaxial growth contains a high density of defects including sub-boundaries and planar defects, as we discussed in chapter 3. These sub-boundaries and planar defects were basically composed of dislocations and partial dislocations. After annealing in a C-rich environment prior to β-SiC epitaxial growth, the sub-boundary density or misorientation levels were significantly reduced in the TiC_x. The reduction of the defect densities was partly owing to the dislocations moving away from bulk crystal to free surfaces. Subsequently, surface steps were then formed.

The major contributor to surface steps is due to miscut or misorientation. Miscut occurs simply because a crystal is never cut exactly parallel to a crystal plane. For a small angle of miscut, the surface plane will be described by extended terraces of major planes and steps. Fig.4.23 illustrates a miscut of angle θ relative to a $<111>$ major surface plane. The surface step height (h) is given by

$$h = L_0 \tan\theta \qquad (4.8)$$

where L_0 is the step spacing , and θ is the miscut angle.

In a similar way, the surface steps can be formed if the substrate material was grown with a small off-angle from the desired major orientation. This is very common for TiC_x bulk crystals, because the growth technique used is far from perfect. Most of the TiC_x crystals used in this study have several degrees off from $<111>$ orientation, as determined from X-ray Laue patterns.

From equation (4.8), the larger the off angle, the smaller of the step spacing or the larger of the step height. Consequently, a rough surface was formed if the substrate has a large misorientation. This expection was actually observed in our TEM examinations.

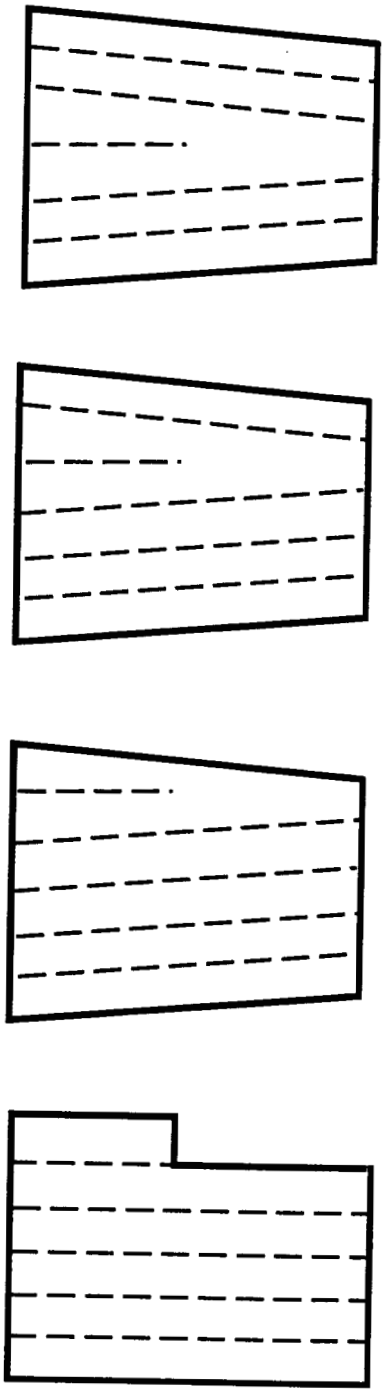

Fig.4.22 Surface steps generated by termination of an edge dislocation at the free surface.

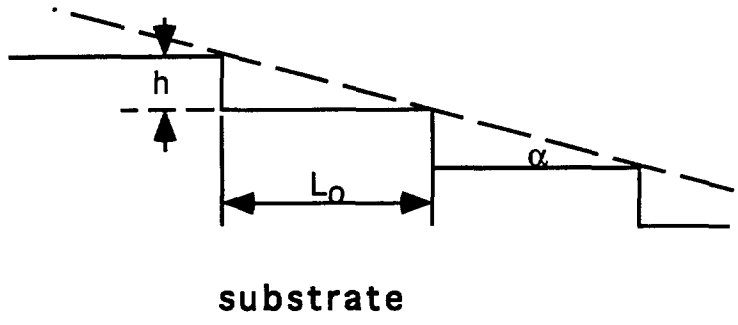

Fig.4.23 Surface steps formed due to miscut or misorientaiton crystal growth relative to the desired low index orientation.

As shown in Fig.4.10, a rough interface was formed for the β-SiC epilayer grown on a 16.5° off-(111) TiC_x substrate. Therefore, it is very important to use substrates with correct orientation and high quality surface.

The surface steps were observed to be the microtwin initiation sites. Fig.4.24(a) and (b) are the TEM images obtained from β-SiC films grown on a (111)-TiC_x substrate. It can be noticed that twins were initiated from the high energy step sites. The step spacing was measured from Fig.4.24(a) as about 456 nm, and the step height measured from Fig.5.24(b) was 12 nm, and therefore, the angle θ is about 1.5° from equ.(4.8). The substrate used for this sample has a (111) orientation according to Laue pattern. The small off angle (1.5°) can be considered as a measurement deviation of the X-ray Laue technique.

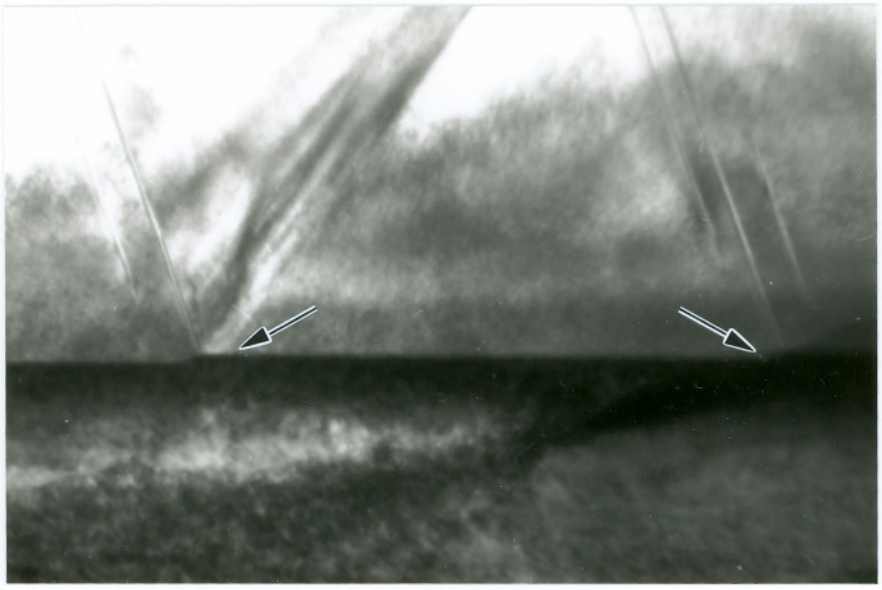

(a) 0.2 μm

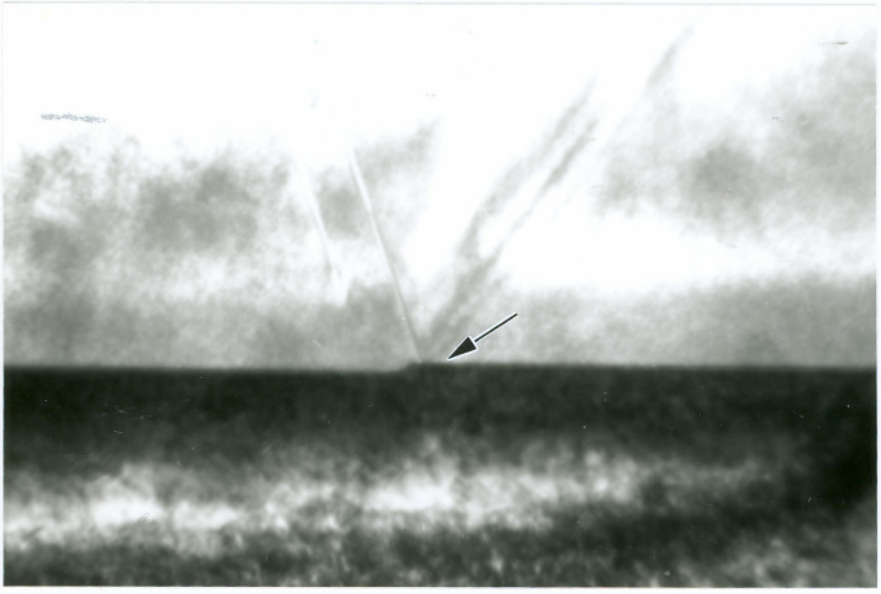

(b) 0.1 μm

Fig.4.24 Cross-sectional TEM micrographs showing that microtwins initiated from the surface steps.

4.4.2 Comparison of (111) and (110) β-SiC/TiC Interfaces

Although both TiC and β-SiC have cubic crystal structures, the lattice symmetry is different for the two materials. TiC has a rocksalt structure and β-SiC has a zincblend structure, which then determines the dependence of epitaxial β-SiC/TiC interfaces on the TiC substrate orientation.

4.4.2.1 TiC Surface Configurations

The substrate surface is the first place the deposited atoms come in contact with, therefore, its configuration will certainly affect the crystallinity of the subsequent deposits. It has been reported that, clean (111) and (100) TiC surfaces remain in stable (1x1) configurations, and also the stable (111) surface is a (1x1) Ti-terminated configuration, while (110) and (112) surfaces reveal (111) facets.[148-150] In fact, the (111) facets formed on (112) TiC surface have been observed by Chien.[151]

The stable (1x1) configuration of (111) TiC surface should produce higher quality of β-SiC epilayer compared to the (110) TiC, because a (110) TiC surface contains many (111) facets which act as surface steps or surface defects. From the origins of defects discussed in section 4.4.1, the surface steps are the initiation sites of defects in epitaxial films.

4.4.2.2 Ideal β-SiC/TiC Interface

The (111) and (110) surfaces of TiC and β-SiC are depicted in Fig.4.25 and Fig.26, respectively, along the <110> projection. As shown in Fig.4.25, both TiC and β-SiC have a polar (111) plane, which means each (111) plane contains two separate atomic layers of Ti and C in TiC, and Si and C in β-SiC. According to previous reports,[148-150] the (111) TiC substrate surface is Ti-terminated (1x1) stable surface. During deposition of β-SiC, incoming C atoms will first be absorbed by forming Ti-C bonds and followed by deposition of Si atoms on top of them to form β-SiC. The (111) β-SiC/TiC interface is illustrated in Fig.4.25, atoms can be matched very well at the interface.

The (110) TiC and (110) β-SiC are non-polar, both Ti and C atoms in TiC (Si and C atoms in β-SiC) lie on the same plane, see Fig.4.26. The Ti atoms on the (110) TiC surface will form Ti-C bonds with depositing C atoms, and then followed by the formation of Si-C bonds. While there are also C atoms on the surface, these atoms can (i) remain as the original C atoms belonging to TiC substrate, (ii) absorb Si atoms to form C-Si bonds, and (iii) absorb C atoms to form C-C bonds. For the first case, C atoms produce dangling bonds. This not only degrade the electrical properties of the metal/semiconductor junction, but also have a deleterious effect in the interface lattice structure by attracting neighboring atoms. In the latter two cases, if the C atoms form C-Si or C-C bonds, the ideal periodic lattice structures near the interface are then destroyed.

From the above analysis, (111) TiC substrate is superior to (110) TiC as the substrate for β-SiC epitaxial growth. This expectation matches with our TEM observations that β-SiC epitaxial films grown on (110) TiC substrates which contain a higher density of defects including microtwins and DPBs.

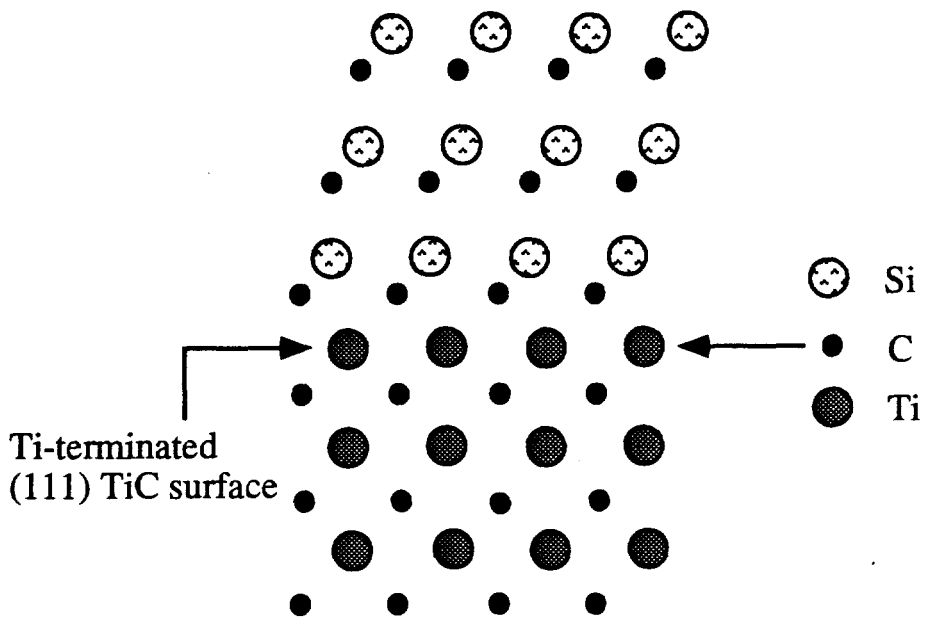

Fig.4.25 (111) planes of TiC and β-SiC along [1$\bar{1}$0] projection.

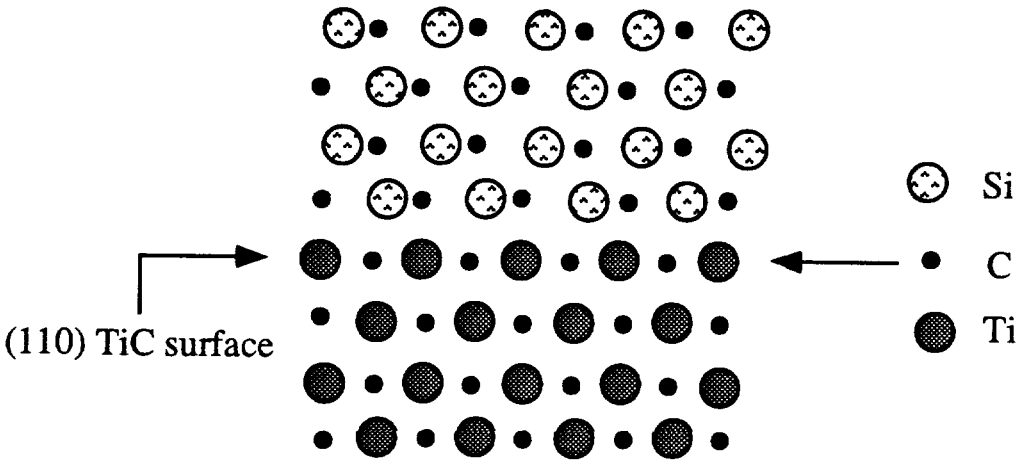

Fig.4.26 (110) planes of TiC and β-SiC along [$\bar{1}$10] projection.

4.5 Conclusions

Single crystal β-SiC films were successfully synthesized on bulk grown (111), off-(111), and (110) TiC_x substrates. Defects formed in the β-SiC epilayers were examined extensively in cross-section. It was found that heteroepitaxial growth of a zincblend structure β-SiC on a rocksalt structure TiC_x was strongly influenced by the growth conditions, and the choice of substrate crystal orientations. The major characteristic of the defects in the epitaxial structures were summarized in Table 4.2. A higher concentration of microtwins and DPBs were observed in β-SiC films especially near the interface region, when a non-optimum growth condition (either high growth temperature or high flow rate) was used. The TiC_x substrate with a small angle off from the desired (111) orientation resulted in a rough surface, which led to a rough β-SiC/TiC_x interface and higher density of defects in the β-SiC epilayers.

Two main differences were observed for the defects formed in (111) and (110) β-SiC epilayers. In the (110) β-SiC epilayer, most microtwins were stacked on top of each other and were almost parallel to the interface. While the majority of microtwins in (111) β-SiC were initiated from the β-SiC/TiC interface and propagated perpendicular to the interface plane. Another difference between the two orientations of β-SiC epilayers was the density of defects. A high density of microtwins and DPBs were formed in the (110) β-SiC films, the DPBs extended all the way to the top surface of β-SiC, however, the DPBs formed in (111) β-SiC terminated within the film as it thickened.

The main barriers to the development of β-SiC using TiC_x as the substrate are: (i) the low quality of bulk-grown TiC_x crystals and (ii) the dissimilar thermal expansion coefficient between β-SiC and TiC. Due to the imperfection of the TiC_x growth technique, substructures are formed in the nonstoichiometric TiC_x, which largely degrade the use of TiC_x as the substrate material. The thermal property mismatch between TiC and SiC makes it very difficult to obtain high quality β-SiC thin films.

Table 4.2 Effect of Growth Condition and Substrate Orientation on the Defect Structures Formed in β-SiC

Influencing Factor	Defect Structures
Growth Condition	(1) Optimum growth condition: Ts = 1157-1180°C, and flow rate of 1,2 disilylethane reactant source = 3.2 sccm. (2) Non-optimum condition: result in higher concentration of microtwins and DPBs.
TiC_x Substrate Off-(111) Level	Misorientation led to a rough TiC_x surface, thus a rough β-SiC/TiC interface and high density of microtwins and DPBs.
TiC_x Substrate Orientation	(1) Higher density of microtwins and DPBs in (110) β-SiC than these defects in (111) β-SiC; (2) Microtwins were stacked on top of each other and were parallel to interface plane in (110) β-SiC, while microtwins were initiated from interface and propagated perpendicular to the interface plane.

Chapter 5

Epitaxial Growth of TiC on β-SiC and 6Hα-SiC Substrates

5.1 Introduction

The physical and electronic properties of TiC indicate that it can play an integral role in SiC semiconductor device and circuit technology. Its low workfunction (≈3 eV),[152,153] low resistivity,[152,153] and thermal stability[58] are desirable attributes for ohmic contacts to n-type SiC and rectifying contacts to p-type SiC.[84]

The rock salt structure of TiC_x can exist as a single phase in the composition range $0.6 \leq x < 1.0$.[58] The minimum lattice parameter mismatch between TiC_x (4.331 Å at x=0.85)[58] and ß-SiC (4.3582 Å),[57] is about 0.6%. The melting temperature of TiC is about 3100°C,[58] and it does not decompose or undergo phase transformations in any temperature range of interest for ß-SiC epitaxial growth, or for SiC device applications at high temperature.

Single crystal interfaces of TiC on SiC can form nearly ideal electrical contacts.[81] Epitaxial growth of stoichiometric TiC on single crystals of SiC, and the properties of the resulting TiC epilayer and the TiC/SiC interface have not been reported. However, extensive studies have been conducted on the reaction layers including (1) thin film growth of Ti on β-SiC,[154] 6Hα-SiC,[155], and Si,[156] (2) metal matrix composite Ti-SiC,[157,158] (3) SiC-SiC joints using Ti-containing alloys brazing.[159] It is generally accepted that the reaction products are Ti_5Si_3, TiC and Ti_3SiC_2. It was also observed that the formation of TiC during the deposition of Ti on SiC was performed by consuming the

C atoms covering the surface and followed by an attack of the SiC substrate with the Si being expelled to the surface as elemental Si.[154,155] However, a good lattice match was also observed between TiC and SiC.[157] Therefore, it is possible to form an abrupt TiC/SiC interface both from thermodynamic or from crystallographic points of view.

In this study, TiC epitaxial growth conditions were established. These conditions were used to grow TiC epilayers on (0001) 6Hα-SiC bulk single crystal substrates, and on (111) and (110) ß-SiC epilayers. The defects, crystallinity and thermal stability of TiC epilayers and TiC/SiC interfaces were investigated using transmission electron microscopy (TEM).

5.2 Experiment

Thin film growth of TiC was performed by atmospheric pressure chemical vapor deposition in a cold wall, inverted-vertical CVD reactor as shown in Fig.2.2. The growth sources were $TiCl_4$ (in a liquid state and therefore contained in a stainless steel bubbler at 15 °C), and 10 volume % C_2H_4 in balance H_2. Hydrogen was used to transport $TiCl_4$, and to provide the make-up gas required to give a total flow rate of 2.9 SLPM for each growth run.

Substrates, either β-SiC epilayers grown on bulk TiC_x substrates or 6Hα-SiC substrates, were first cleaned using the standard cleaning procedures in hot TCE, hot acetone, and hot methanol for 5 minutes, respectively, followed by a 2 minute etching in 4.8% HF to remove the native oxide surface layer. Substrates were subsequently loaded into the CVD reactor and heated to the designed growth temperature in 2.9 SLPM H_2. The surfaces of (111) ß-SiC epilayers, grown on (111) bulk TiC surfaces, were used as substrates to establish TiC epitaxial growth conditions. The conditions for TiC epitaxial growth were identified by a parametric study of growth rate, surface morphology, and crystallinity as a function of substrate temperature (1027 - 1277 °C) and C_2H_4 to $TiCl_4$ flow rate ratios (0.6 - 2.4). Substrate temperatures (T_s) were read by a Leeds and Northrup disappearing filament optical pyrometer, through a water cooling

jacket at 20° relative to the substrate surface. The $TiCl_4$ flow rate was 0.85 sccm for each growth run. Growth rates were measured from micrographs of angle lapped surfaces. The as-grown surface morphologies and crystallinities were examined using scanning electron microscopy (SEM) by secondary electron imaging and selected area electron channeling patterns (SAECP), respectively.

Titanium carbide thin films were grown on three types of substrates: (110)-oriented β-SiC, (111)-oriented β-SiC, and (0001) 6Hα-SiC. The heterostructures of TiC/SiC were then annealed at 1400 °C for two hours after deposition of TiC. The defect structures and interface properties were examined in thinned TiC/SiC cross-sections, using a Hitachi-800 transmission electron microscope (TEM) at an operating voltage of 200 kV. The TEM samples were prepared following the conventional "sandwich method". Slices were cut perpendicular to the interface using a low speed diamond saw. Two slices were then glued together using epoxy to form a sandwich with the TiC layers facing each other. The sandwich was mechanically thinned to about 20-30 μm and subsequently dimpled. Final thinning was performed with a 4 Kev Ar ion beam, until the TiC/SiC interface was perforated.

5.3 Results

5.3.1 TiC Epitaxial Growth Condition

Epitaxial growth of TiC was obtained at $T_s > 1200$ °C. Mirror-like as-grown TiC surface were obtained at $1 \leq C:Ti \leq 2$. The surface morphology and growth rate were functions of growth temperature T_s and C:Ti ratio at all growth conditions investigated. Rough surfaces were obtained at all T_s when $C:Ti < 1$. As-grown surfaces obtained below 1200 °C were grainy under microscopic examination. The growth rate of TiC epilayers (1.7 ± 0.1 μm/hr) was dependent only on $TiCl_4$ flow rate at 1200 °C $\leq T_s \leq$ 1277 °C. The optimum TiC epitaxial growth conditions were identified as: growth rate = 1.7 μm/hr, growth temperature T_s = 1238 °C, and the C_2H_4 to $TiCl_4$ flow rate ratio (C:Ti) = 1.

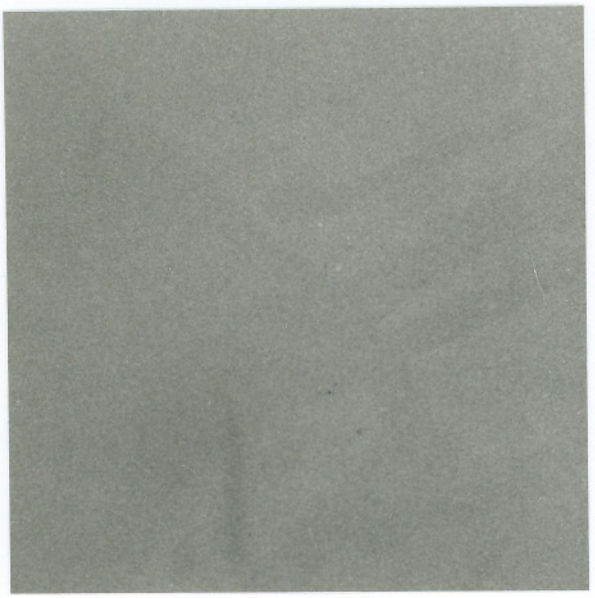

(a) 5 μm

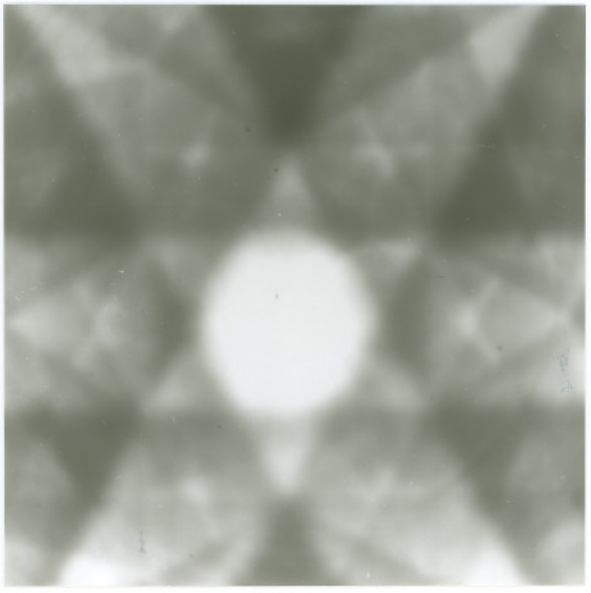

(b)

Fig.5.1 SEM micrographs showing a as-grown TiC epilayer on a (0001) 6Hα-SiC substrate with: (a) surface morphology and (b) SAECP.

Fig.5.1(a) shows an example of the TiC epilayers, with specular as-grown surface morphologies, grown on a (0001) 6Hα-SiC substrate. The epitaxial character and orientation of the TiC films were confirmed by selected area electron channelling patterns (SAECPs) obtained from their surfaces. A sharp SAECP with three fold symmetry obtained from the (111) TiC epilayer revealed in Fig.5.1(a) is shown in Fig.5.1(b).

5.3.2 Interfacial Structures of TiC/β-SiC

Six cases of TiC epitaxial thin films were studied as listed in Table 5.1, which include TiC on (110)-oriented β-SiC, TiC on (111)-oriented β-SiC, TiC with thicknesses of 1800 Å, 1750 Å, 160 Å, and 70 Å on (0001)-oriented 6Hα-SiC.

Table 5.1 TiC Epitaxial Thin Films Examined

Case	Growth Structure
1	TiC on (110) β-SiC
2	TiC on (111) β-SiC
3	TiC on 6Hα-SiC, TiC thickness = 1800 Å
4	TiC on 6Hα-SiC, TiC thickness = 1750 Å
5	TiC on 6Hα-SiC, TiC thickness = 160 Å
6	TiC on 6Hα-SiC, TiC thickness = 70 Å

5.3.2.1 TiC on (110)-oriented β-SiC

Epitaxial TiC films grown on (110)-oriented β-SiC contain defects including threading dislocations, microtwins, and DPBs, although the density of these defects in

TiC is substantially lower in comparison to β-SiC epilayers on which TiC were deposited. Fig.5.2 is a TEM image showing the threading dislocations, microtwins, and DPBs formed in a 1800 Å thick TiC epilayer, which was grown on a (110) β SiC.

Threading dislocations are the primary defects formed in TiC films, as shown in Fig.5.2. The dislocation density was roughly estimated as $\approx 250/\mu m^2$. From the observed dislocation visibility and the dislocation invisible criteria $g \cdot b = 0$,[135] it was found that these threading dislocations are unit dislocations with a Burger's vector $b = a/2<110>$, as expected for dislocations in a fcc crystal.

The microtwins and DPBs formed in TiC were the result of extension of microtwins and DPBs present in the (110) β-SiC. The direct correlation between a DPB in TiC and a DPB in β-SiC can be noticed in Fig.5.2. The (110) β-SiC used as the substrate for TiC epitaxial growth, was grown epitaxially on a bulk-grown (110) TiC_x substrate. In chapter 4, it has been shown that β-SiC grown on (110) TiC_x substrates contained a high density of microtwins and DPBs. These microtwins and DPBs extended from β-SiC/TiC_x interface to the free surface of β-SiC epilayers. During the epitaxial growth of TiC thin films, these microtwins and DPBs were then reproduced into the epilayers. However, it should be mentioned that not every DPB or microtwin can extend into TiC epitaxial film.

It may be difficult to identify a DPB from a dislocation in morphologies shown in TEM micrographs. To determine whether it is a dislocation or a DPB, one thing should be borne in mind that is, a dislocation is a linear defect surrounded by perfect matrix , and a DPB is a planar defect which is the boundary between two twinning-oriented domains. Therefore, a dislocation is revealed as a dark line and a DPB is revealed as a boundary between two regions which have different contrast.

5.3.2.2 TiC on (111)-oriented β-SiC

Threading dislocations, along with a small number of microtwins, were seen as the primary defects formed in TiC films grown on (111) β-SiC, no DPBs were observed in this case. Threading dislocations formed in a TiC epilayer grown on a (111)-oriented

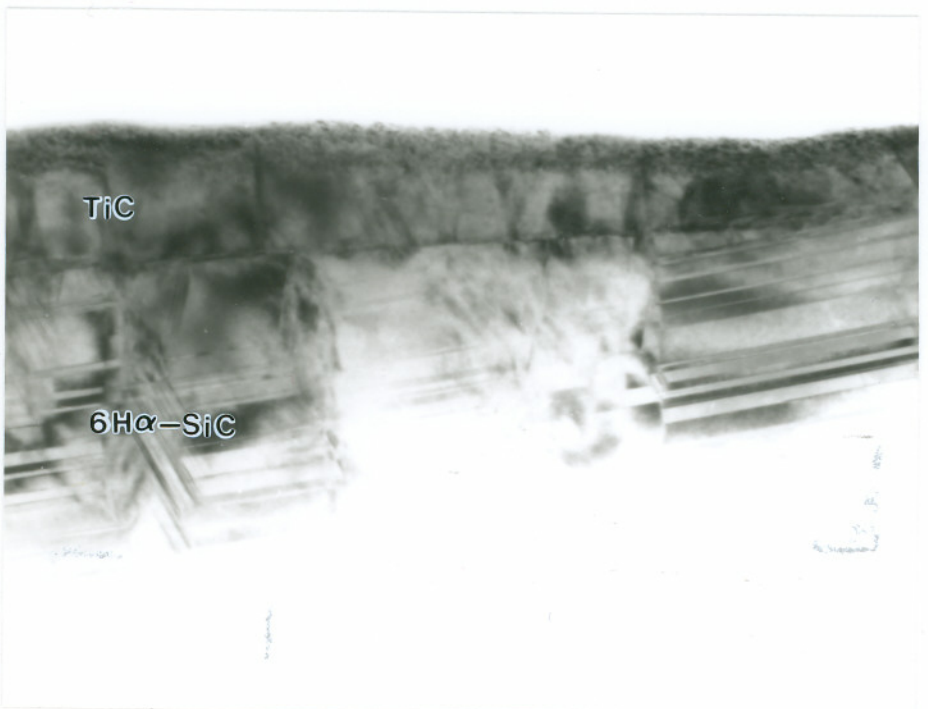

125 nm

Fig.5.2 XTEM micrograph showing defects formed in a TiC epilayer grown on a (110)-oriented β-SiC epilayer.

β-SiC epilayer are shown in Fig.5.3. The density of threading dislocations in (111)-oriented TiC epilayer, however, was higher than that in a (110)-oriented TiC epilayer, from our TEM observations. The density of threading dislocations in (111) TiC was roughly at $400/\mu m^2$ which was 1.6 times the value of threading dislocations observed in (110) TiC epilayers.

The lack of DPBs in (111) TiC is certainly attributed to the low density of DPBs in (111) β-SiC. The (111) β-SiC used as a substrate for TiC epitaxial growth, grown epitaxially on a (111) bulk-grown TiC_x substrate. TEM observations in chapter 4 showed two main differences for the β-SiC epilayers grown on (110) and (111) TiC_x substrates. First, microtwins formed in (110) β-SiC and (111) β-SiC epilayers revealed different orientations relative to the interface. In the (110) β-SiC epilayer, most microtwins were stacked on top of each other and were almost parallel to the interface. While the majority of microtwins in (111) β-SiC were initiated from the β-SiC/TiC interface and propagated perpendicular to the interface plane. Another distinguished difference between the two orientation β-SiC epilayers is the density of defects. Higher densities of microtwins and DPBs were formed in the (110) β-SiC films, and also these DPBs extended all the way to the top surface of β-SiC, while the DPBs formed in (111) β-SiC terminated within film as it thickening. These two differences are believed to attribute for the lower number of microtwins and lack of DPBs in the TiC thin film grown on a (111)-oriented β-SiC.

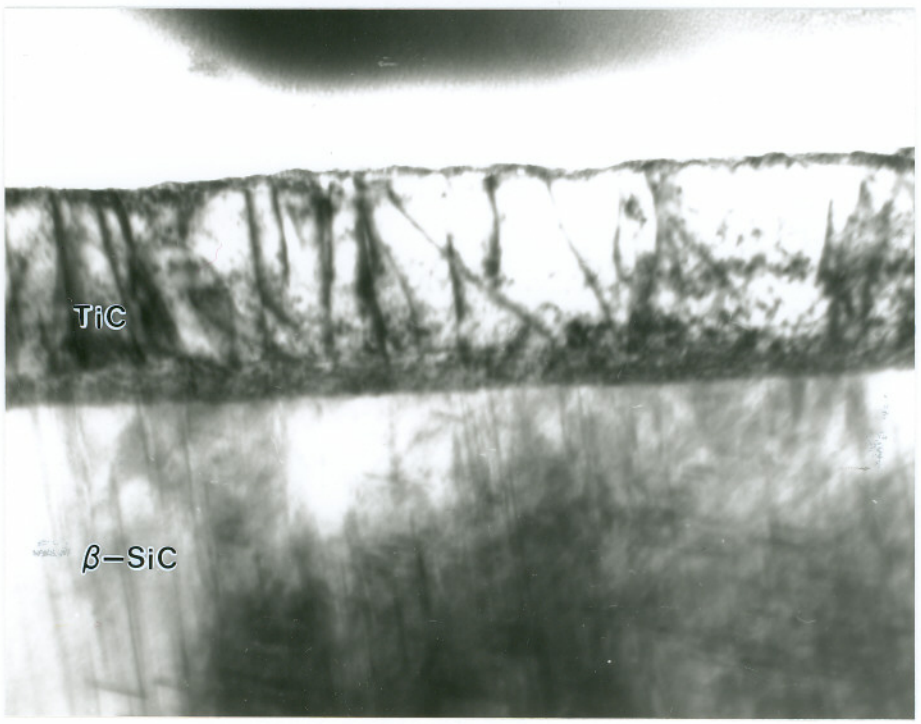

0.1 μm

Fig.5.3 TEM micrographs showing defects formed in a TiC epilayer grown on a (111)-oriented β-SiC epilayer, which was obtained using g = (002) and B = [$\bar{1}$10].

5.3.3 Interface Structures of TiC/(0001) 6Hα-SiC

Four thicknesses of TiC thin films were grown on (0001) 6Hα-SiC substrates, which are 1800 Å, 1750 Å, 160 Å, and 70 Å, respectively. Generally, TiC thin films grown on 6Hα-SiC substrates were superior to these grown on β-SiC. The epitaxial TiC/6Hα-SiC interfaces were flat and did not chemically react, even after being annealed for 2 hours at 1400 °C. The variation of the TiC epilayer quality with its thickness was examined using TEM in cross section.

Fig.5.4 is a TEM image of the TiC/6Hα-SiC interface showing a very low density of threading dislocations formed in the TiC epitaxial thin film. These cloud-like dark shadows present at the TiC/6Hα-SiC interface were the result of coherency loss between TiC and 6Hα-SiC. The threading dislocation density was about $100/\mu m^2$.

For a thinner TiC epilayer, the TiC/6Hα-SiC interface became more sharp, although threading dislocations were still present. Fig.5.5(a) shows a TEM image of the 1750 Å thick TiC on 6Hα-SiC in cross section. The lattice fringes were formed by (0006) planes in the 6Hα-SiC substrate. From Fig.5.5(a), it can be seen that the interface was flat and contained no inter-diffusion or phase transformation products. The flat interface demonstrates the difference in thermal stability of TiC/SiC interfaces formed by epitaxial TiC growth and those formed by Ti deposition and subsequent annealing.[155-159] In the case of Ti deposition on a SiC substrate, TiC was formed at expense of SiC; thus, creating free Si. Therefore, the TiC was in contact with free Si, which then reacted with the free Si to form Ti_3Si_2 and Ti_5Si_3 above 800 °C. However, in the case of stoichiometric TiC deposition on a SiC, there was no free Si with which the TiC could react; thus, the interface was thermally stable to at least 1400 °C. Fig.5.5(b) and (c) are the selected area diffraction (SAD) patterns acquired from the TiC and 6Hα-SiC two regions in Fig.5.5(a). The SAD patterns indicate that the TiC layer and the 6Hα-SiC substrate have a crystal orientation relation: $[\bar{1}10]_{TiC}$ // $[2\bar{1}\bar{1}0]_{6H\alpha\text{-}SiC}$ and $(111)_{TiC}$ // $(0001)_{6H\alpha\text{-}SiC}$. This agrees with the result reported previously.[159]

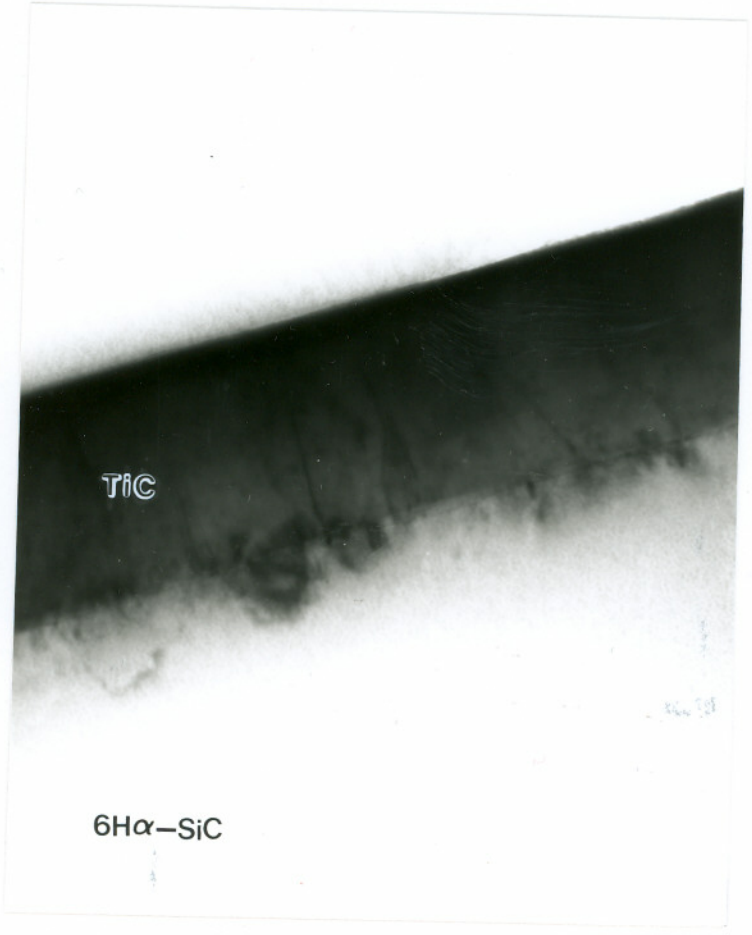

Fig.5.4 A TEM micrograph showing a 1800 Å TiC epilayer grown on a (0001) 6Hα-SiC substrate.

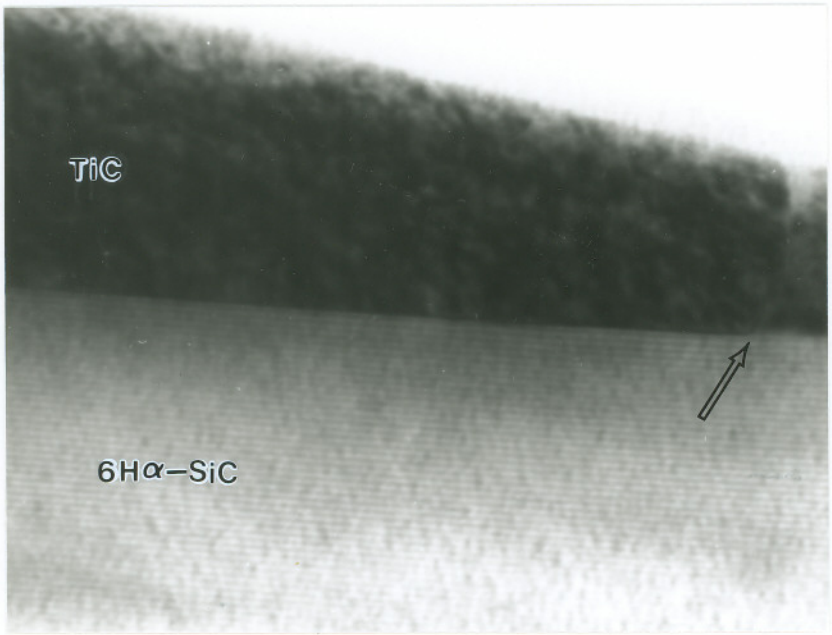

(a) 0.05 μm

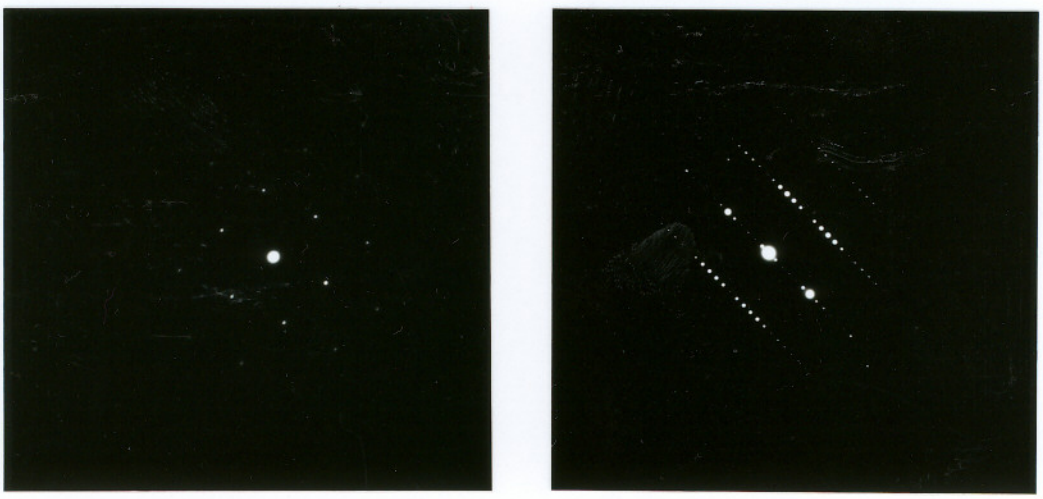

(b) (c)

Fig.5.5 (a) A TEM image showing a 1750Å TiC epilayer grown on a (0001) 6Hα-SiC substrate, (b) SADP from TiC region, and (c) SADP from 6Hα-SiC region.

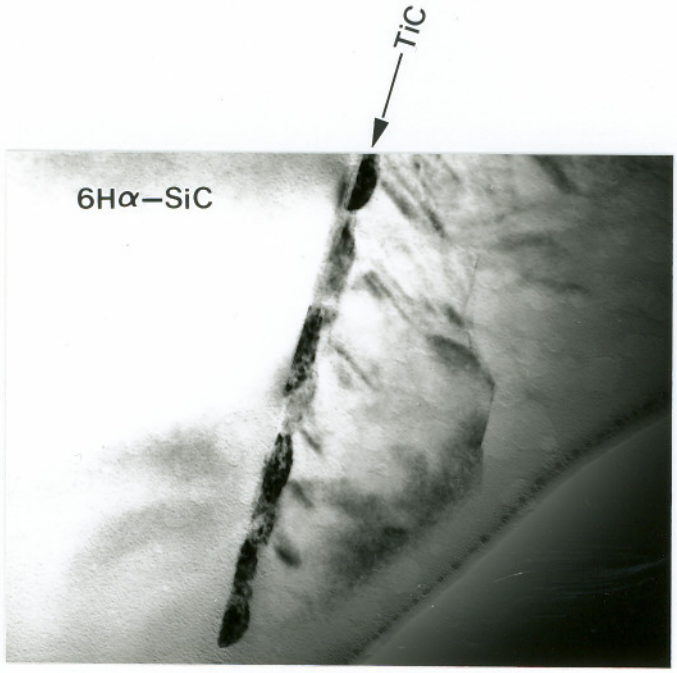

(a) 0.1 μm

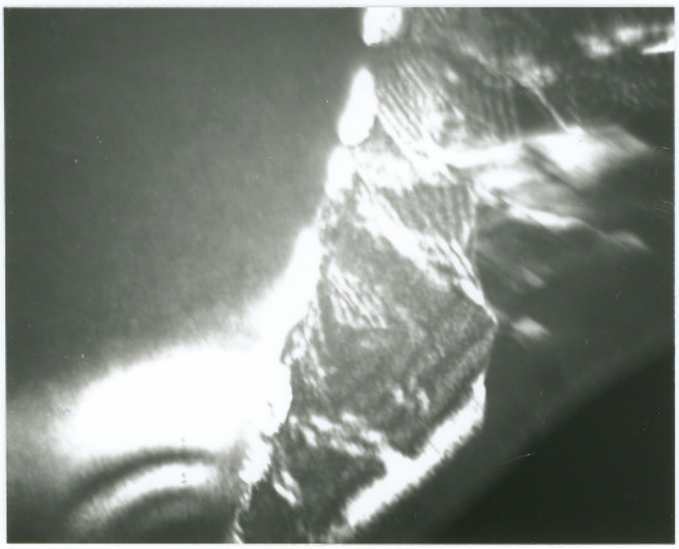

(b) 0.1 μm

Fig.5.6 TEM images showing a 160Å TiC epilayer grown on a (0001) 6Hα-SiC substrate with (a) BF and (b) DF, using g = (0006) and B = $[11\bar{2}0]$.

0.05 μm

Fig.5.7 A TEM image showing 70 Å TiC grown on a (0001) 6Hα-SiC substrate.

When a thin TiC layer was deposited, a non-uniform layer was observed. Fig.5.6(a) and (b) are the TEM images of a 160Å thick TiC layer in bright field (BF) and dark field (DF), respectively. It can be seen that the thin TiC layer is not a continuous film but consists of discrete islands. The TiC thickness 160 Å was determined based on a rough average value. The nonuniform TiC layer was due to island nucleation mode.[88] During the nucleation and the initial growth of vapor phase epitaxial growth, nuclei are first formed on the substrate randomly. These nuclei grow three dimensional; and eventually agglomerate into a continuous film. However, if the deposit is too thin, the growth was over before these island-shape nuclei reach each other in the lateral direction, then a non-continuous layer is generated.

This non-uniform TiC growth was also observed in a 70 Å thick TiC film, as shown in Fig.5.7. However, no defects such as threading dislocations were observed within the TiC.

5.4 Discussion

5.4.1 Formation of Threading Dislocations in TiC Film

TEM observations showed that threading dislocations as the primary defects are formed in TiC epitaxial films grown on either β-SiC or 6Hα-SiC substrates. A basic concept in dislocation theory is that a dislocation line can never terminate within a crystal.[149,152] Dislocations must form either closed loops, branch into other dislocations, or terminate at a grain boundary or crystal surface.

A misfit dislocation usually lies in the interface plane formed by the two materials. Since misfit dislocations can not terminate within the crystal, it then extends its way through the thin overlayer and terminates at the growth surface. Part of the dislocation network is envisioned as threading through the epilayer film; such a dislocation is known as a threading dislocation, as shown in Fig.5.8.

The formation of threading dislocations is associated with misfit dislocations. Due to the lattice parameter difference between TiC and SiC, misfit dislocations were

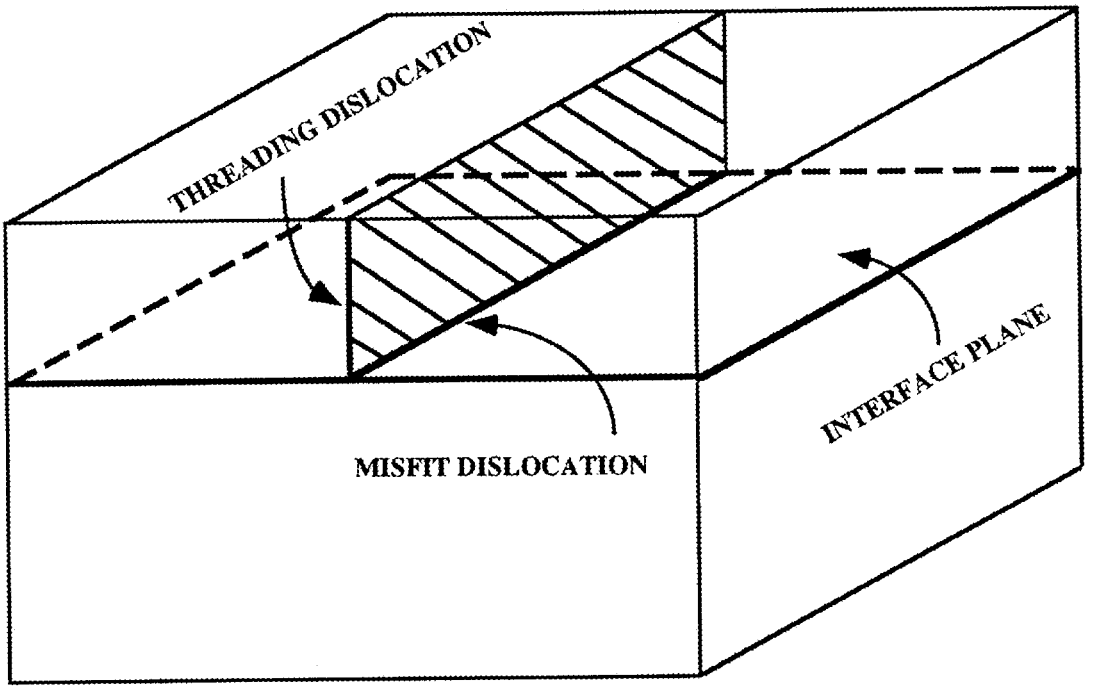

Fig.5.8 Illustration of a threading dislocation connected with a misfit dislocation buried in the interface plane.

formed in the TiC epitaxial films when its thickness was over a critical value for pseudomorphic growth, see section 2.4.2. Threading dislocations were then created when misfit dislocations glided across the epilayer. Misfit dislocations are an intrinsic part of the structure and cannot be avoided in an equilibrium configuration, however, threading dislocations are a function of the experimental situations (i.e. purity, surface cleanliness, growth condition etc.) and can be varied by a large factor.

The variation of threading dislocation density formed in TiC epilayers grown on (110) and (111)-oriented β-SiC are due to the differences in the distribution of microtwins in the two orientation β-SiC epilayers. It was shown in chapter 4, microtwins formed in the (111) β-SiC epilayer were almost perpendicular to the β-SiC free surface, and therefore, led to a rough surface for subsequent TiC epitaxial growth. These high energy surface steps on a (111) β-SiC became the initiation sites of threading dislocations. For the (110) β-SiC, most microtwins were stacked on top of each other and were almost parallel to the β-SiC surface. In this case, TiC thin film was deposited on a flatter surface, which then produced a lower density of threading dislocations.

5.4.2 Reproduction of Defects From β-SiC To TiC

Some of the microtwin or DPBs formed in the TiC epilayers were reproduced from β-SiC substrate. From the TEM observations, Fig.5.2 and Fig.5.3, defects present in β-SiC extended into the TiC epitaxial films. The reproduction of these microtwins or DPBs can be explained using the island nucleation mechanism. The island mode is the most common nucleation mechanism in a chemical vapor deposition process. Fig.5.9 and Fig.5.10 schematically illustrate the rough β-SiC surface caused by the presence of microtwins in β-SiC, and the stacking sequence variations across a DPB, respectively. Discrete nuclei were first formed randomly on the substrate surface. Each nucleus had the same stacking sequence or crystal orientation relative to the substrate below it, as shown in the first stage (a) of Fig.5.9. The nucleus on top of the twinning area had the same stacking sequence Abcabc... in comparison to the neighboring nuclei, however,

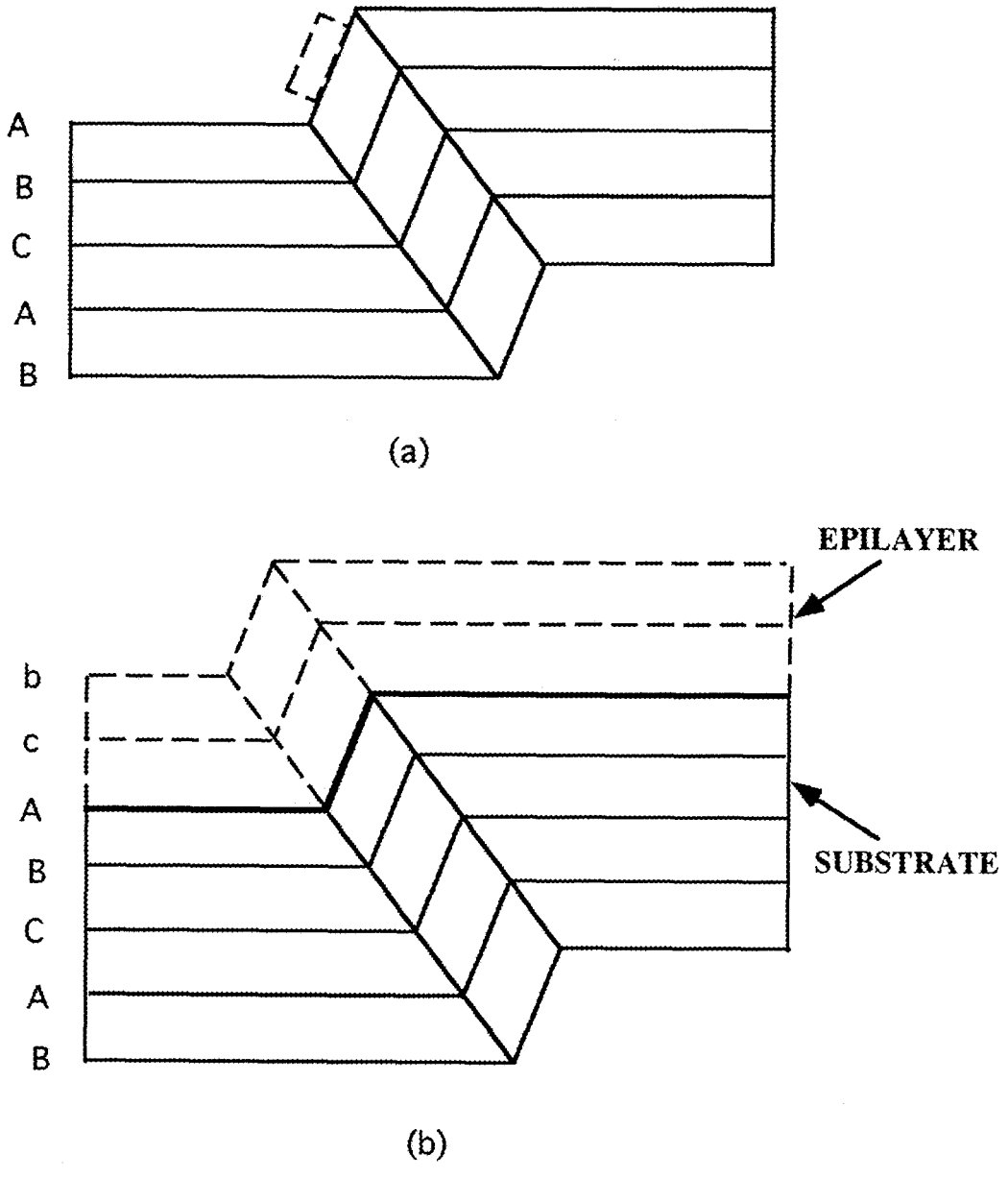

Fig.5.9 Reproduction of microtwins from β-SiC into TiC films due to island nucleation and epitaxial growth.

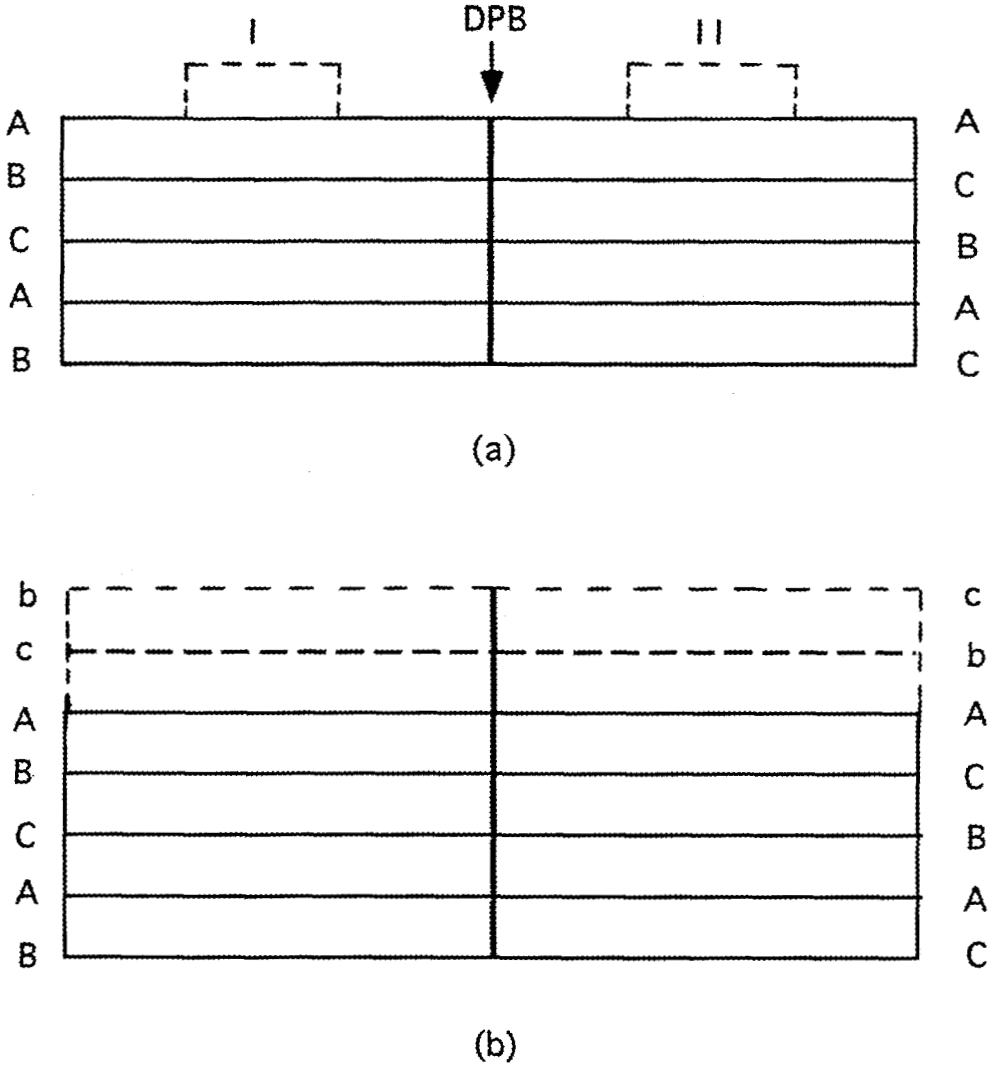

Fig.5.10 Reproduction of DPBs from β-SiC into TiC films due to island nucleation and epitaxial growth.

there was a twinning relation between them. In the case of Fig.5.10, the nucleus I deposited in the order of Abcabc..., and the nucleus II continued in the order of Acbacb.... Lateral growth of these nuclei resulted in the impingement of neighboring islands, therefore, microtwins and DPBs were formed in the TiC film.

5.4.3 Dependence of Strains in TiC Epilayer on Its Thickness

Strains were introduced in the TiC epilayer grown on a β-SiC or 6Hα-SiC substrate due to the lattice mismatch. The strain versus TiC thin film thickness can be illustrated using reduced strain unit as:

$$\epsilon_{red}=\frac{\epsilon^*}{\epsilon_{max}} \tag{5.1}$$

where ϵ^* is the critical strain, ϵ_{max} is the maximum strain (ϵ_{max} = f, the misfit).

The critical strain ϵ^* is the value which minimize the total strain and therefore relates to strain of film at the critical thickness h_c. The ϵ^* is a function of the thin film thickness as discussed in chapter 2, it is given by

$$\epsilon^* = \frac{b}{8\pi(1+\nu)h}\left[\ln\left(\frac{h}{b}\right)+1\right], \qquad h > h_c \tag{5.2a}$$

and

$$\epsilon^* = f. \qquad h < h_c \tag{5.2b}$$

The critical thickness h_c is defined as:[108]

$$h_c = \frac{b}{8\pi\ (1+\nu)\ f}\left[\ln\left(\frac{h_c}{b}\right)+1\right] \tag{5.3}$$

In the epitaxial structures of TiC on β-SiC or TiC on 6Hα-SiC system, lattice misfit f is 0.006, the Burgers' vector b is a/2[110] = 3.06×10^{-8} cm. The Poisson's ratio of TiC is 0.2.[141] The equ.(5.3) was satisfied when h_c/b = 22.8, and therefore, the critical thickness value of TiC films was about 70 Å.

When the TiC film thickness is over h_c, the reduced strain can be obtained using equation (5.1), (5.2a), and (5.3),

$$\epsilon_{red} = \frac{1}{h_{red}} \frac{[\ln[(\frac{h}{b}) + 1]}{[\ln(\frac{h_c}{b}) + 1]}, \qquad h>h_c \qquad (5.4)$$

By defining the reduced thickness as $h_{red} = h/h_c$, this strain versus thickness in reduced units can be shown in Fig.5.11 for TiC thin film grown on a β-SiC or on a 6Hα-SiC substrate, respectively. Beyond the critical thickness, strain decreases approximately as $1/h_{red}$. When the TiC layer thickness was less than h_c, the TiC epilayer was strained to precisely match the SiC substrate at the interface. As TiC thickened, this mismatch strain was reduced and the interface lost its coherency by forming misfit dislocations. Therefore, the incoherency at the TiC/SiC interface became larger in a thicker TiC epilayer, as observed in Fig.5.2. The strain does not reduce infinitely with TiC thickness, but becomes stable when the thickness is over about 10 times the critical value, which is about 700 Å.

The critical thickness of 70 Å for a TiC on a 6Hα-SiC also implys that, a pseudomorphic TiC layer can be obtained within this thickness. No dislocations were observed for the TiC epilayer with a 70 Å thickness, as shown in Fig.5.8. Unfortunately, a non-uniform layer was produced when very thin TiC was deposited.

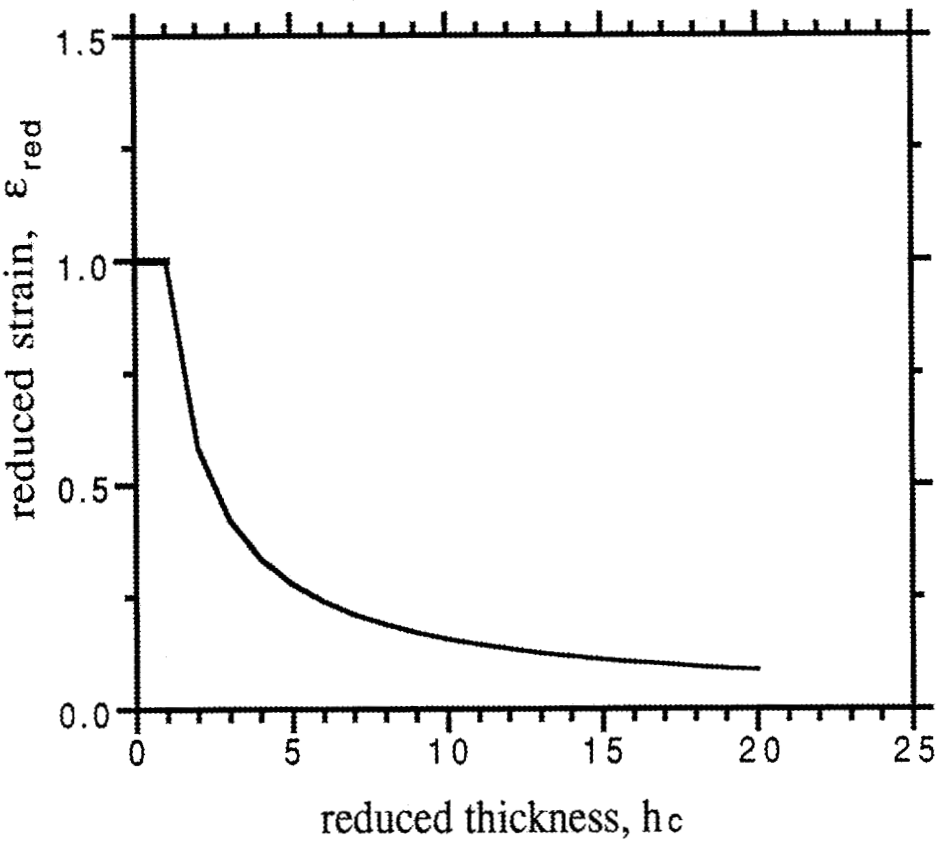

Fig.5.11 Strain versus thickness relationship of a TiC thin film grown on a 6Hα-SiC substrate.

5.5 Conclusions

Conditions were established for epitaxial growth of TiC (rocksalt structure) on β-SiC (zincblend) and 6Hα-SiC (wurtzite) structures. Epitaxial growth of TiC on (110) ß-SiC, (111) ß-SiC, and (0001) 6Hα-SiC, was demonstrated, and the TiC/SiC interfaces remained flat and free of titanium silicides even after annealed at 1300-1400°C for two hours.

Along with the primary defects of threading dislocations, microtwins and DPBs were also formed in a TiC film grown on a (110) β-SiC, but no DPBs were observed in a TiC grown on a (111) β-SiC. The lack of DPBs in the (111) TiC epilayer was attributed to the terminations of DPBs present in the (111) β-SiC on which TiC was grown. The formation of microtwins or DPBs in the TiC films were the result of reproductions of these defects present in β-SiC substrates.

The TiC epitaxial films grown on (0001) 6Hα-SiC were superior to that grown on (110) or (111) β-SiC, owning to the good crystal quality of bulk grown 6Hα-SiC substrate. Threading dislocations were the only defects observed in TiC epilayers grown on (0001) 6Hα-SiC. The TiC/6Hα-SiC interface coherency was dependent on the TiC epilayer thickness, interface incoherency became visibly large when TiC thickness exceeded 1750 Å. when a thin TiC with thickness less than 160Å was deposited on a 6Hα-SiC substrate, non-uniform TiC layer was produced due to the slow lateral growth.

Chapter 6

CONCLUSIONS AND FUTURE WORK SUGGESTIONS

A potential high performance semiconductor material β-SiC was synthesized on (111), off-(111), and (110) bulk-grown TiC_x substrates using a CVD process and 1,2-disilylethane as the reactant source. Epitaxial growth of TiC thin films were also obtained on (110)β-SiC, (111)β-SiC, and (0001)6Hα-SiC substrate. Defects formed in β-SiC and TiC epilayers were characterized using TEM in cross-section.

The TiC_x material used as the substrates for β-SiC epitaxial growth was obtained by a high-pressure float-zone technique. These TiC_x crystals are nonstoichiometric with carbon deficiency, and also contain substrates and inter-subgrain defects. The sub-boundaries were classified by their structures as: (i) wide-extended, fault-like defects (WEFLD), (ii) edge dislocation arrays, and (iii) dislocation networks. The planar defects, observed on sub-boundaries and within sub-grains, resemble an stacking fault-like characteristics. This is the first reported observation of planar defects formed within TiC_x subgrains, to our knowledge. Annealing of TiC_x at 2300 °C in contact with graphite, caused a significant reduction in the misorientation level and/or density of subgrains.

Single crystal β-SiC films grown on the TiC_x substrates contain microtwins and DPBs. The density of these defects were found to be affected by the growth conditions and the TiC_x substrate orientations. An optimum growth condition was growth temperature T_s = 1157 - 1180 °C and the reactant source flow rate Q_{DSE} = 3.2 sccm. Deviation of either growth temperature or flow rate led to higher concentration of microtwins and DPBs in β-SiC. The TiC_x substrate with a small angle off from the

desired (111) orientation resulted in a rough surface, which then led to a rough β-SiC/TiC_x interface and higher density of defects in the β-SiC epilayers. Two main differences were observed for the defects formed in (111) and (110) β-SiC epilayers. In the (110) β-SiC epilayer, most microtwins were stacked on top of each other and were almost parallel to the interface. While the majority of microtwins in (111) β-SiC were initiated from the β-SiC/TiC interface and propagated perpendicular to the interface plane. Another difference between the two orientation β-SiC epilayers was the density of defects. High density of microtwins and DPBs were formed in the (110) β-SiC films, and also the DPBs extended all the way to the top surface of β-SiC, however, the DPBs formed in (111) β-SiC terminated within film as it thickened.

Epitaxial growth of TiC on (110) ß-SiC, (111) ß-SiC, and (0001) 6Hα-SiC, was demonstrated, and the TiC/SiC interfaces remained flat and free of titanium silicides even after annealing at 1300-1400°C for two hours. Along with the primary defects of threading dislocations, microtwins and DPBs were also formed in a TiC film grown on a (110) β-SiC, but no DPBs were observed in a TiC grown on a (111) β-SiC. The TiC epitaxial films grown on (0001) 6Hα-SiC were superior to those grown on (110) or (111) β-SiC, owing to the good crystal quality of bulk grown 6Hα-SiC substrate. Threading dislocations were the only defects observed in TiC epilayers grown on (0001) 6Hα-SiC. The TiC/6Hα-SiC interface coherency was dependent on the TiC epilayer thickness, interface incoherency became visibly large when TiC thickness exceeded 1750 Å. When a thin TiC with thickness less than 160 Å was deposited on a 6Hα-SiC substrate, non-uniform TiC layer was produced due to the slow lateral growth.

The main barriers to the development of β-SiC using TiC_x as the substrate are lying in two aspects: (i) the low quality of bulk-grown TiC_x crystals. Substructures formed in the nonstoichiometric TiC_x largely degrade its use as the substrate material although the substrate density was reduced substantially through an annealing process. (ii) the dissimilar crystal structures, thermal expansion coefficient, and chemical compositions between β-SiC and TiC make it very difficult to obtain high quality β-SiC thin films. Epitaxial growth of β-SiC on a intermediate layer TiC, which was deposited

epitaxially on a (0001) 6Hα-SiC substrate, seems to be a promising approach. In this heterostructure, the interface plane lattice mismatch is very small for both interfaces TiC/6Hα-SiC and β-SiC/TiC. Secondly, the thermal properties of β-SiC and 6Hα-SiC are similar, and therefore, thermal stress will be at a very low level if the intermediate TiC layer is substantially thin. The problem with this approach at the present time, however, is that conditions for a uniform thin TiC layer on 6Hα-SiC have not been obtained. The suggestion for future work is the growth condition optimization of thin TiC epilayer on (0001) 6Hα-SiC substrate, and the study of TiC growth on off-(0001) 6Hα-SiC.

REFERENCES

1. J. A. Powell and L. G. Matus, "Recent Developments in SiC (USA)", in *Amorphous and Crysatlline Silicon Carbide*, Springer Proc. in Phys., Vol. 34, edited by G. L. Harris and C. Y. Yang, (Springer-Verlag, Berlin, 1989), p.2.

2. R. J. Trew, J. B. Yan, P. M. Mock, "The Potential of Diamond and SiC Electronic Devices for Microwave and Millimeter-wave Power Applications", *Proc. IEEE*, **79** (5), 598 (1991).

3. M. G. Spencer, "The Prospects for Beta Silicon Carbide Materials and Devices", *Proc. of Int. Semiconductor Device. Res. Symp.*, (Charlettesville, VA, 1991), p. 503.

4. B. J. Baliga, "Impact of SiC on Power Devices", in *Amorphous and Crysatlline Silicon Carbide IV*, edited by C. Y. Yang, M. M. Rahman, and G. L. Harris (Springer-Verlag, Berlin, 1992), p. 305.

5. P. A. Ivanov and V. E. Chelnokov, "Recent Developments in SiC Single Crystal Electronics", *Semicond. Sci. Tech.*, **7**, 863 (1992).

6. L. A. Hemstreet and C. Y. Fong, "Recent Band Structure calculation of Cubic Silicon Carbide", *Proc. 3rd Int. Conf. on SiC*, (Miami Beach, FL, USA, Sept.17-20, 1973), p.284.

7. H. R. Phillip and E. A. Taft, "Intrinsic Optical Absorption in Single Crystal Silicon Carbide", in *Silicon Carbide - A High Temperature Semiconductor*, edited by J. R. O'Connor and J. Smithens (Pergamon Press, 1960), p.366.

8. S. M. Sze, *Physics of Semiconductor Devices*, (John Wiley & Sons, New York, 1981).

9. C. van Opdorp and J. Vrakking, "Avalanche Breakdown in Epitaxial SiC p-n Junction", *J. Appl. Phys.*, **40**, 2320 (1969).

10. M. Shinohara, M. Yamanaka, H. Daimon, E. Sakuma, J. Okumuram S. Misawa, K. Endo, and S. Yoshida, "Growth of High-Mobility of 3C-SiC Epilayers by Chemical Vapor Deposition", *Japan J. Appl. Phys.*, **27**, LA34 (1988).

11. D. M. Caughey and R. E. Thomas, "Carrier Mobilities in Silicon empirically Related to Doping and Field", *Proc. IEEE*, **55**, 2192 (1967).

12. W. von Muench and E. Pettenpaul, "Saturated Electron Drift Velocity in 6H Silicon Carbide", *J. Appl. Phys.*, **48**, 4823 (1977).

13. L. Patrick and W. J. Choyke, "Static Dielectric Constant of SiC", *Phys. Rev. (B)*, **2**, 2255 (1970).

14. G. A. Slack, "Thermal Conductivity of Pure and Impure Silicon Carbide and Diamond", *J. Appl. Phys.*, **35**, 3460 (1964).

15. A. R. Verma, P. Krishna, *Polymorphism and Polytypism in Crystals*, (John Wiley & Sons, New York, 1966).

16. R. I. Space and G. R. Slack, *Silicon Carbide, A High Temperature Semiconductor*, edited by J. R. O'Connor and J. Smiltens, (Pergamon Press, New York, 1960), p.24.

17. W. S. Yoo, S. Nishino, and H. Matsunami, "Polytype Change of Silicon Carbide at High Temperature", in *Amorphous and Crystalline SiC II*, (Springer Proc. in Phys., Vol. 34, 1989), p. 8.

18. S. Nishino, Yoshikazu, H. Matsunami, and T. Tanaka, "Chemical Vapor Deposition of Single Crystalline ß-SiC Films on Silicon Substrate with Sputter SiC Intermediate Layer", *J. Electrochem. Soc.*, **127**, 2674 (1980).

19. S. Nishino, J. A. Powell, and H. A. Will, "Production of Large-Area Single-Crystal Wafers of Cubic SiC for Semiconductor Devices", *Appl. Phys. Lett.*, **42**, 460 (1983).

20. K. Shibahara, S. Nishino, and H. Matsunami, "Surface Morphology of Cubic SiC (100) Grown on Si (100) by Chemical Vapor Deposition", *J. of Crystal Growth*, **78**, 538 (1986).

21. K. Shibahara, S. Nishino, and H. Matsunami, "Antiphase-Domain-Free Growth of Cubic SiC (100)", *Appl. Phys. Lett.*, **50**, 1888 (1987).

22. K. Takahashi, S. Nishino, and J. Saraie, "Low-Temperature Growth of 3C-SiC on Si Substrate by Chemical Vapor Deposition Using Hexamethyldisilane as a Source Material", *J. Electrochem. Soc.*, **139**, 3565 (1992).

23. C. M. Chorey, P. Pirouz, J. A. Powell, and T. E. Mitchell, "TEM Investigation of ß-SiC Grown Epitaxially on Si Substrate by CVD", in *Semiconductor-Based Heterojunctions Interfacial Structure and Stability*, edited by M. L. Green et.al., (Warrendal, PA: Metallurgical Soc.), **115** (1992).

24. P. Pirouz, C. M. Chorey and J. A. Powell, "Antiphase Boundaries in Epitaxially Grown ß-SiC", *Appl. Phys. Lett.*, **50**, 221 (1987).

25. J. A. Powell, " ß-SiC Heteroepitaxial Films Using Off-axis Si Substrates", *Appl Phys. Lett.*, **51**, 823 (1987).

26. P. Liaw, and R. F. Davis, "Epitaxial Growth and Characterization of ß-SiC Thin Films", *J. Electrochem. Soc.*, **132**, 642 (1985).

27. C. H. Carter, Jr., R. F. Davis and S. R. Nutt, "Transmission Electron Microscopy of Process-Induced Defects in ß-SiC Thin Films", *J. Mater. Res.*, **1**, 811 (1986).

28. H. S. Kong, Y. C. Wang, J. T. Glass, and R. F. Davis, "The Effect of Off-axis (100) Substrates on the Defect Structure and Electrical Properties of ß-SiC Thin Film", *J. Mater. Res.*, **3**, 521 (1988).

29. H. S. Kong, J. T. Glass, and R. F. Davis, "Epitaxial Growth of ß-SiC Thin Films on 6Hα-SiC Substrates via Chemical Vapor Deposition", *Appl. Phys. Lett.*, **49**, 1074 (1986).

30. H. S. Kong, J. T. Glass, and R. F. Davis, "Chemical Vapor Deposition and Characterization of β-SiC Thin Films on Off-axis 6Hα-SiC Substrate", *J. Appl. Phys.*, **64**, 2672 (1988).

31. H. S. Kong, J. T. Glass, and R. F. Davis, "Growth Rate, Surface Morphology, and Defect Microstructures of ß-SiC Films Chemical Vapor Deposition on 6Hα-SiC Substrates", *J. Mater. Res.*, **4**, 204 (1989).

32. H. S. Kong, H J. Kim, J. A. Edmond, J. W. Palmour, J. Ryu, C. H. Varter, Jr., J. T. Glass, and R. F. Davis, "Growth, Doping, Device Development and Characterization of CVD Beta-SiC Epilayers on Si (100) and Alpha-SiC (0001)", *Mater. Res. Soc. Symp. Proc.*, **97**, 233 (1987).

33. Y. C. Wang, R. F. Davis, "Growth Rate and Surface Microstructure in 6Hα-SiC Thin Films Grown by Chemical Vapor Deposition", *J. of Electronic Materials*, **20**, 869 (1991).

34. J. D. Parsons, R. F. Bunshah and O. M. Stafsudd, "Unlocking the Potential of the Beta Silicon Carbide", *Sol. State Tech.*, **11**, 133 (1985).

35. J. D. Parsons, "Single Crystal Epitaxial Growth of β-SiC for Device and Integrated Circuit Applications", *Mat. Res. Soc. Symp.*, **97**, 271 (1987).

36. J. D. Parsons, G.B. Kruaval, and J. A. Vigil, "β-SiC on Titanium Carbide for Solid State Devices", *Springer Proc. in Phys.*, **43**, p. 171.

37. F. C. Frank, "The Growth of carborundum: Dislocations and Polytypism", *Phil. Mag.*, **42**, 1014 (1951).

38. L. S. Ramsdell and J. A. Kohn, "Development in Silicon Carbide Research", *Acta Cryst.*, **5**, 215 (1952).

39. C. J. Schneer, "Polymorphism in One Dimension", *Acta Cryst.*, **8**, 279 (1955).

40. H. Jagodzinski, "Polytypism in SiC Crystals", *Acta Cryst.*, **7**, 300 (1954).

41. W. S. Yoo and H. Matsunami, *Springer Proc. in Physics*, **71**, (Springer-Verlag, Berlin, 1992), p.66.

42. Y. M. Tairov and Y. A. Vodakov, *Electroluminesence*, edited by J. I. Pankove, (Springer-verlag, Berlinheideberg, New York, 1977), p.31.

43. E. O. Johnson, "Physical Limitation on Frequency and Power Parameters of Transistors", *RCA Review*, **26**, 163 (1965).

44. R. W. Keyes, "Figure of Merit for Semiconductors for High-Speed Switches", *Proc. IEEE*, **60**, 225 (1972).

45. K. Shenai, *Fourth International High Frequency Power Convention Conf. Proc.*, Naples, Fla., USA, May 14-18, 1989, (Intertec. Communications. Inc.), p.1-23.

46. J. A. Lely, "Dartellung von Einkristallen von Siliziumcarbid und Beherrschung von Art und Menge der eigebauten Verunreinigunen", *Ber. Deut. Keram. Ges.*, **32**, 229 (1955). (in German)

47. Y. M. Tairov and V. F. Tavetkov, "Investigation of Growth Processes of Ingots of Silicon carbide Single Crystals", *J. Cryst. Growth*, **43**, 209 (1978).

48. Y. M. Tairov and V. F. Tavetkov, "General Principles of Growing Large-Size Single Crystals of Various Silicon Carbide Polytypes", *J. Cryst, Growth*, **52**, 146 (1981).

49. G. Ziegler, P. Lanig, D. Theis, and C. Weyrich, "Crystal Growth of SiC Substrate Material for Blue Light Emitting Diodes", *IEEE Trans. Dev.*, **ED-30**, 277 (1983).

50. D. M. Jackson, Jr. and R. W. Howard, "Fabrication of Epitaxial SiC Films on Silicon", *Trans. Met. Soc. AIME*, **233**, 468 (1965).

51. J. J. Rohan and J. L. Sampson, "Heteroepitaxial beta-SiC on Sapphire", *Proc. Int. Conf. Cryst. Growth*, 1966, pp. 523-529.

52. K. E. Bean and P. S. Gleim, "Some Properties of Vapor Deposited SiC", *J. Electrochem. Soc.*, **114**, 1158 (1967).

53. R. B. Campbell and T. L. Chu, "Epitaxial Growth of Silicon Carbide by the Thermal Reduction Technique", *J. Electrochem. Soc.*, **113**, 825 (1966).

54. R. W. Bartlett and R. A. Mueller, "Growth, Processing and Characterization of beta-SiC Single Crystals", *Report AFCRL-69-0114 (AD685-172)*, Standford Res. Inst. Menlo Park, Calif., 1969, p. 26.

55. G. K. Safaraliev, Y. M. Tairov, V. F. Tsvetkov, and M. A. Chernov, *Pis'ma Zh. Tekh. Fiz.*, **2**, 699 (1976). (in Russion)

56. V. J. Jennings, A. Sommer, and H. C. Chang, "The Epitaxial Growth of Silicon Carbide", *J. Electrochem. Soc.*, **113**, 728 (1966).

57. P. Villars and L. D. Calvent, *Pearson's Handboob of Crystallographic Data for Intermetallic Phases*, **2**, (American Society for Metals, Metals Park, OH, 1985), p.1577.

58. E. K. Storms, "The Refractory Carbides", in *Refractory Materials*, **2**, (Academic Press, 1967), p.8.

59. H. Matsunami, S. Nishino, M. Odaka, and T. Tanaka, "Epitaxial Growth of a alpha-SiC Layer by Chemical Vapor Deposition Technique", *J. Cryst. Growth*, **31**, 72 (1975).

60. I. H. Khan and R. N. Summergrad, "The Growth of Single Crystal Films of Cubic SiC on Si (Part E)", *Appl. Phys. Lett.*, **11**, 12 (1967).

61. A. J. Learn and I. H. Khan, "Growth Morphology and Crystallographic Orientation of beta-SiC Films Formed by Chemical Conversion", *Thin Solid Films*, **5**, 145 (1970).

62. I. H. Khan, "The Structure of Epitaxial beta-SiC Films as Studied by Electron Diffraction", *Acta Cryst.*, **25**, p. S55 (1969).

63. K. E. Haq and I. H. Khan, "Surface Characteristics and Electrical Conduction of beta-SiC Films Formed by Chemical Conversion", *J. Vac. Sci. Tech.*, **7**, 490 (1970).

64. C. J. Mogab, H. J. Leamy, "Conversion of Si to Epitaxial SiC by Reaction with C_2H_4", *J. Apll. Phys.*, **45**, 1075 (1974).

65. A. S. Brown and B. E. Watts, "Growth of beta-SiC on Silicon", *J. Cryst. Growth*, **3**, 172 (1970).

66. J. Mercier and C. Roussel, *3rd Inter. Conf. on CVD*, 1972, p.426.

67. W. G. Spitzer, D. A. Kleinman, and C. J. Frosch, "Infrared properties of Cubic SiC Films", *Phys. Rev.*, **113**, 133 (1959).

68. H. Nakashima, T. Sugano, and H. Yanai, "Epitaxial Growth of SiC Films on Si Substrate and its Crystal Structures", *Japan. J. Appl. Phys.*, **5**, 874 (1966).

69. J. Graul and E. Wagner, "Growth Mechanism of Polycrystalline beta-SiC layers on Si Substrate", *Appl. Phys. Lett.*, **21**, 67 (1972).

70. A. Addamiano, and J. A. Sprague, "Buffer-Layer Technique for the Growth of Single Crystal SiC on Si", *Appl. Phys. Lett.*, 44(5), 1 March 1984, pp. 525-527.

71. S. Nishino and J. Saraie, "Heteroepitaxial Growth of Cubic SiC on a Si Substrate Using Si_2H_6 - C_2H_2 - H_2 System", in *Amorphous and Crystalline SiC II*, (Springer Verlag, Berlin, 1989), p. 8.

72. I. Golecki, F. Reidinger, and J. Marti, "Single Crystalline, Epitaxial Cubic SiC Films Grown on (100) Si at 750°C by Chemical Vapor Deposition", *Appl. Phys. Lett.*, **60**, 1703 (1992).

73. A. J. Steckl and J. P. Li, "Uniform β-SiC Thin Film Growth on Si by Low Pressure rapid Thermal Chemical Vapor Deposition", *Appl. Phys. Lett.*, **60**, 2107 (1992).

74. J. Yong, P. Pirouz and J. A. Powell, in *Amorphous and Crystal SiC II*, edited by Rahman et. al. (Springer Verlag, Berlin, 1989), p.14.

75. Y. C. Wang, H. S. Kong, J. T. Glass, and R. F. Davis, "Effect of Substrate Orientation on Interfacial and Bulk Character of Chemically Vapor Deposited Monocrystalline Silicon Carbide Thin Film", *J. Am. Ceram. Soc.*, **73**, 1289 (1990).

76. T. Ueda, H. Nishino, and H. Matsunami, "Crystal Growth of SiC by Step-Contralled Epitaxay", *J. Cryst. Growth*, **104**, 695 (1990).

77. J. A. Powell, J. B. Petit, J. H. Edgat, I. G. Jenkins, L. G. Matus, J. W. Yang, P. Pirouz, W. J. Choyke, L. Clemen, and M. Yoganathan, "Controlled Growth of 3C-SiC and 6H-SiC", *Appl. Phys. Lett.*, **59**, 333 (1991).

78. J. A. Powell, D. J. Larkin, J. B. Petit, and J. H. Edgar, "Investigation of the Growth of 3C-SiC and 6H-SiC Films on Low-Tilt-Angle Vicinal (0001) 6H-SiC Wafers", in *Amorphous and Crystalline Silicon Carbide IV*, edited by C. Y. Yang, M. M. Rahaman and G. L. Harris, (Springer Verlag, Berlin, 1992), p.23.

79. J. D. Parsons, *Ph.D Dissertation*, UCLA, 12/1981.

80. R. F. Bunshah, J. D. Parsons, and O. M. Stafsudd, *U. S. Patent No. 4,767,666* (8/30/1988).

81. J. D. Parsons, "Beta-SiC Power IMPATT Development", in *Interim Technical Report 3*, Sept./1987 to Spet./1988", Novel Weapons Center, Contract No. N60530-85-C-0163, No.3, 1989.

82. J. D. Parson, "High Temperature Electronics Workshop", (Albuquerque, N.M., Marriot Hotel, June 6-8, 1989).

83. J. D. Parsons, "Inverted-Vertical OMBPE Reactor: Design and Characterization", *J. Cryst. Growth*, **116**, 387 (1992).

84. J.D. Parsons, *U.S. Patent No. 4,738,937* (4/19/1988).

85. S. H. Tan, C. P. Beetz, Jr., J. M. Carulli, Jr., B. Y. Lin, and D. F. Cummings, "Space-Charge-Limited-Current Conduction in Heteroepitaxial 3C-SiC (111) on TiC (111)", *J. Mater. Res.*, **7**, 1816 (1992).

86. D. W. Brown and J. D. Parsons, in *Novel Refractory Semiconductors*, (Materials Res. Soc. Symp. Proc., **97**, 1987), p. 271.

87. D. W. Brown and J. D. Parsons, *U. S. Patent No.4,923,716* (5/18/1990).

88. M. J. Stowell, "Defects in Epitaxial Deposites", in Epitaxial Growth (part B), edited by J. W. Matthews (Academic Press, 1975), p. 457.

89. J. A. Venables and G. L. Price, *Epitaxial Growth (part B)*, edited by J. W. Matthews, (Academic Press, 1975), p.429.

90. A. Masson, J. J. Metois, Kern R., in *Advances in Epitaxy and Endotaxy*, edited by V. Ruth and H. G. Schnerider, (V. E. B. Deutscher Verlag für Grundstffindustrie, Leipzig, 1971).

91. J. J. Metois, M. Granch, A. Masson, and R. Kern, "Brownian Migration of Crystallinities on a Surface and Relation to Epitaxy", *Surface Sci.* **30**, 43 (1972).

92. J. J. Metois, M. Granch, A. Masson, R. Kern, "Example of Discontinuous Thin Films of Al and Au on (100) Patassium Chloride", *Thin Solid Films*, **11**, 205 (1972).

93. B. A. Joyce, "Growth and Structure of Semiconducting Thin Films", *Rep. Prog. Phys.*, **37**, 363 (1974).

94. B. A. Joyce, R. R. Bradley, and G. R. Booker, "Nucleation in Chemically Grown epitaxial Si Films Using Molecular Beam Technique (I)", *Phil. Mag.*, **14**, 289 (1966).

95. B. A. Joyce, R. R. Bradley, and G. R. Booker, "Study of Nucleation in Chem. Grown Epitaxial Si Films Using Mol. Beam Technique (III)", *Phil. Mag.*, **15**, 1167 (1967).

96. B. A. Joyce, R. R. Bradley, B. E. Watts, and G. R. Booker, "Study of Nucleation in Chem. Grown Epitaxial Si Films Using Mol. Beam Technique (V)", *Phil. Mag.*, **19**, 403 (1969).

97. B. A. Joyce, J. H. Neave, ,and B. E. Watts, "Influence of Substrate Conditions on the Nucleation and Growth of Epitaxial Si Films", *Surface Sci.*, **15**, 1 (1969).

98. D. W. Pashley, *Thin Films*, (ASM, Metals Park, Ohio, 1964), p.59.

99. J. W. Matthews, "A Study of Growth Defects in FCC Metal Foils Prepared by Evaporation", *Phil. Mag.*, **4**, 1017 (1959).

100. V. A. Phillips, "Direct Observation of Defects in Evaporated Siliver", *Phil. Mag.*, **5**, 571 (1960).

101. G. A. Bassett, D. W. Pashley, "The growth Structure and Mechanical Properties of Evaporated Metal Films", *J. Inst. Metals*, **87**, 449 (1959).

102. D. W. Pashley, "High-resolution Electron microscopy of Crystals", *Phil. Mag.* **4**, 324 (1959).

103. G. A. Bassett, *Proc. Eur. Regional Conf. Electron Microscopy*, edited by A. L. Houwink and B. J. Spits, (De Nederlandse Vereniging voor Electronmikrosc, Delft, 1960), p. 270.

104. M. H. Jacobs, D. W. Pashley,and M. J. Stowell, "Nucleation and Growth of Thin Films as Observed in the Electron Micorscopy", *Phil. Mag.*, **13**, 129 (1966).

105. R. H. Finch, H. J. Queisser, G. Thomas, and J. Washburn, "Structure and Origin of Stacking Faults in Epitaxial Si", *J. Appl.Phys.*, **34**, 406 (1963).

106. D. Pomerantz, in *Proc. Collq. Thin Film*, (Hungarian Acad. of Sci., Budapest, 1967), p. 63.

107. D. B. Holt, "Antiphase Boundaries in Semiconducting Compounds", *J. Phys. Chem. Soli.*, **23**, 1353 (1969).

108. King-Ning Tu, James W. Mayer, and Leonard C. Feldman, in *Electronic Thin Film Science for Electrical Engineers and Materials Scientists*, (Macmillan Publishing Company, 1992).

109. W. A. Jesser, J. W. Matthews, and D. Kuhlmann-Wilsdorf, *J. Vac. Sci. Tech.*, **2**, 276 (1965).

110. J. W. Matthews, "Role of Contaminants in the Epitaxial Growth of Au on NaCl", *Phil. Mag.*, **13**, 1207 (1966).

111. J. W. Matthews, S. Mader, and T. B. Light, "Accomodation of Misfit Across the Interface Between Crystals of Semiconducting Elements or Compounds", *J. Appl. Phys.*, **41**, 3800 (1970).

112. J. W. Matthews and A. E. Blakeslee, "Defects in Epitaxial Multilayers (I): Misfit Dislocation", *J. Crystal Growth*, **32**, 265 (1974).

113. J. W. Matthews, in *Epitaxial Growth (part B)*, edited by J. W. Matthews (Academic Press, 1975).

114. J. H. van der Merwe, "Strains in Crystalline Overgrowth", *Phil. Mag.*, **7** (80), 1433 (1962).

115. J. H. van der Merwe, "Crystal Interface (Part II): Finite Overgrowth", *J. Appl. Phys.*, **34** (1), 123 (1963).

116. J. M. van der Merwe, in *Single Crystal Films*, edited by M. H. Francombe and H. Sato, (Pergamon, Oxford, 1964), p.139.

117. W. A. Jesser and J. H. van der Merwe, in *Dislocation in Solids*, edited by J. W. Matthews, (Armsterdam, the Netherland, North Holland, 1989), p.421.

118. J. R. Willis, S. C. Jain, and R. Bullough, "The energy of an Array of Dislocations: Implications for Strain Relaxation in Semiconductor Heterostructures", *Phil. Mag.*, **A62** (1), 115 (1990).

119. R. Hull and J. C. Bean, "Misfit Dislocations in Lattice Mismatched Epitaxial Films", *Critical Reviews in Solids and Materials Sciences*, **17**, 507 (1992).

120. D. L. Tonsing, P. M. Stoop, and J. H. van der Merwe, "The Formation of Misfit Dislocations by Climb in Pseudomorphic Monolayers", *Surface Sci.*, **277**, 193 (1992).

121. J. W. Cahn, "On Spinodal Decomposition in Cubic Crystals", *Acta Metall.*, **10**, 179 (1962).

122. F. Yajima, T. Tanaka, E. Bannai, and S. Kawai, "Preparation of TiC_x Single Crystal With Homogenous Composition", *J. Cryst. Growth*, **47**, 493 (1979).

123. S. Otani, S. Honama, T. Tanaka, and Y. Ishizawa, "Preparation of TiC_x Single Crystal with Maximum Carbon Content by a Float Zone Technique", *J. Cryst. Growth*, **61**, 107 (1983).

124. S. Otani, T. Tanaka, and Y. Ishizawa, "Preparation of TiC_x Single Crystal with Nonstoichiometric Compositions by a Floating Zone Technique", *J. Cryt. Growth*, **71**, 615 (1985).

125. S. Shimada, J. Watanabe, K. Kodaira, T. Matsushita, *J. of Mater. Sci.*, **24**, 2513 (1989).

126. F. R. Chien, S. R. Nutt, and D. Cummings, "Defect Structures in Single Crystal TiC", *Phil. Mag. A*, **68(2)**, 325(1993).

127. W. S. Williams, "Physics of Transition Metal carbides", *Mater. Sci. Engineering (A)*, **105/106**, 1(1988).

128. W. S. Williams, R. D. Schaal, "Elastic Deformation, Plastic Flow, and Dislocations in Single Crystals of TiC", *J. of Appl. Phys.*, 33(3), 955(1962).

129. W. S. Williams, "Mondrian Precipitation Patterns in Single Crystals of TiC", *J. of Appl. Phys.*, 32, 552(1961).

130. G. E. Hollox, R. E. Smallman, "Plastic Behavior of TiC", *J. Appl. Phys.*, **37**(3), 818(1966).

131. J. Venables, "Stacking Faults in TiC", *Phys. Stat. Sol.*, **15**, 413(1966).

132. J. Venables, "The Nature of Precipitates in Boron-doped TiC", *Phil. Mag.*, **16**, 873(1967).

133. J. Venables, "Influence of Impurities on Stacking Fault Energy Determination", *Metall. Trans.*, **1**, 2471(1970).

134. P. B. Hirsch, A. Howie, R. B. Nicholson, and D. W. Pashley, *Electron Microscopy of Thin Crystals*, (Butterworth, London, 1965).

135. J. W. Edington, in *Practical Electron Microscopy*, (N. V. Phillips' Gloeilampenfabrieken, Eindhoven, 1976).

136. A. Seegar, in *Dislocations and Mechanical Properties of Crystals*, (John Wiley & Sons, New York, 1957).

137. R. E. Reed-Hill and R. Abbaschian, in *Physical Metallurgy*, 3rd edition (PWS-Kent Pub., Boston, 1991).

138. W. A. Tiller, in *The Science of Crystallinizations: Macroscopic Phenomena and Defects Generations*, (Cambridge University Press, 1991), p.336.

139. R. E. Smallman, in *Modern Physical Metallurgy*, (London Butterworths, 1970).

140. J. P. Hirth, J. Lothe, in *Theory of Dislocations*, (McGraw-Hill, Inc., 1968).

141. J. Friedel, in *Dislocations*, (Pergamon Press, 1964).

142. D. E. Newbury and H. Yakowitz, " Contrast Mechanisms of Special Interest in Materials Science", in *Practical Scanning Electron Microscopy*, edited by J. I. Goldstein, H. Yakowitz, (Plenum Press, New York, 1975).

143. D. W. Pashley, M. J. Stowell, *Phil. Mag.*, **8**, 1605 (1963).

144. T. P. Pearsall, "Strained Layer Superlattice Science and Technology", in *Semiconductors and Semimetals*, **33**, edited by R. K. Willardson, A. C. Beer,

(Academic Press, NY, 1990).

145. M. Neuberger, "Group IV Semiconductor Materials", in Handbook of Electronic Materials, **5**, (IFI/PLENUM, 1971), p.58.

146. J. H. Westbrook and E. R. Stover, "Carbides For High Temperature Application", edited by I. E. Campbell, E. M. Sherwood, in *High-Temerpature Materials and Technology*, (John Wiley & Sons, Inc., 1967), p.324.

147. G. A. Somorjai, *Chemistry in Two Dimensions: Surfaces*, (Cornell University Press, Ithaca, 1981).

148. C. Oshima, M. Aono, S. Zaima, Y. Shibata, and S. Kawai, "The Surface Properties of TiC (001) and TiC (111) Surfaces", *J. Less-Common Metals*, **82**, 69 (1981).

149. S. Zaima, Y. Shibata, H. Adachi, C. Oshima, S. Otani, M. Anoto, and Y. Ishizawa, "Atomic Chemcial Composition and reactivity of the TiC (111) Surface", *Surface Science*, **157**, 180 (1985).

150. J. H. Weaver, A. M. Bradshaw, J. F. van der Veen, F. J. Himpsel, D. E. Eastman, and C. Politis, "Angle-resolved Photoemission Studies of TiC (111) and TiC (100)", *Physical Review B*, **22**, 492 (1980).

151. F. R. Chien, *Ph.D Dissertation*, Brown University, 1994.

152. L.E. Toth, *Transition Metal Carbides and Nitrides*, (Academic Press, New York, 1971), p. 188.

153. D.T. Morelli, "Thermal Conductivity and Thermoelectric Power of TiC Single Crystals", *Phys. Rev. B*, **44** (11), 5453 (1991).

154. J. J. Bellina Jr. and M. V. Zeller, in *Novel Refractory Semiconductors*, edited by D. Emin, T. Aselage, and C. Wood, (MRS, Pittsburgh, PA, 1987), p. 265.

155. J. S. Bow, L. M. Porter, M. J. Kim, R. W. Carpenter, and R. F. Davis, "High Spatial Resolution TEM Study of Thin Film Metal/6H-SiC Interfaces", *Mat. Res. Soc. Symp. Proc.*, **280**, 571 (1993).

156. M. A. Taubenvlatt and C. R. Helms, "Interaction of Ti with C- and SiC-contaminated Si surfaces", *J. Appl. Phys.*, **59**(6), 1994 (1986).

157. S. K. Choi, M. Chandrasekaran, M. J. Brabers, "Interaction between titanium

VITA

The author was born September 21, 1964 in Henan Province, China. She received her B.S. and M.S. degree in Materials Science and Engineering (MSE) from Central-South University of Technology, Changsha, P. R. China in 1985 and 1988, respectively. She then worked as an assistant engineer for two years with China National Non-Ferrous Metals Industry Corp., Beijing, China.

She jointed Oregon Graduate Institute of Science and Technology in 1990, and received M.S. degree in MSE in January, 1993, on "Microstructural Characterization of Ni-Alloy Cladding onto Low Alloy Steel". She then started her Ph.D research on the defect study of semiconductor β-SiC thin films, and fulfilled the requirements for the degree of Ph.D in MSE in October, 1994.